공학박사학위논문

Strategies to Suppress Early Bone Resorption Induced by High Dose Bone Morphogenetic Protein-2

고농도 골형성 단백질 2형 적용시 나타나는 초기 골 흡수 억제 전략

2016년 2월

서울대학교 대학원

치의과학과 두개악안면세포및발생생물학전공

김 리 연

Strategies to Suppress Early Bone Resorption Induced by High Dose Bone Morphogenetic Protein-2

고농도 골형성 단백질 2형 적용시 나타나는 초기 골 흡수 억제 전략

지도교수 황 순 정

이 논문을 공학박사 학위논문으로 제출함

2016년 2월

서울대학교 대학원

치의과학과 두개악안면세포및발생생물학전공

김 리 연

김리연의 박사학위논문을 인준함

2016년 2월

위 원 장 (인)

부위원장 (인)

위 원 (인)

위 원 (인)

위 원 (인)

-ABSTRACT-

Strategies to Suppress Early Bone Resorption Induced by High Dose Bone Morphogenetic Protein-2

Ri Youn Kim

Program in Craniomaxillofacial Cell and Developmental Biology,

Department of Dental Science,

Graduate School, Seoul National University

(*Directed by Professor* **Soon Jung Hwang**, Dr. med. Dr. med. dent)

Objectives

Recombinant human morphogenic protein-2 (rhBMP-2) can induce new bone formation by differentiation of mesenchymal stem cells(MSCs) into chondrocytes and osteoblasts, and it is used in clinical treatment for skeletal repair. However, there were many experimental data and clinical papers reporting that successful bone regeneration using rhBMP-2 required supra-physiological, high dosages which can induce several side effects including early bone resorption. Our goal in current study is (1) to identify factors which linkes to early bone resorption caused by supra-physiological dose of rhBMP-2, (2) to find specific factors leading suppression of early

bone resorption, and (3) to establish a carrier system for the application of high dose rhBMP-2. First, in vivo and in vitro experiments were performed to investigate dose dependent effect of rhBMP-2 on early bone resorption and to evaluate the expression pattern change of early bone resorption and formation-related factors by supra-physiological dose of rhBMP-2. Nuclear factor of activated T-cells (NFAT)-c1 plays osteoclastogenesis inducer via c-fos pathway and is induced by BMP2. We investigated the effect of NFAT-c1 inhibitor on early bone resoprtion and long-term bone regeneration by high dose rhBMP-2. Sclerostin(SOST), as osteoclastogenesis inducer, is regulated by Receptor activator of nuclear factor kappa-B ligand(RANKL)/Osteoprotegerin(OPG) rate, which is up-regulated by rhBMP-2, was the second target in our study. Our study was performed to identify crosslink of estrogen and BMP2 signaling pathway in regulation of SOST expression for providing the mechanism of bone formation and resorption by high dose BMP2. The release kinetics of a carrier system can have a crucial influence on clinical effect of BMP-2. To overcome the shortcomings of absorbable collagen sponge (ACS), which shows initial burst release pattern of BMP-2 on bone regernation, we established a system for the sustained release of rhBMP-2 using heparin conjugated collagen sponge (HCS). In this carrier system, it was expected to modulate the functions of several heparin-binding molecules and we investigated the effect of high dose rhBMP-2 (40ug) on early bone resorption, long-term bone regeneration, bone erosion, and heterotopic ossification in HCS. The final goals of this study was to identify the target molecules which played key factors for osteoclast activation and to enhance the effect of rhBMP-2 treatment in short and long-term bone regeneration in bone therapy.

Materials and methods

To examine the local and peripheral effects of high dose BMP-2 release in vivo, 8mm critical-sized rat calvarial defect model was used, and the total region was divided into the defect area and the surrounding calvariae. New bone formation area was also divided into central original defect area and outside area of cental defect. To investigate the effect of NFAT-c1 inhibitor, the experimental groups were implanted with ACS including buffer only, rhBMP-2 (5 μg/defect), rhBMP-2 (20 μg/defect), or rhBMP-2 (20 μg/defect) + NFAT-c1 inhibitor (150 μM). To investigate the effect of HCS on early and long-term bone formation by high does rhBMP-2 (40μg/defect), HCS was used in a rat calvarial defect model. To confirm the appropriate dose of heparin in HCS for the experiments, HCS was prepared at different concentrations of heparin (0.2, 0.5 and 1.0 %) and characterized by scanning electron microscope (SEM), MTT assay, and Alizarin red s. As a result, 0.5% HCS and ACS was chosen as the control and 40 μg of rhBMP-2 was loaded in each scaffold for further animal experiments. For *in vitro* experiments, primary human MSCs (hMSCs), primary rat MSCs (rMSCs), and primary human osteoblasts were also cultured and used. 1 ng/μL of TOPFlash luciferase or Smad reporter plasmids, 30 pM human estrogen receptor (ER) alpha or SMAD family member 4 (Smad4) si-RNA, rhBMP-2 (50, 200 ng), estradiol (E2) (100 nM), and NFAT-c1 inhibitor (200 nM) each or together were treated in cells and the treated cells were then additionally cultured after 7 days. To evaluate mRNA relative expression of target genes, including insulin-like growth factor-1(IGF1), BMP2, and SOST, in each experiment as well as bone resorption- or formation-related marker genes, including RANKL, OPG, tartrate-resistant acid phosphatase

(TRAP), cathepsin K, c-Fos, NFAT-c1, core binding factor α1 (Cbfa1), osterix, alkaline phosphatase (ALP), and vascular endothelial growth factor (VEGF), reverse transcription polymerase chain reaction (RT-PCR) and quantitative reverse transcription polymerase chain reaction(qRT-PCR) were performed. Based on mRNA expression levels, RANKL/OPG rate was also calculated. ELISA assay, Western blotting, ALP staining, TRAP staining, and immunofluorescence (IF) or immunohistochemistry (IHC) staining were performed to evaluate the expressions or activations of proteins including Sost, Beta-catenin, ER alpha, Smad4, Alp, Trap, Rankl, Opg, and Cbfa1. To evaluate the effect of rhBMP-2, NFAT-c1 inhibitor, or HCS on long-term bone regeneration, micro-CT analysis was also performed and bone volume (BV), tissue volume (TV), BV ratio (BV/TV), trabecular number (Tb.N), trabecular thickness (Tb.Th), trabecular separation (Tb.Sp), and bone mineral density (BMD) were calculated. Masson trichrome staining (MT staining) was also performed. To determine the statistical significance of all experimental data, statistical analyses were performed using IBM SPSS 20.0 or 22.0 software. Groups were compared using a two-tailed Student's t-test, a one-way ANOVA or two-way ANOVA, and Bonferroni's test. Differences with $p < 0.05$ were considered significant.

Results

In 8mm critical-sized calvarial defects, 20ug or 40ug rhBMP-2 increased not only the expression of bone formation-related genes but also several bone resorption-related markers including osteoclast activation, RANKL/OPG rate, and the expression of bone resorption-related genes than 5ug rhBMP-2 did. NFAT-c1 inhibitor treatment with rhBMP-2 significantly reduced rhBMP-2 effect on

those bone resorption-related markers. However, co-treatment of NFAT-c1 inhibitor also reduced the expression of bone formation-related genes. Micro-CT analysis of long term bone regeneration also reveal that co-treatment of NFAT-c1 inhibitor could lead to increased BV and BV/TV indicating effective new bone formation compared to rhBMP-2 only treatment, while BMD and other markers were similar in two groups. In hMSCs, rhBMP-2 (200ng/mL) increased SOST expression at 7 days. However, co-treatment of 100nM E2 supressed SOST induction by rhBMP-2 and increased the activation of beta catenin as key factor in Wnt signaling pathway. On the other hand, ER alpha siRNA and ICI 182,780 which was Wnt and ER alpha inhibitor could Smad-independently reduce the repressive effect of E2 on SOST induction by BMP2 and beta-catenin activation. In osteoblasts, the effect of E2 on SOST induction by rhBMP-2 differed among the human osteoblast lines. RANKL/OPG rate in two human osteoblast cell lines, which showed estrogen-mediated suppression of SOST induction by BMP2, also showed a similar pattern to SOST expression. All concentrations of heparin could lead to sustained release of rhBMP-2 for 4 weeks in HCS. 0.5% HCS showed different reponses to rhBMP-2 treatment between the defect area and the surrounding marginal bone. At the defect area in HCS, OPG expression was very low and RANKL expression, RANKL/OPG rate was increased 14.5 fold and 145 fold by rhBMP-2, and the expression of bone resorption-related genes was also increased. Especially, the increase in RANKL/OPG rate by rhBMP-2 was higher 51.9 fold and osteoclast activation was also more increased in HCS than in ACS. The expression of bone formation-related genes also showed similar pattern to those of bone resorption-related genes. In micro-CT

analysis, BV and Tb.N indicating more effective long term bone regeneration at central defect was higher to a certain degree by rhBMP-2 in HCS than in ACS at 8 and 12 weeks, Histological staining was consistent with results of micro-CT analysis. On the other hand, the portion of the bone erosion region of ACS in rhBMP-2 treatment was 1.8 fold higher than that of HCS in rhBMP-2 treatment. Heterotopic ossification by rhBMP-2 was detected in ACS at 4 weeks. However, this side effect was less as time goes by and completely disappeared after 12 weeks.

Conclusions

Supra-physiological dose of rhBMP-2 caused early bone resorption with bone formation by regulation of bone formation and resorption-related genes via BMP2 signaling in vivo. NFAT-c1 inhibitor reduced the effect of rhBMP-2 on early bone resorption-related factor and also led to better long term bone regeneration. However, the effect of NFAT-c1 was not showed in rMSCs, suggesting these roles of NFAT-c1 in rhBMP-2 signaling was limited via RANKL/OPG mechanism in osteoclasts. These results indicated that the limited repression of rhBMP-2 signaling in osteoclast during early phase can be an effective strategy for the reduction of early bone resorption and the induction of long-term bone regeneration. However, NFAT-c1 inhibitor also repressed early bone formation-related marker leading less effective bone regeneration. Therefore, additional studies were needed to conform suitable conditions of NFAT-c1 inhibitor. The increase in RANKL/OPG rate by rhBMP-2 also implied potential regulation of SOST as bone resorption-related marker by BMP2. In hMSCs, estrogen could smad4-independently repress the induction of SOST

by BMP2 signaling cascade via Wnt signaling pathway including ER alpha and activated beta-catenin, indicating crosstalk between estrogen and BMP2 which might have a clue about the regulation of bone homeostasis by estrogen in osteoblast. Although further studies were needed to investigate estrogen's effect on bone regeneration process including early bone formation and resorption, SOST regulation by estrogen might be a target in bone regeneration by rhBMP-2. Our studies showed that HCS reduced rhBMP-2-induced early bone erosion and heterotopic ossification and also enhanced long-term bone regeneration by low initial burst and sustained release of rhBMP-2 as well as heparin itself effect. Although not significant, site specific regulation of OPG by rhBMP-2 could be also observed. However, accumulation of rhBMP-2 by sustained release at defect area in HCS might be able to intensified early bone resorption, suggesting that sustained release of rhBMP-2 was considered with side effects in defect area. Our in vivo study using HCS also showed low initial burst and sustained release of rhBMP-2 could reduce rhBMP-2-induced early bone erosion and early heterotopic ossification and enhance long-term bone regeneration.

Keywords : rhBMP-2, new bone formation, early bone resorption, heparin, NFAT-c1 inhibitor, estrogen, SOST

Student number : 2009-31130

CONTENTS

Strategies to Suppress Early Bone Resorption Induced by High Dose Bone Morphogenetic Protein-2

Ri Youn Kim

Program in Craniomaxillofacial Cell and Developmental Biology,

Department of Dental Science,

Graduate School, Seoul National University

(*Directed by Professor* **Soon Jung Hwang**, Dr. med. Dr. med. dent)

Introduction

Bone regeneration in bone defects has been a focus of tissue engineering and has involved methods to understand bone healing mechanism and progress toward clinical application [1-3]. In tissue engineering, recombinant human bone morphogenetic protein (rhBMP)-2 has been regarded as a molecule involved in promoting clinical osteoinduction in bone repair, and has also been approved for clinical applications such as bone defect healing [4, 5]. Many studies reported that a high dose of rhBMP-2 was needed to promote successful bone regeneration for clinical therapy [6, 7]. However, an overdose of rhBMP-2 can also trigger negative side effects including ectopic bone formation, inflammation, and bone resorption [8-11]. These unexpected effects are potential obstructions to endorsing clinical bone regeneration by rhBMP-2. Several studies implied that

the osteoclastic resorption during bone healing period should be considered as a critical part of bone regeneration [12, 13]. Recent studies revealed a complex role of BMP signaling in bone metabolism related to the coupling of bone resorption with bone formation [14]. BMPs exhibit biphasic functions encompassing bone formation as well as bone resorption, which is regarded as a regulatory mechanism to control bone mass through a balance between bone formation and resorption[14, 15]. This dual function of BMP signaling is reflected in bone regeneration using rhBMP-2. Treatment with high-dose rhBMP-2, via collagen sponges, dose-dependently and transiently caused osteoclastic resorption of peri-implant bone in surrounding bone [16, 17].

The Smad-dependent and Smad-independent p38 MAPK pathways play a central role in BMP signaling by accelerating osteoblastogenesis [18, 19]. However, Smad pathways activated by BMPs also activate the bone resorption process, representing a classic feedback inhibition loop [20]. This feedback inhibition involves the expression of BMP antagonists such as Noggin and Sclerostin (SOST), both of which are also secreted from osteoblasts. While Noggin prevents BMPs from binding their receptors [21], the regulatory route of SOST expression involves an interplay between BMP and Wnt signaling. SOST is up-regulated by BMP through the Smad pathway, and it then inhibits Wnt signaling by binding to the co-receptors, low-density lipoprotein receptor-related proteins 5 and 6 (LRP5 and LRP6) [22]. SOST eventually enhances resorption by triggering receptor activator of nuclear factor-kappa B ligand (RANKL)-osteoprotegerin (OPG) pathway-induced osteoclastogenesis, leading to a decrease in bone mass [23, 24]. The RANKL/RANK/OPG system has been considered a central signaling pathway governing

osteoclastogenesis [25]. RANKL mediates osteoclast differentiation via TNF receptor-associated factor 6-activated c-Jun Nterminal kinase upregulation and subsequent activation of c-Jun and c-Fos signaling coupled with nuclear factor of activated T cells(NFAT) [26, 27].

Many studies tried to explain the mechanisms of bone resorption in molecular aspect [14]. A relationship between the receptor activator for the nuclear factor (NF)-κB ligand (RANKL) pathway with rhBMP-2-induced-osteoclastogenesis has frequently been reported in studies [28, 29]. RANKL is a key molecule for osteoclast differentiation and activation to induce bone resorption in bone [30-32]. Itoh et al reported BMP-2 increased RANKL activation via BMP receptor type 1A (BMPR1A) and then induced osteoclast formation and activation [33]. Therefore, RANKL inhibition can be a promising method to block early osteoclast activation and enhance bone formation in clinical treatment using an over-dose rhBMP-2. RANKL is a critical factor in osteoclastogenesis. RANKL can regulate osteoclast formation, activation and survival in bone modeling by binding to the receptor activator of nuclear factor-κB (RANK) and this mechanism was the target for effective bone formation [34, 35].

Osteoprotegerin (OPG) is an important regulator as an antagonist to the RANKL / RANK signaling pathway [31, 36]. OPG can bind to RANKL and repress the interaction with RANK and RANKL that causes bone resorption [37]. For this reason, the RANKL/OPG ratio can represent osteoclast activation *in vivo* and *in vitro* [34]. This current study revealed that a combined treatment of OPG with rhBMP-2 enhanced the effect of rhBMP-2 on bone formation and simultaneously repressed bone resorption [28]. For this reason, several types of RANKL inhibitor provides an encouraging stategy targeting anti-resorption in the treatment of bone-disorders. Among these,

Denosumab also was a promising RANKL inhibitor to reduce bone resorption by directly binding to RANKL [38-40]. Sclerostin is a glycoprotein inhibitor of osteoblast Wnt signaling produced by osteocytes that may become a therapeutic intervention in patients with osteoporosis [41]. Sclerostin was first recognized as a molecular target for the treatment of osteoporosis when disorders with inactivating mutations of the sclerostin gene SOST were found to be associated with increased bone mass [42, 43]. These observations suggested that inhibitors of sclerostin might be used to increase BMD. Pre-clinical and clinical data report that anti-SOST antibody can dose-dependently increase bone formation with efficacy and safety [44-48]. However, the inhibitors directly targeting RANKL / RANK signaling may cause potential side effects. OPG can block activation of TNF-related apoptosis-inducing ligand as tumor inhibitor [49]. Denosumab has also been associated with a frozen bone, immunosuppression, and osteonecrosis of the jaw by repressing RANKL / RANK pathway [50]. Therefore, the inhibition of the RANKL-linked-pathway involving ERK, p38, and NF-kB pathway or through ROS production lead to decreased bone resorption [51, 52]. After all these efforts, the short or long-term effects of these inhibitions on bone defects *in vivo* were uncertain.

NFAT-c1 was considered a crucial factor in downstream of RANKL including p38 pathway for differentiation of osteoclasts [53-57]. In the RANKL pathway, NFAT-c1 can regulate several key players including OSCAR, LTBP3, ClC7, cathepsin K, MMP9, and c-Src to induce osteoclast activation [57, 58]. Several studies reported that BMP-2 could also lead to RANKL dependent-induction of NFAT-c1 [29, 59]. Based on all of these studies, we can assume that NFAT-c1 might play a role as a factor that can increase

RANKL-induced bone resorption via a high dose of rhBMP-2 in short and long-term bone regeneration. In this regard, we also can consider a combined treatment of NFAT-c1 inhibitor with rhBMP-2 to arrest the effect of rhBMP-2 on bone resorption. Combined treatment of rhBMP-2 with other molecules has been tried to enhance bone regeneration rhBMP-2 [60]. For example, Kempen et al. reported that local sequential delivery of BMP-2 and VEGF enhanced early bone formation [61]. NFAT-c1 also has been safely used for generating an immune response through the whole-body in clinical situations [62]. Therefore, we tried to investigate the effect of local treatment with rhBMP-2 and NFAT-c1 inhibitor on early bone resorption and bone formation *in vivo.*

Estrogen also can be considered as an inhibitor to the RANKL-induced osteoclastogenesis via c-Jun pathway [63]. Many studies reported that estrogen plays a role in skeletal formation and bone homeostasis in both men and women, especially the elderly [64-66]. Estrogen prevents the increase of bone resorption markers as well as maintaining bone formation [67]. Estrogen also regulates osteoclast formation and activation, and treatment with high-dose estrogen represses bone resorption [68]. In postmenopausal osteoporosis, estrogen inhibited bone resorption by various actions including direct induction of apoptosis of osteoclasts via estrogen receptor - mediated mechanism and induction of Fas Ligand (FasL) in osteoclasts [69]. Especially, estrogen receptor alpha (ER α) mediated most actions of estrogen on bone cells including prevention of bone resorption [70]. Moreover, induction of transforming growth factor (TGF) - beta in osteocytes and Interleukin (IL)-7 in mice was regulated by estrogen and this regulation led to apoptosis of osteoclasts and repression of osteoclastogenesis [70-72]. In the

RANKL pathway, 17β-Estradiol also dose-dependently increased OPG expression in human osteoblasts [73]. Although all of these reports implied a role for estrogen in osteoclastogenesis, however, estrogen was rarely reported as an inhibitor of osteoclastogenesis in clinical data. In addition, the mechanism of estrogen in the RANKL pathway was unclear for application as an inhibitor of osteoclastogenesis. Some papers reported that estrogen might regulate SOST expression associated with osteoclast activation [74, 75]. Clinical reports also showed that reduction of estrogen was associated with to higher serum levels of SOST in postmenopausal women [74, 76]. Furthermore, chronic treatment with estrogen in postmenopausal women led to a reduction in SOST levels [77, 78]. . According to other studies, SOST expression was also regulated by BMP-2 in human osteogenic cells [23, 79]. Reversely, SOST also inhibits bone formation by antagonizing BMP-induced alkaline phosphatase (ALP) activity as well as stimulating apoptosis of osteoblasts via caspase-3 [80]. Kamiya et al. showed that BMPR1A signaling in osteoblasts negatively regulated endogenous bone mass indirectly by a reduction in canonical Wnt signaling via SOST as Wnt inhibitor and a bone mass mediator, indicating that SOST might be related to BMP-2 induced bone resorption in bone regeneration [81]. Although the role of Wnt pathway was reported in SOST regulation by BMP-2, it did partially explain the mechanism of SOST regulation and why effective and safe modulators of SOST did not exist *in vivo* or in clinical applications. However, subsequent reports implied that estrogen and BMPs might converge on the mechanism of SOST regulation via overlapped paths including Wnt / Beta-catenin pathway [81-84].Taken together, we hypothesized that estrogen might regulate SOST expression indirectly via the BMP-2 pathway and we expected

this mechanism to be helpful in modulation of bone resorption caused by an over-dose of rhBMP-2 in clinical application.

Although rhBMP-2 involved bone resorption-related mechanism, rhBMP-2-induced bone resorption mostly occurred in high-dose rhBMP-2, implying that the molecular event in rhBMP-2-induced osteoclastogenesis *in vivo* or *in vitro* might be able to be regulated by a controlled release rate of rhBMP-2 into a target site to stimulate successful bone regeneration. In clinical rhBMP-2 treatment, the regulation of the release rate of rhBMP-2 into a target region was steadily studied for higher efficiency of rhBMP-2 on bone regeneration [85-88]. Uludag et al. reported that delivery scaffolds, showing difference in pharmacokinetics, had different release and retaining rates of BMP-2 [89], and Winn et al. reported the release kinetics of a scaffold system could have a crucial influence on clinical effects of BMP-2 [90]. The osteoinductive effect of rhBMP-2 can also be influenced by its mode of delivery to a target site [91, 92]. The osteogenic response can also be more efficaciously promoted by its gradual liberation from a specific scaffold [87]. A hyaluronic acid based scaffold can release low levels of rhBMP-2 into the local environment in a sustained manner [93]. The sustained delivery of BMP-2 via the poly lactic-co-glycolic acid (PLGA) microsphere system also resulted in greater bone healing [94]. For more effective bone regeneration, these scaffold systems can be conjugated with specific factors that can regulate the release rate of target molecules [95-97]. PLGA / polyethylene glycol (PEG) scaffolds induced an increase in new bone volume by loading with 1μg BMP-2 [98]. Heparin conjugated PLGA scaffold also enhanced the osteogenic efficacy of BMP-2 by sustained release of 1 μg BMP-2 [99]. Among various modulators applied to a scaffold, heparin, which can modulate

the functions of heparin-binding molecules including BMP-2, was a promising candidate for regulation of BMP-2 release [100]. Heparin-conjugated fibrin can also lead to sustained delivery of BMP-2 [101]. However, most heparin-conjugated scaffolds have investigated methods for targeting bone formation, including ALP activation, and using a low dose of BMP-2 such as 1 μg, which was insufficient to promote clinical bone regeneration [98, 99, 102]. On the other hand, Bhakta et al. reported that heparin conjugated hydrogels attenuated the release of BMP-2 reduced osteogenic effect of BMP-2, compared to hydrogels lacking heparin, indicating a need for an optimal burst release of rhBMP-2 for bone formation [103]. The coupling of bone resorption with bone formation also indicated that a loading dose of molecules should be considered to optimize the balance between bone-formation and bone-resorption activities [87]. In this point, over-dose treatment of rhBMP-2 might cause initial burst release via scaffold in bone defects that promotes early bone resorption as well as bone formation. Therefore, the sustained release of rhBMP-2 might lead to less bone resorption. However, bone resorption caused by an initial burst of rhBMP-2 had not yet been examined in pre-clinical or clinical studies. Especially, the combination of proper dose of rhBMP-2 with scaffolds for successful bone regeneration and repression of bone resorption by high-dose rhBMP-2 has not been defined in clinical trials. For these purposes, an absorbable collagen sponge (ACS) was deemed suitable for studies to investigate the dosage and scaffold dependent effect of rhBMP-2 on bone resorption as well as formation [104, 105]. The efficacy and safety of ACS as a scaffold for rhBMP-2 in pre-clinical and clinical applications have been clearly proven in both animal and human examples [104]. Since ACS showed rapid release of rhBMP-2, it also

was an ideal scaffold for studies to investigate the effect of the release rates on bone resorption by being conjugated with heparin [106]. Therefore, we tried to investigate the effect of a heparin conjugated collagen sponge (HCS) on release rates of high-dose rhBMP-2 release and bone regeneration including both bone formation and bone resorption, for short and long-term clinical application.

As our approach encompasses various views they might provide an integrating viewpoint about the mechanism of bone regeneration, including bone formation and resorption, as well as a clinical application for induced bone healing. For this purpose, we tried to confirm early bone resorption caused by high-dose rhBMP2 via ACS *in vivo* using a rat calvarial defect model. Next, we tried to investigate the local effect of NFAT-c1 inhibitor on bone regeneration as a target molecule to overcome early bone resorption caused by an initial burst release of rhBMP-2 *in vivo* for practical applications. We also tried to find molecular mechanism of SOST regulation by estrogen in association with BMP-2 signaling including Wnt pathway as target for preclinical and clinical applications. Lastly, we tried to develop HCS as a scaffold that can effectively regulate the release rate of rhBMP-2 safely *in vivo* and to investigate the effect of sustained release of rhBMP-2 via HCS in short and long-term bone regeneration. This study aimed to reduce early bone resorption without any repressive effect on rhBMP-2-induced bone formation and to find the implications in bone regeneration via an integrating viewpoint.

Part I

Enhanced osteogenic efficacy of high dose BMP-2 using heparin-conjugated collagen sponge by controlled release-mediated modulation

A. Materials and Methods

1. Fabrication of HCS

ACS was fabricated by freeze-drying a 1 % (w/v) collagen solution (Dalim Tissen Co., Ltd., Seoul, Korea) in 0.1 M acetic acid (Junsei Chemical, Tokyo, Japan). Lyophilized collagen sponges were cross-linked with 20 mM 1-ethyl-3-(3-dimethylaminopropyl) carbodiimide hydrochloride (EDC; Tokyo Chemical, Tokyo, Japan) in ethanol (Merck Millipore, Darmstadt, Germany) for 4 hours. The cross-linked collagen sponges were washed out 5 times in order to remove residual EDC and ethanol. The collagen sponges were then re-lyophilized. For heparin immobilization, freeze-dried collagen sponges were soaked in 50 mM 2-(N-Morpholino) ethanesulfonic acid hydrate (MES; Sigma, St. Louis, MO, USA) buffer supplemented with 0.2, 0.5, and 1.0 % (w/v) heparin (Wako Pure Chemical, Osaka, Japan), 20 mM EDC, and 7.8 mM N-Hydroxysuccinimide (NHS; Sigma) for 2 hours. The resulting collagen sponges were washed out and lyophilized.

2. rhBMP-2 release test

ACS and HCS loaded with 5 μg rhBMP-2 (Novosis®-Dent, BioAlpha Inc., Seongnam, Korea) were incubated for 1 hour at 37 ℃. The rhBMP-2-loaded collagen sponges were soaked in 2 ml PBS (Sigma) in sealed glass vials and then incubated at 37℃ while shaking at 15 rpm. The whole incubation media were collected at 0.5, 1, 2, 4, 8, 12, 24, and 48 hours. The amount of rhBMP-2 was

determined with a BMP-2 ELISA kit (RHF913CKX, Antigenix America Inc., Melville, NY, USA) according to the manufacturer's manual. The cumulative release of BMP-2 was then expressed as a percentage of the initial loading amount.

3. Scanning electron microscopy (SEM)

To investigate morphology and porosity, SEM was performed on cross sections and surfaces of scaffolds. The sponges were coated with an ultrathin layer (300 Å) of gold/Pt in an ion sputter (E1010, HITACHI, Tokyo, Japan). The ultrastructure of the sponges was observed by scanning electron microscope (S-800, HITACHI).

4. Cell proliferation

Bone marrow mesenchymal stem cells (BM-MSCs) which were isolated from femurs and tibias of Sprague Dawley (SD) rat (male, 8 - 12 weeks) were seeded on ACS and HCS at a density of 5×10^4cells per sponge. Rat BM-MSCs (rBM-MSCs)were cultured in Dulbecco's Modified Eagle's Media (DMEM;Gibco, Waltham, MA, USA) supplemented with 10 % fetal bovine serum (FBS; Gibco), 1 % antibiotics (Gibco) at 37 °C in 5 % CO_2. After 3, 7 and 14 days of culture, a MTT colorimetric assay was performed. The cells on the sponges were incubated at 37 °C in 1 ml DMEM containing 10% MTT solution. After an hour, the solution was discarded completely and 800μl of Dimethyl sulfoxide (DMSO;Junsei Chemical) was added to the sponges. Using a microplate reader, the absorbance of the DMSO from the sponges was measured at a wavelength of 570nm.

5. Quantitative real-time reverse transcription-polymerase chain reaction (RT-PCR)

Total RNA was isolated from rBM-MSCs cultured on ACS and HCS using the RNeasy Mini kit (Qiagen, Valencia, CA, USA) mRNA extraction. Equivalent amount of RNA were reverse transcribed for cDNA synthesis using an Omniscript RT kit (Qiagen). Then the qRT-PCR for *alkaline phosphatase (ALP), osteocalcin (OCN)* and *osteopontin (OPN)* was performed on a real-time polymerase chain reaction (PCR) machine (Bio-Rad, Hercules, CA, USA) using the QuantiTect SYBR Green PCR Kit (Qiagen). The PCR cycling was carried out under the following conditions: 15 seconds at 95 ℃, 30 seconds at 58 ℃, and 30 seconds at 72 ℃ for 40 cycles after an initial denaturation step for 5 minutes at 95 ℃. Oligonucleotide primers for real-time RT-PCR were designed for product sizes under 200 bp using real-time PCR system Sequence Detection Software v1.3 (Applied Biosystems, Foster City, CA, USA). The sequence of each primer is listed in Table 1.

6. Alizarin red s staining

To assess *in vitro* mineralization, collagen-coated microplates were prepared by treating with 300 μl of 1 % (w/v) collagen solution in 0.1 M acetic acid. After air-drying, a fresh solution of 20 mM EDC in ethanol was added into the microplates for cross-linking of collagen for 4 hours. This was then rinsed with PBS for 5 times. For heparin immobilization, 1 ml of 50 mM MES buffer supplemented with 1 % (w/v) heparin, 20 mM EDC, and 7.8 mM NHS was added to the collagen coated multi-well microplates for 2 hours, which was

followed by rinsing of the collagen coated surface with PBS 5 times. BM-MSCs were cultured on collagen or heparin-collagen coated plates with osteogenic differentiation media containing 10 mM b-glycerophosphate (Sigma), 50 μg/ml ascorbic acid (Sigma), and 10 nM dexamethasone (Sigma) for 14 days and then were stained by Alizarin red (Sigma). Cells were fixed with 10 % formaldehyde for 15 minutes at room temperature and then washed three times with distilled water. Alizarin red solution (2 % w/v, pH 4.2) was added in each collagen- coated plate and cells were incubated for 20 minutes. Then, excess dye was removed by washing four times with distilled water.

7. Preparation of rhBMP-2 - loaded scaffold

Escherichia coli-derived rhBMP-2 powder (Novosis®-Dent, BioAlpha Inc.) was dissolved at a concentration of 1 mg/mL with stabilizing buffer obtained from the manufacturer. The collagen sponges were 8 mm in diameter and 1 mm thickness for the calvarial defect model. rhBMP-2 was rapidly loaded onto each scaffold before *in vivo* implantation at a total volume of 30 μL, which was controlled at an amount not exceeding 0.1 % of the total scaffold volume. For control experiments, the scaffold was loaded with buffers, which are dissolving solutions for rhBMP-2.

8. Surgery

Eight-week-old Sprague - Dawley rats (total n=80) were used. The experimental protocol was approved by the Animal Care and Use

Committee of Seoul National University. After disinfection of the calvarial skin with 10 % betadine (Potadines; Sam-Il Pharm, Seoul, Korea) and subcutaneous injection of 2 % lidocaine containing 1:100,000 epinephrine (Lidocaine HCL Injs.; Yuhan, Seoul, Korea), an incision was made along the sagittal suture. The periosteum was elevated and an 8-mm-diameter calvarial bone defect was created with a trephine burr without dural perforation. An rhBMP-2-loaded collagen sponge was then implanted into the defect area. The experimental groups were divided into ACS and HCS groups, and then these two groups were treated with buffer (ACS or HCS, n=20/each group) or rhBMP-2 (40 μg/defect) (ACS-BMP or HCS-BMP, n=20/each group). Rats in each group were evaluated for RT-PCR and tartrate-resistant acid phosphatase (TRAP) staining one week after implantation (each n=5), and were analyzed after four- (each n=5) or eight- (each n=5) or twelve-week (each n=5) healing periods using micro-CT and histological observation to evaluate new bone formation. A calvarium containing 11-mm radius around the defect from each group was removed 7 days after surgery and separated into collagen sponges and the surrounding calvariae adjacent to the defect. Then, each area was cut in half for reverse-transcription polymerase chain reaction (RT-PCR) analysis and TRAP staining.

9. Quantitative real-time RT-PCR

The collagen sponges removed from calvarial defect or surrounding calvariae of sponges were separately washed with PBS and chopped

into small pieces. After adding 0.5 mL of Trizol reagent (Invitrogen, Life Technologies, Carlsbad, CA, USA) directly to the chopped sponge or bone, total RNA was extracted and then subsequently treated as described in the manufacturer's instructions. Oligonucleotide primers for real-time RT-PCR were designed for product sizes under 200 bp using real-time PCR system Sequence Detection Software v1.3 (Applied Biosystems), and their sequences are provided in Table 1. Fold differences of each gene were calculated for each treatment group using normalized CT values of the housekeeping gene *beta-actin,* according to the instructions of Applied Biosystems.

10. TRAP staining

Collagen sponges were implanted onto 8 mm critical sized defects of rat calvariae. After 7 days, whole calvariae including the collagen sponge were removed. Half of each sponge was fixed and decalcified before paraffin embedding. Tissue sections were deparaffinized, dehydrated, and then cut vertically into 5-mm-thick pieces. Tissue sections were stained for TRAP activity to examine osteoclastogenesis as follows. TRAP staining buffer was prepared by dissolving Naphthol AS-MS phosphate disodium salt (5 mg/mL) in 10% formalin, followed by addition Fast Red Violet LB salt (1 mg/mL; Sigma). Slides were incubated with TRAP staining buffer for 30 min at 37 ℃, washed for 15 min in tap water, and mounted with Crystal/Mount solution. After capture of representative 40x fields under a phase microscope for whole sections of each group, the numbers of TRAP-positive multinucleate cells (MNC), which have more than three nuclei per cell, were counted using Image J software (NIH, NY, USA).

11. Immunohistochemical (IHC) staining

Rankl and Opg expression *in vivo* were observed 7 days after implantation. The collagen sponges were removed and decalcified through incubation in ethylenediaminetetraacetic acid solution (7 %, pH = 7.0) for 3-4 days (with a solution change on day 2). The specimens were then dehydrated in 70 % ethanol and embedded in paraffin. Ten paraffin sections were cleaned for 10 min with xylene, and the deparaffinized sections were treated with an undiluted serum solution for 30 min. Specimens were then incubated with anti-RANKL (1:200; Novus Biologicals, Littleton, CO, USA) or anti-OPG (1:1000; Abcam, Cambridge, England) at 4 ℃ overnight. After incubation, the sections were incubated with R.T.U biotinylated universal antibody using Vectastatin kit (Vector Laboratories, Burlingame, CA, USA) according to the manufacturer's instructions. Staining was detected with diaminobenzidine (Sigma) substrate, and slides were mounted with Crystal/Mount (Biomeda; Foster City, CA, USA). Images of stained cells were captured by bright field microscopy.

12. Micro-CT analysis

After sacrifice of animals 4 or 8 weeks post-surgery, each calvarium containing a collagen sponge was removed from the skull. New bone formation was analyzed for two regions; one region included just the real defect, while the other included both the real defect and the defect exterior. All calvaria were fixed in 10 % formalin for 1 week. Micro-CT scans were then taken to quantitatively evaluate new bone formation using the Sky-Scan 1172®

Microfocus X-ray System (SkyScan) with CT software, including CTAn 1.8®, CTvol, and NRecon Reconstruction® (SkyScan). The SkyScan 1172 microfocus X-ray system is equipped with a microfocus X-ray tube with a focal spot of 2 mm, producing a cone beam that is detected by a 12-bit cooled X-ray camera CCD that is fiber-optically coupled to a 0.5 mm scintillator. The resulting images were 1000 × 1000-pixel square images with an aluminum filter used to produce optimized images. Reconstructions and analyses were performed using NRecon reconstruction and CTAn 1.8 software, respectively. A second-order polynomial correction algorithm was used to reduce the beam-hardening effect for all samples. To measure newly formed bone, a circular area of pre-defined size was selected as the region of interest (ROI) in two-dimensional images. The pixel zone representing ossification in the defined ROI was then reconstructed in 3D by creating a volume of interest (VOI) in the lower and upper ranges of the threshold using grayscale units. After using CTAn 1.8 on each reconstructed BMP file, bone volume (BV), tissue volume (TV), trabecular number (Tb.N), trabecular thickness (Tb.Th), trabecular separation (Tb.Sp)), and the relative ratio of BV/real defect were obtained using a CT-analyzer in 3D based on a surface-rendered volume model according to the manufacturer's instructions. To measure bone mineral density (BMD), attenuation data for ROI or VOI were converted to Hounsfield units and expressed as a value of BMD using a phantom (SkyScan). This phantom contained rods of calcium HA (CaHA) with a standard density corresponding to mouse or rat bone, which ranges from 0.25 to 0.75 g/cm^3. BMD values were expressed in grams per cubic centimeter of CaHA in distilled water. A zero value for BMD corresponded to the density of distilled water alone (no additional

CaHA), and a value greater than zero corresponded to nonaerated biologic tissue.

13. Histochemical staining

After micro-CT reconstruction, the operative field of each calvaria was removed and decalcified through incubation in ethylenediaminetetraacetic acid solution (7 %, pH = 7.0) for 3-4 days (with a solution change on day 2). The specimens were then dehydrated in 70 % ethanol and embedded in paraffin. Decalcified paraffin sections were cleaned for 10 min with xylene and stained with hematoxylin and eosin (H&E) for the detection of cells and bone structures, respectively. Digital images of the stained sections were collected using a transmission and polarized light Axioskop microscope, Olympus BX51 (Olympus Corporation, Tokyo, Japan).

14. Statistical analysis

All data are presented as means±standard errors of the mean (SEM) for *in vitro* tests, or as standard deviations (SD) for *in vivo* animal experiments. Statistical analyses were performed using IBM SPSS statistics 22.0 software (IBM, Armonk, NY, USA). Groups were compared using a one-way ANOVA or two-way ANOVA, using Bonferroni's test. Differences with $p < 0.05$ were considered significant.

B. Results

1. In vitro rhBMP-2 release and bioactivity in HCS

HCS was prepared at multiple heparin concentrations (0.2, 0.5 and 1.0 %) to choose the appropriate dose of ACS, which contained no heparin for the control. *In vitro* release kinetics of rhBMP-2 from HCS and ACS and the biological properties of HCS were compared over 28 days (Figure 1). The cumulative release of rhBMP-2 from 0.2, 0.5, and 1.0 % HCS was 27.0, 30.4 and 32.9 % (all, $p<0.05$) in 1 day, compared to 57.1 % from ACS (Figure 1A). All types of HCS showed a low burst release pattern of rhBMP-2, which corresponded to 54.3-67.3 % of the loaded rhBMP-2 over a period of 28 days. ACS had an initial burst, releasing over 90 % of the rhBMP-2 within 4 days. All HCS concentrations exhibited sustained release of rhBMP-2 for 28 days, indicating that HCS could stably control rhBMP-2 release for a longer time than ACS. The amount of rhBMP-2 released from HCS differed slightly based on heparin concentration; the 1.0 % HCS showed the lowest level of cumulative release during the first four days. Although there was no significant difference in the amount of rhBMP-2 between the 0.2 and 0.5 % HCS, the 0.5 % HCS was chosen for further animal experiments.

Next, HCS was characterized *in vitro* by SEM, MTT assay, real-time PCR, and Alizarin red S staining. SEM photographs revealed that average pore diameters on the surface differed significantly between ACS and HCS. The HCS pores were 0.75- and 0.77-fold smaller than ACS pores on the surface of the sponges

(Figure 1B). Proliferation of BM-MSCs was 1.3 fold higher ($p<0.05$) on HCS as compared to ACS at 3 days, but there was no significant difference at 7 and 14 days (Figure 1C). However, there was significant difference in the expression of osteogenic marker genes (*ALP, OCN* and *OPN*) in BM-MSCs cultured on ACS and HCS (Figure 1 D). Alizarin red s staining of BM-MSCs also showed that osteoblast differentiation and *in vitro* mineralization progressed more intensively on heparin/collagen-coated plates than collagen-coated plates (Figure 1 E).

2. Early osteogenic regulation of HCS-BMP in vivo

We examined the early osteogenic process after the implantation of rhBMP-2 near the collagen sponge-implanted defect and the surrounding calvariae to examine the local and peripheral effects of BMP-2 release *in vivo*. The gene expression of bone-forming and bone-resorbing markers was examined by real-time PCR one week after rhBMP-2 implantation. We investigated early bone resorption by assessing *RANKL* and *OPG* expression, calculating the relative ratio of *RANKL* to *OPG* (R/O), and counting the number of TRAP-positive MNCs (Figure 2B and 3B). rhBMP-2 increased *RANKL* expression in HCS and ACS at the defect area, though it increased 14.9 fold in HCS ($p<0.01$) and 2.4 fold ($p<0.01$) in ACS over each vehicle control (Figure 2A and B). However, *RANKL* expression in the surrounding calvariae showed a consistent 6.5-fold increase ($p<0.05$) in ACS-BMP, while it was slightly increased without significance in HCS-BMP. *OPG* expression exhibited a different response to rhBMP-2 between the defect area and the

surrounding calvariae. The expression of *OPG* was reduced by rhBMP-2 in the defect area in ACS- and HCS-BMP. In particular, *OPG* expression in HCS alone was significantly reduced ($p<0.01$) over ACS alone in the defect area. BMP-2 increased *OPG* expression 3.8 fold ($p<0.05$) in ACS in the surrounding calvariae, compared to the vehicle control. However, HCS-BMP did not change *OPG* expression over the HCS control, and even less level than ACS alone, although the difference of OPG level between ACS alone and HCS-BMP was not significant difference. AS *OPG* expression in HCS showed lower levels, the resulting R/O ratios of HCS-BMP to ACS-BMP differed significantly, with a 145.0-fold ($p<0.01$) versus a 4.7-fold ($p<0.05$)in the defect area; therefore, the HCS-BMP group showed a 51.9 fold ($p<0.01$) higher level of R/O than the ACS-BMP group. In the surrounding calvariae, ACS-BMP and HCS-BMP had a similar R/O ratio. ACS-BMP showed a 4.3-fold ($p<0.05$) increase in R/O ratio over the ACS control, but the increased value of the R/O ratio of HCS-BMP was not significant. IHC staining for Rankl and Opg was consistent with real-time PCR data for *RANKL* and *OPG* expression in the defect area (Figure 2C).

TRAP-positive MNCs, which have more than three nuclei per cell, were counted as an index of osteoclast activation (Figure 3). Consistent with our previous study, ACS-BMP increased the number of TRAP-positive MNCs to about 25.6, while the ACS control showed almost zero counts (Figure 3A and B). However, the number of TRAP-positive MNCs in the HCS vehicle control was about 7.0, while HCS-BMP had 49.4 MNCs, which was 1.9-fold higher ($p<0.05$) than ACS-BMP. We observed bone erosion at the margin of the defect scaffold in the ACS-BMP and HCS-BMP groups, which is probably caused by initial BMP-2 release (Figure 3C). The existing

bone at the scaffold margin showed an irregular bone surface and activated osteoclasts in both BMP groups, while the ACS and HCS groups without rhBMP-2 showed a relatively sharp defect margin around the scaffold. The total marginal area of necrotic bone in the ACS-BMP group was greater than that of the other groups including the ACS-control or HCS-BMP, indicating that ACS might cause aggressive release of rhBMP-2.

Next, we examined the expression of osteoblast activation-related markers (*ALP, osterix, VEGF,* and *Cbfa1*) and osteoclast activation-related markers (*TRAP, cathepsin K, c-fos,* and *NFAT-c1*) in the defect area and the surrounding calvariae (Figure 4). The expression of these genes was similar to *RANKL* or *OPG* expression (Figure 2). ACS-BMP significantly increased the expression of bone-forming and bone - resorbing genes both in the defect area and the surrounding calvarie, except for *ALP* and *c-fos*. The HCS-BMP group showed different trends between bone forming genes and resorbing genes, especially in the surrounding calvariae. The expression of bone-forming genes (*osterix, VEGF,* and *Cbfa1*) in the HCS-BMP group was not changed except for the *ALP* gene ($p<0.01$), compared to the HCS control, which was induced in the surrounding calvariae. Resorbing markers (*TRAP, c-fos,* and *NFAT-c1,* all $p<0.01$) were all upregulated over the HCS control, with the exception of *cathepsin K*. As seen in *RANKL* expression, HCS-BMP in the defect area increased the expression of most bone formation- and resorption-related markers (*ALP, osterix,* and *Cbfa1; NFAT-c1* and *cathepsin K,* all $p<0.01$), and HCS-BMP increased their expression more than ACS-BMP.

3. Comparison between HCS-BMP and ACS-BMP

in bone regeneration in vivo

We chose an extremely high dose (40 mg/ml) for an 8mm defect in rats to imitate a supra-physiological dose in clinical therapy. Bone regeneration was evaluated after a 4, 8, and 12-week healing period using micro-CT and histological staining (Figure 5, 6, and 7, Table 2). Micro-CT-based evaluation was performed to analyze new bone formation at two areas of the central defect and outside the defect area. We assessed the central defect area to evaluate how efficiently HCS guides new bone formation within this targeted defect area. In addition, we assessed excessive bone formation at the defect exterior to evaluate whether HCS could minimize bone formation outside the defect as an index for heterotopic ossification.

In the central defect, the ACS-BMP and HCS-BMP groups showed significant increases over the control vehicle group in bone parameters including BV/real defect volume, Tb.N, and BMD (Figure 5A, B and D). On the contrary, the Tb.Th and Tb.Sp of the ACS-BMP and HCS-BMP groups were reduced at the central defect (Figure 5C and E, Table 2). HCS-BMP exhibited higher values of BV and Tb.N by 31 % ($p<0.05$) and 61 % ($p<0.01$) at 8 weeks and by 23 % ($p<0.05$) and 34 % ($p<0.01$) at 12 weeks, respectively, over ACS-BMP, while the difference between these groups was minor at 4 weeks (Figure 5D and Figure 6B). ACS and HCS without BMP-2 showed few differences.

Heterotopic ossification was determined by measuring TV and BV at the defect area. The TV of the ACS-BMP and HCS-BMP group showed a 147 % and 37 % increase (both, $p<0.01$) compared to each vehicle control at 4 weeks (Figure 5G). The HCS-BMP group had half the TV change rate of the ACS-BMP group at 4 weeks.

However, the TV of the ACS-BMP group significantly declined as time passed, while the TV of the HCS-BMP group was nearly equivalent over the whole period. As a result, the TVs were similar at 8 weeks. The BV of the ACS-BMP group at the full region gradually decreased with time, while the BV of the HCS-BMP group did the opposite (Figure 6C). Namely, the BV of the HCS-BMP group was 0.7 fold lower ($p< 0.01$) at 4 weeks, equivalent at 8 weeks, and 1.2 fold higher ($p< 0.01$) at 12 weeks than that of the ACS-BMP group. The ACS-BMP group had an 8.2-fold increase in excessive BV outside the defect compared to the HCS-BMP group, but this declined over time and completely disappeared at 12 weeks (Figure 6D). For HCS-BMP, excessive bone, which was one-eighth of ACS-BMP at 4weeks, temporarily increased to about 50% of the level of ACS-BMP at 8 weeks, although the excessive bone completely disappeared at 12 weeks. This transient increase in bone formation at 8 weeks is probably due to sustained release of BMP-2 and the resulting osteogenic capacity of HCS.

Micro-CT images showed that all animals implanted with both HCS-BMP and ACS-BMP had bony union in the defect region (Figure 7A). Histological observation using MT-stained sections was consistent with micro-CT-based evaluation (Figure 7B). New bone formation outside the defect area in the vertical section was observed in both the ACS-BMP and HCS-BMP groups. The central defect space in the HCS-BMP group was more densely filled with new mineralized bone than that of the ACS-BMP group over the whole period. Successful union with existing calvarial bone was detected in both the ACS-BMP and HCS-BMP groups, although there was bone erosion at the margin of the defect at 7 days. In addition, HCS-BMP resulted in less excessive bone formation outside the defect than

ACS-HCS did, indicating less heterotopic ossification in the HCS-BMP group. At 12 weeks, HCS-BMP showed a compacted bone structure while ACS-BMP resulted in remodeled regenerated bone that was less compact than HCS-BMP.

C. Discussion

To achieve successful outcomes in BMP-2 therapy, current investigations have focused on developing a smart delivery vehicle to control BMP-2 release and finding appropriate doses of BMP-2 in skeletal sites. While an initial burst has a negative effect, a recent report suggested that a sufficient burst followed by a sustained release is more favorable for efficient bone formation than just a high burst with no sustained release [100]. Nevertheless, controlled release of BMP-2 might be critical for patient safety if severe postoperative swelling occurs in the treatment of alveolar bone healing [104, 105]. Because this poor stability arises in high BMP-2 dosing scientists have developed a variety of alternatives associated with established bone grafts or scaffolds to avoid initial burst and induce sustained release [82, 91, 106]. Heparin-associated delivery enhances bone formation at low doses of BMP-2 [107]. However, there is no evidence for heparin application with a collagen sponge for high dose BMP-2, which is critical for clinical applications. We evaluated the potential of HCS as an alternative high-dose rhBMP-2 delivery vehicle. We investigated the ability of HCS to overcome clinically relevant and undesired effects induced by high-dose BMP-2 and to enhance short- and long-term bone formation through controlled BMP-2 release.

Despite successful bone formation outcomes with no immune rejection *in vivo*, ACS showed an initial burst release of BMP-2, like other kinds of scaffolds [108]. Heparin shows binding affinity for BMP-2 and slowly releases it from the matrix *in vivo* [109]. To take advantage of this, we manufactured HCS at three concentrations of heparin and selected 0.5 % heparin after release analysis. An *in vitro*

BMP-2 release profile revealed that the HCS exhibited a lower burst followed by a sustained release phase for BMP-2, while the ACS released most BMP-2 within the first four days. Our manufactured HCS successfully immobilized BMP-2, leading to release of BMP-2 in a controlled manner, like other heparin-conjugated materials [96, 110-112]. Recent studies using heparin-conjugated fibrin or hydrogel showed controversial results that were dependent on BMP-2 dose or ectopic vs. orthotopic bone formation [103, 113, 114]. This is a unique study that has directly compared ACS and HCS in high-dose BMP-2 delivery for clinical applications. Johnson et al. reported that pre-complexed BMP-2 and heparin may be more effective than a collagen/heparin matrix at a low dose of BMP-2 in bone regeneration of femoral defects [114]. Although we concluded that a collagen/heparin matrix is ineffective when used for low dose BMP-2 delivery, HCS was effective in high dose BMP-2 delivery.

The rat calvarial defect model is most commonly used to determine bone regeneration capacity in response to certain stimuli, but its results have limited applications for patients. We chose a dose of 40 mg in an 8 mm defect to imitate a supra-physiological dose in people because 5 mg is a sufficient dose to fill a defect of this size completely at 4 weeks [115, 116]. By implanting an overdose of BMP-2, we intended to evaluate the clinical feasibility of HCS. However, calvaria defects in rodents do not normally undergo swelling as a critical side effect, which sometimes occurs when a supra-physiological dose of rhBMP-2 is applied in alveolar bone regeneration. Instead, we examined other side effects which can be observed in the rodent model. These include early transient bone resorption, excessive bone formation, and bone at undesired sites, also called heterotopic ossification [117].

We analyzed the capacity of HCS to efficiently deliver high-dose BMP-2 in three ways. First, we evaluated its ability to suppress early bone resorption induced by BMP-2. The early osteogenic response was examined 7 days after BMP-2 administration in the central defect area and the surrounding calvaria because we hypothesized that different release profiles of HCS- and ACS-BMP might be reflected in the early osteogenic process in these two regions. The influence on the surrounding calvaria is important because previous reports warned that rhBMP-2 delivered in a collagen sponge for metaphyseal fracture repair should be avoided due to severe transient bone resorption of surrounding tissue induced by a supra-physiological dose of rhBMP-2 [118]. The initial osteogenic process accompanied the simultaneous amplification of bone formation and resorption during bone regeneration in a BMP-2-loaded scaffold in the defect area [115]. In addition, the absence of a BMP dose-dependent increase in bone mass was attributed to concurrent bone resorption and formation. We used double the concentration of BMP-2 (40 mg), which resulted in a higher number of activated osteoclasts than the previous study (data not shown). As expected, the early osteogenic process in bone formation and resorption was correlated with the *in vitro* release profile of BMP-2 from HCS and ACS. Within the defect area, the HCS-BMP group had greater bone resorption indices, including TRAP-positive MNC number, R/O ratio, and *cathepsin K* expression, than the ACS-BMP group, probably due to a lower initial burst and higher long-term BMP-2 levels. However, the surrounding calvaria showed the opposite; the ACS-BMP group had greater bone resorption indices than the HCS-BMP group. Moreover, the HCS-BMP group had significantly increased activated osteoclasts on the scaffold compared to the ACS-BMP group at the

defect area, which was correlated with the R/O ratio. Although the HCS-BMP and ACS-BMP groups showed no difference within the scaffold due to greater osteoclast activation, the use of HCS might be beneficial because HCS alleviates the exposure of surrounding tissue to the rhBMP-2 burst, resulting in relatively weakened bone necrosis. As mentioned above, HCS probably effectively diminishes the potential risk of high dose rhBMP-2 use for metaphyseal fracture repair better than ACS [118]. The expression of bone forming markers (*ALP, osterix, Cbfa1*) trended with bone resorption indices both in defect area and surrounding calvariae in the ACS- and HCS-BMP groups, respectively. The more rapid release of rhBMP-2 from ACS may stimulate an increased response in the surrounding calvariae when compared with the HCS, which controlled the release of rhBMP-2 better. Higher BMP-2 concentrations in the defect area in the HCS-BMP group may stimulate a more aggressive response of infiltrated cells to BMP-2. This result was consistent with a carrier-dependent differential response to rhBMP-2, which is attributed to the release rate of rhBMP-2 from the carrier [118, 119]. In the initial response to BMP-2, HCS enhances bone formation in the defect area better than ACS, but this was counterbalanced by amplified bone resorption, finally leading to no difference in bone mass between the two groups.

OPG expression *in vivo* after high dose BMP-2 implantation differed between the defect area and the surrounding calvariae, while *RANKL* expression showed a consistent increase in response to BMP-2 treatment. Opg, which was secreted from osteoblasts, reduced RANKL signaling as a decoy receptor for RANKL, which plays a critical role in the regulation of bone resorption [120, 121]. rhBMP-2 induces *OPG* expression in murine cells *in vitro* [122, 123]. In

contrast, our previous study revealed that high dose rhBMP-2 reduced *OPG* expression at the defect area *in vivo* and in rat mesenchymal stem cells *in vitro* [115]. Additionally, *OPG* expression was reduced by BMP-2 both in human mesenchymal stromal cells and human osteoblasts [124]. In this study, *in vivo OPG* expression was also significantly reduced in the defect area in ACS-BMP over ACS alone, consistent with our previous study [115]. In addition, *OPG* expression in HCS alone and HCS-BMP was minor compared to that of ACS alone in the defect area, consistent with reports that heparin can enhance osteoclastic bone resorption by inhibiting *OPG* binding activity [109]. As a result, the R/O ratio in the HCS-BMP group at the defect area was enormously increased, which was consistent with a greater level of osteoclast activation than ACS-BMP. TRAP staining consistently showed abundantly distributed osteoclasts within defect area, and this increased significantly in the HCS-BMP group. However, BMP-2's effect on *OPG* expression was completely different between the surrounding calvariae and the bone defect. BMP-2 increased *OPG* expression in existing bone areas of the surrounding calvariae while it did the opposite in the defect area, which undergoes new ossification. This difference can probably be attributed to differential BMP-2 concentrations caused by release kinetics or to the differentiated stage of cells localized in each tissue. Further study is necessary to confirm the effect of rhBMP-2 on *OPG* expression, depending on a diverse range of dosages of rhBMP-2 or time.

We then investigated the effect of HCS on heterotopic ossification four weeks after surgery. Heterotopic ossification occurs when a supra-physiological dose of BMP-2 is rapidly released, resulting in less compact bone formation at the desired site and excessive bone

formation at undesired sites outside the original defect region [117]. Lateral growth of the newly formed bone was induced outside and inside the original defect area in BMP-2 treated scaffolds. Linde et al. showed that high dose rhBMP-2 (10 μg) could induce excessive bone formation, spreading outside the original contour in rats [125]. rhBMP-2 may affect new bone formation differently inside and outside the membranes [126]. Therefore, the effect of the delivery vehicle on early heterotopic ossification, especially at high doses of BMP-2, might indicate the release rate of BMP-2. We evaluated the effect of HCS on excessive bone formation by assessing new bone formation at the central defect only or in the full region including the central and exterior defect. Micro-CT-based evaluation showed little difference in new bone formation between HCS-BMP and ACS-BMP at the central defect at 4 weeks. This was probably due to greater bone resorption of HCS-BMP at the initial phase, which might counteract bone formation. ACS-BMP had much greater BV in the defect exterior than HCS-BMP when compared to the BV formed at the central defect. Although the excessive bone in the ACS-BMP group was rapidly remodeled and almost disappeared at 12 weeks, this result indicates a suppressive effect on excessive bone formation by HCS. Histological observation using MT-stained sections showed that total tissue and dead space within new bone tissue is definitely less in the HCS-BMP group over the whole period. This is probably caused a by lower burst and better controlled release of BMP-2, implying that HCS is able to alleviate early heterotopic ossification and may reduce adverse effects of an initial burst of high-dose BMP-2.

Finally, HCS was evaluated to determine whether sustained release of rhBMP-2 could continuously induce bone formation. Johnson et al.

showed that heparin alone was incorporated in a collagen matrix to potentially sequester endogenous BMP-2 at the defect site [114]. However, our data did not show any difference between HCS and ACS alone in new bone formation, but demonstrated an excellent effect when exogenous BMP-2 was delivered by HCS. Many researchers expected that a heparin-mediated sustained release of BMP2 would increase bone formation long-term. However, these systems have been mainly tested within 4 weeks and have not been evaluated over 12 weeks. Moreover, most studies used low dose BMP-2 or an ectopic assay. A research group investigated the effects of heparin on long-term bone formation at 12 weeks, and reported that heparin addition failed to increase bone formation over a collagen sponge with or without low-dose BMP-2 (3 mg) [114]. In contrast, our results showed that HCS was more effective than ACS at long-term formation of new bone at eight and 12 weeks when used with high dose BMP-2 (40 mg). ACS-BMP showed similar trends to HCS-BMP, but formed excessive bone at the defect exterior more than at the central defect, which rapidly disappeared as time passed, implying bone remodeling. Bhakta et al. proposed that BMP-2 delivery from a collagen sponge after an 8-week observation of an ectopic assay relies mostly on desorption rather than physical entrapment [127], thus failing to sustain release if the collagen sponge is fully degraded [103]. However, the collagen sponge is almost degraded within 4 weeks, as shown by MT staining in the ACS-BMP and HCS-BMP groups. BMP-2 dosed with either ACS or HCS continued to form new bone in the implanted defect region at 8 and 12 weeks despite the degradation of the collagen sponge. Micro-CT and histological staining revealed that heparin-immobilized rhBMP-2 developed compact bone structure and exerted active

osteogenic activity to form new bone more efficiently than a non-conjugated collagen sponge over 12 weeks.

Under *in vivo* conditions, the release of BMP-2 from collagen is reportedly more sustained, exhibiting a burst release followed by a sustained release until day 14 [128] Although we did not present *in vivo* pharmacokinetic data for BMP-2 from HCS and ACS, our *in vivo* data at from 7 days to 12 weeks were consistent with the prediction derived from the *in vitro* release profile and reflected the estimate derived from lower initial burst and sustained release of rhBMP-2 from HCS. Improved long-term bone formation in HCS-BMP was presumed by sustained release of BMP-2 from HCS. However, HCS-BMP had slightly better effects on early osseous healing than ACS-BMP despite a greater level of bone resorption and formation, which was assumed by the lower initial burst and the resultant higher retention of BMP-2 on the scaffold. The half-life of exogenous BMP-2 rapidly declines. However, HCS- and ACS-delivered BMP-2 guided new bone formation over 12 weeks in the central defect, despite degradation of the bulk of the collagen sponge within 4 weeks. This indicates that a bound form of BMP-2 with heparin might form new bonds with endogenously formed extracellular matrix, which may allow it to be continuously active *in vivo* or protected from proteolysis. Taken together, the HCS used here may be advantageous for rhBMP-2 delivery at high doses and may reduce the associated safety concerns that counteract the benefits of BMP-2 in patients.

Part Ⅱ

The effect of dose on rhBMP-2 signaling, delivered via collagen sponge, on osteoclast activation and in vivo bone resorption

Part of this work was published in Journal of Biomaterials 35 (2014) 1869-1881

A. Materials and Methods

1. Preparation of rhBMP-2/NFAT inhibitor-loaded scaffold

Escherichia coli-derived rhBMP-2 powder was provided from Daewoong Co. (Seoul, Korea), and dissolved with stabilizing buffer which was obtained by manufacture, at a concentration of 1 mg/mL. NFAT inhibitor (Sigma-Aldrich, St. Louis, MO, USA) was prepared by dissolving 50% acetic acid at a concentration of 5 mM. Each collagen sponge was prepared from the cross-reaction of chondroitin-6-sulfate (CS; Sigma Chemical Company, St. Louis, MO, USA) and type I collagen as described previously [129]. A type I atelocollagen powder (KOKEN Corp., Osaka, Japan) was dissolved in 0.05 M acetic acid, at a concentration of 5.0 mg/mL, which was co-precipitated by the dropwise addition of CS while stirring in a homogenizer. The resulting collagene-CS solution was placed in a freezer at 80 ℃ for 6 h, and was then lyophilized by freeze-drying at 80 ℃ for 48 h, yielding a collagen sponge. Subsequently, the collagen sponges were placed in a vacuum oven and subjected to a vacuum of 1.3 in. of Hg at 105 ℃ for 24 h. After a series of treatments with 40% ethanol containing 50 mM 2-morpholineoethane sulfonic acid (MES; Fluka Chemie, Buchs, Switzerland) (pH 5.5), and washings, collagen sponges are finally rinsed with distilled water, lyophilized by freeze-drying and sterilized with g-irradiation at 10 kGy. The collagen disks were 8 mm in diameter and 1 mm thickness for the calvarial defect model. Cocktail solution which contains rhBMP-2, NFAT inhibitor or stabilizing buffer was rapidly loaded onto each

scaffold before in vivo implantation at a total volume 30 μl which was controlled at an amount not exceeding 0.1% of the total scaffold volume. For control experiments, the scaffold was loaded with buffers which are dissolving solutions of rhBMP-2 or NFAT inhibitor.

2. Rat calvarial defect model

Eight-week-old Sprague-Dawley rats (total n = 42) were used. The experimental protocol was approved by the Animal Care and Use Committee of Seoul National University. After disinfection of the calvarial skin with 10% betadine (Potadines; Sam-Il Pharm, Seoul, Korea) and subcutaneous injection of 2% lidocaine containing 1:100,000 epinephrine (Lidocaine HCL Injs.; Yuhan, Seoul, Korea), an incision was made along the sagittal suture. The periosteum was elevated and an 8-mm-diameter calvarial bone defect was created with a trephine burr without dural perforation. A rhBMP-2-soaked collagen disk was then implanted into the defect area. The experimental groups were implanted with buffer-loaded scaffold alone (n = 10), rhBMP-2 (5 μg/defect) (n = 12), rhBMP-2 (20 μg/defect) (n = 12), or rhBMP-2 (20 μg/defect)+NFAT inhibitor (150 μM; 7.5 μg/defect) (n = 10). Half rats in each group was evaluated for RT-PCR at one week after implantation, and the other half was analyzed after four-weeks healing periods using micro-CT and histological observation to evaluate the new bone formation in calvarial defects. Collagen disks removed at one week was cut in half for RT-PCR analysis and TRAP staining to draw consistent results for the effect of BMP-2 with or without NFAT inhibitor on osteoclast activation.

3. Reverse transcription-polymerase chain reaction (RT-PCR) and quantitative real-time RT-PCR

The collagen disks removed from calvarial defect was washed with PBS solution and chopped into small pieces. After adding 0.5 mL of TRIzol reagent (Invitrogen, Life Technologies, Carlsbad, CA, USA) directly to the chopped sponge, total RNA was extracted and then subsequently treated as prescribed in the manufacturer's instructions. One microgram of RNA from each sample was subjected to cDNA synthesis using SuperScript Reverse Transcriptase II and oligo (dT)12-18 primer (Invitrogen) in a 20 μL reaction volume according to the manufacturer's instructions, with an additional step of removing RNA complementary to the cDNA using E. coli RNase H (Invitrogen). One microliter of cDNA was then subjected to PCR with the following amplification profile: predenaturation at 95 ℃ for 40 s, amplification (denaturation at 95 ℃ for 40 s, annealing at 60 ℃ for 40 s, and extension at 72 ℃ for 1 min) for a duration of 30 cycles, with a final extension at 72 ℃ for 10 min. PCR was performed in a DNA thermal cycler (model PTC-200; MJ Research, Waltham, MA, USA). For each of the PCR products, 10 μL was electrophoresed on a 1.5% agarose gel in the presence of ethidium bromide and visualized by the Gel documentation system (Vilber Lourmat, Marne-la-vallee Cedex, France).

For quantitative real-time RT-PCR, total RNA isolation and cDNA synthesis were carried out by the same method as RT-PCR. SYBRGreen PCR Master Mix (Applied Biosystems, Foster City, CA, USA) was used to detect accumulation of PCR product during cycling with the ABI Prism 7700 sequence Detection system (Applied Biosystems). The thermocycling conditions were as follows:

predenaturation at 95 ℃ for 10 min, amplification with denaturation at 95 ℃ for 15 s, and annealing and extension at 60 ℃ for 1 min for a duration of 30 cycles, with a final dissociation cycle at 95 ℃ for 15 s, 60 ℃ for 1 min, and 95 ℃ for 15 s. Real-time RT-PCRs were carried out in triplicate with three independent experiments (n > 3-5). Oligonucleotide primers for real-time RT-PCR were designed for product sizes under 200 bp using real-time PCR system Sequence Detection Software v1.3 (Applied Biosystems), and their sequences are provided in Table 3. Fold differences of each gene were calculated for each treatment group using normalized CT values of the housekeeping gene b-actin according to the instructions of Applied Biosystems.

4. Tartrate-resistant acid phosphatase (TRAP) staining

Collagen disks loaded with rhBMP-2 or PBS buffer were implanted onto 8 mm-critical sized defects of rat calvariae. After 7 days, collagen disks were removed. Half of each disk was fixed, and decalcified before paraffin embedding. Tissue sections were deparaffinized, dehydrated, and then cut vertically into 5-μm-thick pieces. Tissue sections were stained for TRAP activity to examine osteoclastogenesis as follows. TRAP staining buffer was prepared by dissolving Naphthol AS-MS phosphate disodium salt (5 mg/mL) in 10% formalin, followed by addition Fast Red Violet LB salt (1 mg/mL; Sigma-Aldrich). Slides were incubated with TRAP staining buffer for 30 min at 37 ℃, washed for 15 min in tap water, and mounted with Crystal/Mount solution. After capture of representative 200x fields under a phase microscope for whole sections of each

group, the numbers of TRAP-positive multinucleate cells, which have nuclei over three per cell, were counted using Image J software (NIH, USA).

5. Immunohistochemical (IHC) staining

RANKL and Cbfa1 expression in vivo were observed at 7 days after implantation. The collagen disks were removed and decalcified through incubation in ethyl-enediaminetetraacetic acid solution (7%, pH = 7.0) for 3-4 days (with a solution change on day 2). The specimens were then dehydrated in 70% ethanol and embedded in paraffin. Ten, paraffin sections were cleaned for 10 min with xylene, and the deparaffinized sections were treated with an undiluted serum solution for 30 min. Specimens were then incubated with anti-RANKL (1:200; Novus Biologicals, Littleton, CO, USA) or anti-Cbfa1 (1:100; Abcam, Cambridge, England) at 4 ℃ overnight. After incubation, the sections were incubated with R.T.U biotinylated universal antibody using Vectastatin kit (Vector Laboratories, Burlingame, CA, USA) according to the manufacturer's instructions. Staining was detected with dia-minobenzidine (Sigma) substrate, and slides were mounted with Crystal/Mount (Biomeda; Foster City, CA, USA). Images of stained cells were captured by bright field microscopy.

6. Quantitative micro-CT analysis

Animals were sacrificed 4 weeks post-surgery. Each calvaria

containing a collagen disk implant was removed from the skull and fixed in 10% formalin for 1 week. Micro-CT scans were then taken to quantitatively evaluate new bone formation using the Sky-Scan 1172®Microfocus X-ray System (SkyScan) with CT software, including CTAn 1.8®, CTvol, and NRecon Reconstruction®(SkyScan). The SkyScan 1172 microfocus X-ray system is equipped with a microfocus X-ray tube with a focal spot of 2 μm, producing a cone beam that is detected by a 12-bit cooled X-ray camera CCD fiber-optically coupled to a 0.5 mm scintillator. The resulting images were 1000 x 1000-pixel square images with an aluminum filter used to produce optimized images. Reconstructions and analyses were performed using NRecon reconstruction and CTAn 1.8 software, respectively. A second-order polynomial correction algorithm was used to reduce the beam-hardening effect for all samples. To measure newly formed bone, a circular area of pre-defined size was selected as the region of interest (ROI) in two-dimensional images. The pixel zone representing ossification in the defined ROI was then reconstructed in 3D by creating a volume of interest (VOI) in the lower and upper ranges of the threshold using grayscale units. After using CTAn 1.8 on each reconstructed BMP file, bone volume (BV), tissue volume (TV), BV ratio (BV/TV), trabecular number (Tb.N), trabecular thickness (Tb.Th), and trabecular separation (Tb.Sp) were obtained using a CT-analyzer in direct 3D based on a surface-rendered volume model according to the manufacturer's instructions. To measure bone mineral density (BMD), attenuation data for ROI or VOI were converted to Hounsfield units and expressed as a value of BMD using a phantom (SkyScan). This phantom contained rods of calcium HA (CaHA) having a standard density corresponding to mouse or rat bone, which ranges from 0.25

to 0.75 g/cm3. BMD values were expressed in grams per cubic centimeter of CaHA in distilled water. A zero value for BMD corresponded to the density of distilled water alone (no additional CaHA), and a value greater than zero corresponded to nonaerated biologic tissue.

7. Histochemical staining

After micro-CT reconstruction, the operative field of each calvaria was removed and decalcified through incubation in ethylenediaminetetraacetic acid solution (7%, pH = 7.0) for 3-4 days (with a solution change on day 2). The specimens were then dehydrated in 70% ethanol and embedded in paraffin. Decalcified paraffin sections were cleaned for 10 min with xylene and stained with hematoxylin and eosin (H&E) and Masson's trichrome (MT) for the detection of cells and bone structures, respectively. Digital images of the stained sections were collected using a transmission and polarized light Axioskop microscope, Olympus BX51 (Olympus Corporation, Tokyo, Japan).

8. Culture of rMSCs

Primary rMSCs were isolated from bone marrow from tibia collected from 4-week-old SD rats. The marrow suspension was collected in a syringe containing 6000 U/mL heparin and was mixed with phosphate buffered saline (PBS) solution in the same volume ratio and centrifuged at 2500 rpm for 10 min. After aspiration of the upper PBS layer, the marrow suspension was layered on Ficoll-paque

(Amersham Biosciences, Uppsala, Sweden) in a 1:5 ratio and then centrifuged at 1200 g for 30 min. The nucleated cells concentrated at the interface were collected and washed with PBS. Adherent cells were plated at a density of 200 x 10^4 cells/100 mm plate and cultured in an expansion medium containing low-glucose Dulbecco's modified Eagle's medium (DMEM; Welgene, Inc., Daegu, Korea), 100 units/mL of penicillin, 100 mg/mL of streptomycin, and 10% heat inactivated fetal bovine serum (FBS) under a humidified atmosphere of 5% carbon dioxide (CO2) at 37 ℃. The medium was changed every 3 or 4 days. Cells were passaged when they reached 70% confluence, and second-passage cells were used for in vitro experiments. To induce osteogenic differentiation, cells were supplemented with 50 μM of ascorbic acid and 10 mM of bglycerophosphate (Sigma-Aldrich), and then incubated with two different concentrations of rhBMP-2 (Daewoong) at 50 and 200 ng/mL with or without NFAT inhibitor (200 nM; Sigma-Aldrich). To evaluate the gene expression, real time RT-PCR was performed after 7 days culture.

9. Quantitative real-time RT-PCR

Total RNA was extracted from each cell cultures using TRIZOL reagent (Invitrogen Life Technologies, Carlsbad, CA, USA) following the manufacturer's instructions. Following reactions for RT-PCR were performed as described in the Section 3.

10. Statistical analysis

All data are presented as means standard errors of the mean (SEM) or standard deviation. Statistical analyses were performed using IBM SPSS statistics 20.0 software (IBM, USA). Groups were compared using a two-tailed Student's t-test or with Kruskal-Wallis nonparametric test. Differences with $p < 0.05$ were considered significant.

B. Results

1. Early bone-resorbing effect of rhBMP-2 after in vivo implantation

We investigated the early osteogenic process induced by rhBMP-2 when administered in a high-dose to heal bone loss in 8 mm critical-sized calvarial defects in rats. Early bone resorbing effect with high-dose rhBMP-2 (20 μg) in vivo was determined by counting TRAP-positive cell numbers in comparison with vehicle control and 5 μg rhBMP-2 groups at one week post-surgery. TRAP staining using vertically cut sections of collagen sponge showed that TRAP-positive multinucleate cells (MNCs), which have nuclei over three per cell, were significantly increased by rhBMP-2 in a dose-dependent manner. The high-dose group (20 μg) stimulated osteoclast formation by 6 fold, compared to vehicle control and lower-dose (5 μg) groups, where MNCs were rarely found (Figure 8). Real time RT-PCR for bone-resorbing markers was consistent with TRAP staining showing rhBMP-2 dose-dependent increase (Figure 9). RANKL expression was up-regulated by 1.47 and 3.7 fold at 5 μg and 20 μg of rhBMP-2 treatment, respectively, compared to vehicle control. Contrary to RANKL expression, rhBMP-2 led to down-regulation of OPG expression to 0.61 and 0.47 fold in 5 and 20 μg groups, respectively, compared to vehicle control. The relative ratio of RANKL/OPG expression was increased by 2.2 ($p < 0.01$) and 8 fold ($p < 0.01$) in 5 μg and 20 μg rhBMP-treated groups, respectively, over vehicle control, and was increased by 3.7 fold ($p < 0.01$) in the high-dose group compared to the low-dose group (Figure 9C). IHC

staining for RANKL showed intensively stained areas in rhBMP-2 groups, dose-dependently, compared to vehicle control. We further examined the expression of other osteoclast activation-related markers including TRAP, cathepsin K, c-fos, and NFATc1. All these genes were significantly up-regulated in rhBMP- 2-treated groups. TRAP and cathepsin K showed a significant dose-dependent increase by 1.8 versus (vs.) 3.3 fold at 5 vs. 20 μg for TRAP, and by 2.1 vs. 3.7 fold at 5 vs. 20 μg for cathepsin K, compared to vehicle control. rhBMP-2 treatment also increased c-Fos and NFATc1 expression, but did not show dose dependence.

2. Effect of rhBMP-2 on bone-forming activity in vivo during early healing period

We further investigated the early bone formation process induced by rhBMP-2 treatment using the same specimens used for the expression of bone-resorption markers. The expression of early osteoblast differentiation markers, cbfa1, osterix, ALP, and VEGF, was examined by real-time RT-PCR (Figure 10). The expression of all these genes was significantly increased in rhBMP-2-reated groups and showed the same tendency as seen in the expression of bone resorption markers. In particular, osterix, ALP and VEGF expression was greater in the 20 μg group than in the 5 μg group by 5.44 ($p < 0.01$), 5.74 fold ($p < 0.01$), and 1.65 fold ($p < 0.05$), respectively. However, there was no significant difference between two doses of rhBMP-2 in cbfa1 expression. IHC staining for Cbfa1 showed intensively stained areas in rhBMP-2 groups, compared to vehicle control.

3. Involvement of NFAT signaling in rhBMP-mediated bone resorption and formation in vivo

We hypothesized that rhBMP-2-mediated bone resorption might be regulated by c-Fos/NFATc1 signaling, because expression of each was found to be slightly enhanced by rhBMP-2 in the current study, and because they are known as key regulators of osteoclastogenesis [44]. Therefore, we investigated the activity of rhBMP-2 for bone resorption and formation in vivo using NFAT inhibitor, because NFATc1 is downstream of RANKL and c-Fos in osteoclasts [45]. Both TRAP staining and real-time RT-PCR was performed using the same experimental strategy as described above (Figures 8 and 9), and results were compared between 20 μg of rhBMP-2 group and combined treatment of NFAT inhibitor (150 μM; 7.5 μg/defect) with rhBMP-2 20 μg (Figure 11). The number of TRAP-positive MNCs decreased to 21.8% ($p < 0.01$) with NFAT-specific inhibitor, compared to treatment with 20 μg of rhBMP-2 alone group, meaning that NFAT inhibitor partially blocked the bone-resorbing activity of high-dose rhBMP-2. Subsequent RT-PCR analysis showed a consistent trend with TRAP staining. The addition of NFAT inhibitor suppressed the expression of osteoclastogenesis-related markers such as RANKL, c-fos, and cathepsin K, all of which were up-regulated by rhBMP-2. Although NFAT inhibitor treatment did not influence the OPG expression down-regulated by 20 μg of rhBMP-2, the resulting relative ratio of RANK to OPG was also diminished to a similar level as the vehicle control group. Most of these resorption-related markers measured after co-treatment of NFAT

inhibitor with rhBMP-2 were restored either partially or to a similar level to that in vehicle controls. IHC staining for RANKL showed that RANKL expression appeared weakened by combined treatment of NFAT inhibitor and high-dose rhBMP-2, compared to the high-dose rhBMP-2 only group. We also examined the effect of NFAT inhibitor on the expression of bone-forming markers up-regulated by high-dose rhBMP-2 (Figure 12). As seen in the expression of boneresorbing markers, NFAT inhibitor suppressed the up-regulated (by rhBMP-2) expression of bone-forming markers as well. The expression levels of ALP, cbfa1, osterix, and VEGF measured after cotreatment of NFAT inhibitor with high-dose rhBMP-2 were restored to those of vehicle controls, suggesting that NFAT mediates BMP signaling both in bone resorption and formation. As seen in IHC staining for RANKL, Cbfa1 staining was weakened by combined treatment with NFAT inhibitor, compared to the high-dose rhBMP-2 group.

4. Interplay of NFAT signaling with rhBMP-2 signaling in rMSCs

In vivo results showed that rhBMP-2 dose-dependently enhanced the expression of both bone formation and resorption markers, and rhBMP-2 signaling was blocked by NFAT inhibitor. Because the in vivo microenvironment is composed of a multicomplex system including osteoblasts, osteoclasts, and other constituents, we attempted to investigate in vitro rhBMP-2 effect at two different concentrations (50 and 200 ng/mL) and NFAT effect on BMP-2 signaling in osteoblasts, using rMSCs as osteoprogenitor cells (Figure 13). As seen in the in vivo animal model, real-time RT-PCR showed

that RANKL expression was slightly increased ($p < 0.05$) with rhBMP-2 in a dose-dependent manner, while OPG expression was down-regulated with lack of dose dependence. Due to dose-dependent increase of RANKL expression, the relative ratio of RANKL to OPG was dose-dependently increased. NFAT inhibitor treatment exhibited a consistent result with in vivo results, leading to evident suppression of RANKL expression and the ratio of RANKL to OPG, compared to treatment with high-dose rhBMP-2 (200 ng/mL) alone. As like, rhBMP-2 induced dose-dependent increase in the expression of bone-formation markers Cbfa1, osterix, ALP, and VEGF, most of which was also suppressed by NFAT inhibitor. However, increased Cbfa1 expression induced by rhBMP-2 was not suppressed by combined treatment with NFAT inhibitor. These results suggest that Cbfa1 is not regulated by NFAT, while NFAT influences the expression of osterix, ALP, and VEGF. Although RANKL or OPG expression was consistent with in vivo results, there was no change in the expression of other bone resorption markers including TRAP, Cathepsin K, and NFATc1 with rhBMP-2 or additional NFAT inhibitor treatment.

5. Combined treatment of NFAT inhibitor with high-dose rhBMP-2 enhances bone regeneration in vivo

Our previous study, performed using the same strategy as the current study, showed that rhBMP-2 treatment using collagen sponges showed successful bone regeneration at doses of 5 and 20 μg/defect, between which there was less difference in new bone

formation after a 4-week healing period [116]. Although NFAT inhibitor suppressed the bone-resorbing activity of rhBMP-2 at one week after implantation, it was unclear whether NFAT inhibitor improved new bone formation of high-dose rhBMP-2 group after the 4-week healing period, because NFAT inhibitor also suppressed the expression of bone formation-related markers at 7 days post-operation.

Calvarial defects were divided into 4 groups comprised of vehicle controls treated with PBS buffer and defects treated with 5 μg rhBMP-2, 20 μg rhBMP-2, or combination of 20 μg rhBMP-2 and 150 μM NFAT inhibitor (BMP20/INH). Micro-CT images showed that all animals implanted with rhBMP-2 had bony union in the defect region, while visible bone was rare on defect regions in the vehicle control group (Figure 14). Expanded bone formation in the vertical section of defect areas was observed in both 20 μg rhBMP-2 and BMP20/INH group, where there was no apparent difference in images. Micro-CT-based evaluation showed that new BV of rhBMP-2 5 μg and 20 μg groups was increased by 5.6 ($p < 0.01$) and 7.4 fold ($p < 0.01$), respectively, compared to vehicle control. As seen in the vertical section of 3D micro-CT images, TV was dose-dependently increased by rhBMP-2 implantation as well. Thus, both 5 μg and 20 μg groups increased BV/TV at a similar level by 4.5-4.9 fold, compared to vehicle control. The value of BV/TV resulted in no significance dose dependence, as observed in the previous study. Tb.N was increased and Tb.Sp decreased in all rhBMP groups compared to the vehicle alone control group, suggesting that more trabecular structures were densely built in rhBMP-induced bone. Both parameters showed dose-dependence with rhBMP-2 treatment, indicating a denser structure of new bone at higher dose (20 μg).

However, Tb.Th for regenerated bone tissue showed a rather decreased pattern in all rhBMP-2 groups, as observed in the previous study. Micro-CT-based evaluation revealed NFAT inhibitor improved the new bone formation of high-dose rhBMP-2 treatment in BV by 14.5% ($p < 0.01$), TV by 12.2% ($p < 0.05$), and BV/TV by 12.0% ($p < 0.05$), compared to the rhBMP-2 20 μg only group. Among other parameters, Tb.Th was slightly increased by 28% ($p < 0.05$) by NFAT inhibitor treatment, while the values of Tb.N and Tb.Sp were not changed. In addition, BMD in all rhBMP groups and the BMP20/INH group was slightly increased at a similar level by 13% ($p < 0.01$), compared to the vehicle control group.

Histological observation using MT-stained sections confirmed the radiographic findings, with bony bridging seen in rhBMP-2-treated groups and non-union seen in vehicle control (Figure 15). H&E staining showed that there was no inflammatory reaction around or in the scaffold, and that cells were infiltrated into sponge pores. After 4 weeks of healing, the central zone in the defect space was filled with new mineralized bone and showed successful union with existing calvarial bone in all rhBMP-2 groups, whereas collagen fiber implanted into defects still existed with scarce mineralization in the vehicle control group. All rhBMP-2 groups with or without NFAT inhibitor induced new bone formation, which was mineralized within interspaces of collagen fibers with osteocytes structure, before collagen fibers were fully degraded. In addition, these groups induced expanded bone formation, which was united over existing calvarial bone surrounding the defects. However, there was no apparent difference between the rhBMP-2 20 μg group and additional NFAT inhibitor treatment in MT staining.

C. Discussion

BMPs are critical regulators of bone remodeling that modulate two opposing functions: bone formation and resorption [23, 130-132]. Accumulated evidence has revealed that binding of BMP-2 at its specific receptor I/II transduces a strong signal to bone-forming cells including MSCs or osteoblasts, leading to the induction of osteoblast differentiation-markers and matrix mineralization [133]. Conflicting with this anabolic function of BMPs, it is widely known that BMPs stimulate osteoclastogenesis as well, and there are controversial studies supporting the role of BMPs in the direct activation of osteoclasts [9, 132]. In addition, BMPs are negatively regulated by antagonists through feedback inhibition [132, 134]. High dosing of rhBMP-2 induces transient bone resorption in vivo [118], indicating that the resorption process is dominant over a range of rhBMP-2 concentrations during early healing periods, likely corresponding to initial burst release in treatments. However, it is still unclear which mechanisms are signaled by BMP in vivo, when high-dose rhBMP-2 is administered at the target site. This study aimed to investigate the action of high-dose rhBMP-2 delivered by collagen sponges in vivo for bone formation and resorption, and furthermore, to approach anti-resorption by blocking a target molecule that plays a pivotal role in rhBMP-2 mediated osteoclast activation.

The current experiment was designed in a setting of rhBMP-2-induced orthotopic bone formation, because the recruitment of both osteoprogenitors and osteoclast progenitors is more active compared to ectopic bone formation at non-skeletal sites. In particular, a calvarial defect model is very suitable to investigate dose-dependent effects of rhBMP-2 due to simplicity and a rapid healing period

without risks of heterotopic bone formation. Our previous study, performed using the same scheme as current study, showed that after a 4-week healing period, new bone formation in the group treated with 20 μg rhBMP-2 was inferior to the group treated with 5 μg rhBMP-2 [116]. This finding implies either an inhibitory effect by feedback inhibition or osteoclast activation by high-dose rhBMP-2. The absorbable collagen sponge used in then previous and present study is a type of carrier thatwas approved by the FDA for human use as an alternative tobone grafts [135]. However, release kinetics reported that collagen sponge implantation results in a rapid burst release, such that only 5% of the loaded BMP-2 remains after 14 days. This rapid release can be attributed to the low affinity of sponge material to BMP-2, although release is generally slower than with ceramic scaffolds sponges during the initial stages of release in vivo [86, 136]. Multiple studies have reported that a higher-dose treatment of rhBMP-2 induced transient bone resorption owing to rapid release of rhBMP-2 during the early stage of bone formation [118, 137]. Sciadini et al. reported the dose-dependent formation of cyst-like bone voids by rhBMP-2 in animal models [138]. Therefore, the current scheme using collagen sponges in a calvarial defect model would be an appropriate model to investigate high-dose rhBMP-2-mediated signaling related with bone resorption during early phase in BMP-2 implantation.

Using the same scheme as in our previous study, current results showed a clear in vivo tissue response to rhBMP-2 dose, and these were consistent with in vitro results for osteoblast differentiation obtained primarily from osteoblasts or MSCs [139, 140], even though the in vivo microenvironment is composed of a variety of cells and constituents. rhBMP-2 increased the expression of bone-forming

markers such as Cbfa1, osterix, ALP, and VEGF in vivo at 7 days after surgery [141, 142]. Among these, expression of osterix and ALP was dose-dependently increased, while the expression of Cbfa1, a crucial transcriptional activator of osteoblast differentiation [143], did not show dose dependence. The increase in VEGF expression with rhBMP-2 treatment indicates enhanced angiogenesis, which is a critical pre-requisite for promoting bone formation, suggesting that rhBMP-2 application enhances both angiogenesis and osteoblast differentiation during early phase healing [144]. The same tendency was seen in the expression of resorption-related makers including RANKL, TRAP, and cathepsin K and in the number of activated osteoclasts, which increased dependently of dose. RANKL expression was increased in a dose-dependent manner, while OPG expression was down-regulated by rhBMP-2, but the expression of both genes was independent of dose. However, the resulting ratio of RANKL to OPG expression exhibited a definite dose-dependent increase, which probably attributed to increased expression of cathepsin K, which is essential for normal bone resorption as a proteinase to hydrolyze extracellular bone matrix proteins [145]. A previous study showed that constitutively activated BMP receptor type IA (caBMPRIA) mice exhibited a unique phenotype with decreased bone mass due to increased bone resorption mediated by increased RANKL expression and the ratio of RANKL to OPG [23]. High-dose rhBMP-2 treatment creates similar conditions to caBMPRIA mice in that BMP signaling is over-activated. Although information about the expression of bone-forming markers was unavailable from caBMPRIA mice, current results suggest that highdose rhBMP-2 induced cell populations within defect areas to promote both bone-forming and resorbing process without notable feedback inhibition. However, the high-dose

of rhBMP-2 (20 μg) used in the current study was not sufficient to induce severe resorption, as opposed to our initial expectation. Further study is being performed to observe whether bone resorption and formation process is concurrent at an extremely high doses dose where severe resorption appears.

In BMP-2-mediated osteoclastogenesis, activation of the Smad pathway by BMP-2 induces SOST expression, which antagonizes the Wnt pathway by modulating RANKL/OPG expression [20]. We observed that high-dose of rhBMP-2 promoted osteoclast activation via the gene expression of osteoclastic molecules, including RANKL, TRAP, cathepsin K, c-Fos, and NFATc1, at a greater level than with low dose. There is conflicting discussion about whether BMPs regulate osteoclasts directly [9] or through indirect pathways, such that BMP-2 could only stimulate osteoclast cells via stromal cells and the osteoblast-mediated RANKL signaling pathway [132]. Although the contribution of BMP-2 signaling to this argument cannot be evaluated, current in vivo results suggest that exogeneous rhBMP-2 delivered by collagen sponge exerts resorbing activity during the early healing period, dosedependently, when administered at higher-than-physiological doses. Dosage customization for rhBMP-2 and a level of bone resorption in association with collagen sponge is not simple, because both the release kinetics of scaffolds and the availability of appropriate responding cells are variables for determining this relationship [118, 144]. A few studies have suggested that appropriate concentration of rhBMP-2 is necessary to avoid early bone resorption [9, 146]. Furthermore, it has recently been reported that an initial burst release of BMPs followed by sustained release is more beneficial to bone healing than a sustained release after reduced initial burst; however, there is an additional contrasting suggestion

that it is crucial for release to be sustained over time [100, 110]. Nevertheless, the risk for early resorption by rhBMP-2 treatment would be increased, because clinical treatment requires over ~mg level to maintain sustained release over long periods of healing. Therefore, combined treatment of high-dose rhBMP-2 with another factor to suppress the resorptive process might be effective, because bone resorption caused by high-dose rhBMP-2 is transient [9].

Osteoclast differentiation is derived by RANKL binding to RANK, leading to activation of either the JNK/NF-kB or p38/c-Fos signaling pathway, finally resulting in transactivation of NFATc1 and up-regulation of NFATc1-responsive genes related to bone resorption and remodeling [147]. Current results showed rhBMP-2 treatment increased the expression of c-Fos and NFATc1 in vivo, but failed to increase the expression of c-Fos and NFATc1 in vitro using rMSCs, implying that both genes are not downstream markers of rhBMP-2 signaling in osteoblasts. However, NFATc1 up-regulation by rhBMP-2 in vivo suggests that increased RANKL expression in stromal cells probably signals the NFATc1 pathway via RANKL/RANK interactions in osteoclasts, leading to autoamplification of NFATc1 [44], and finally, increased osteoclast activation at high-dose. Our result is consistent with the finding that induction of c-Fos and NFATc1 during RANKL-stimulated osteoclast differentiation is mediated by the p38 signaling pathway [45], which is also a BMP signaling pathway. Although we cannot rule out the possibility that BMP-2 directly stimulates mature osteoclast function [9], the increased RANKL/OPG ratio from stromal cells probably plays a major or synergistic effect in initial triggering of osteoclast activation in BMP-2 signaling.

In order to investigate the involvement of NFATc1 pathway in

high-dose rhBMP-2-mediated regulation of bone resorption, we examined the effect of NFATc1 inhibitor on high-dose rhBMP-2 activity in vivo and in vitro. However, it is known that NFATc1 regulates bone mass by functioning in both osteoblasts and osteoclasts [148]. NFATc1 plays a pivotal role in osteoclast activation via up-regulation of various genes in a series processes, such as osteoclast adhesion, migration, acidification, and degradation of inorganic and organic bone matrix [149]. The binding of RANKL to RANK can also stimulate calcium oscillation followed by calcineurin phosphatase activation and induce the autoamplification of NFATc1, which results in transactivation of osteoclastic genes [44, 150]. However, active NFAT drives osteoblast proliferation in vivo, and calcineurin/NFAT signaling in osteoblasts enhances chemokine expression of CCL8, which may recruit osteoclast precursors to bone and influence osteoclastogenesis [148]. Consistently with these findings, our results showed that co-treatment of NFAT inhibitor with high-dose rhBMP-2 suppressed both bone forming- and resorption markers in vivo. However, there was no change in OPG expression in vivo, as was also found in vitro using rMSCs, indicating that OPG is not transcriptionally regulated by NFAT. Combined treatment of NFAT inhibitor with high-dose rhBMP-2 using rMSCs in vitro did not induce any change in contrast with in vivo results, which was consistent with the results described in the Koga et al. [151]. The difference in Cbfa1 expression between in vivo and in vitro is probably a result of rhBMP-2 dose exposed to cells and different environment, indicating that Cbfa1 expression might be influenced indirectly by diverse NFAT signaling routes in vivo. However, expression of osterix, its downstream marker, ALP, and VEGF was clearly under NFAT control in osteoblasts. This result

agrees with the finding that NFATc1 and Osterix form a complex that binds to DNA, and this interaction is important for the transcriptional activity of Osterix [151]. In addition, NFAT inhibitor failed to influence the expression of TRAP and cathepsin K in rMSCs in vitro, compared to great reduction of these genes' expression in vivo, indicating that rhBMP-mediated resorption is linked to the RANKL/OPG-NFAT pathway in osteoclasts, not in osteoblasts. Notably, the effect of NFATc1 inhibitor on NFATc1 expression differed in vivo and in vitro. There was no change of NFATc1 expression in vitro in the treatment of hBMP-2+NFAT inhibitor in rMSCs, while NFATc1 expression was down-regulated by inhibitor in vivo. This finding is probably attributed to the property of tissue specimen in vivo study that was actually a mixture of bone cells. However, the differences in cell population can also contribute to the differences in the results. Taken together from in vivo and in vitro results, we suggest that NFATc1 is not a responsive gene of BMP-2 signaling, but influences the expression of BMP-2 responsive genes such as osterix or ALP in stromal cells. However, NFATc1 is probably linked to BMP-2 signaling via RANKL/RANK interaction and transcriptionally inhibited by NFAT inhibitor via the autoamplification mechanism of NFAT in osteoclasts. Consistently with the gene expression of bone-resorption markers, the combined treatment of NFAT inhibitor and highdose rhBMP-2 (20 μg) introduced a resulting phenotype in defect regions that showed a significant reduction in the numbers of TRAP-positive multinucleated osteoclasts during the early healing period of 7 day, compared to high-dose rhBMP-2 (20 μg) treatment alone.

Despite a critical role of NFAT both in osteoblasts and osteoclasts, targeting NFATc1 is an alternative strategy to inhibit the high-dose

rhBMP-2-mediated resorption during the early healing period, because NFATc1 is a master modulator for osteoclast fusion, maturation, and activation [149]. We first investigated the bone-regenerating effect of a cocktail treatment of high-dose rhBMP-2 and NFAT inhibitor using collagen sponges under the hypothesis that NFAT inhibitor effect might attenuate bone resorbing effect of high-dose rhBMP-2 during early healing period. NFAT inhibitor is a high-affinity calcineurin-binding peptide that potently inhibits NFAT activation and NFAT-dependent expression of endogenous cytokine genes in T cells [152]. Because there was no information about in vivo application of NFAT inhibitor for local delivery,we first performed the experiment at a concentration of at 150 μM (7.5 μg/defect). Micro-CT-based evaluation showed that there was little difference between 5 μg and 20 μg rhBMP-2 groups in BV and BV/TV, despite 4 fold difference in the dose between two groups, probably due to early resorption in the high-dose group. However, combined treatment with NFATc1 inhibitor increased BV and BV/TV more than 20 μg of rhBMP-2 alone, suggesting that the inhibitor effectively suppressed early bone resorption. In addition, the increase of BV by NFAT inhibition suggests that the effect of NFAT inhibitor might be transient during the early healing period, given the observation that it also inhibited bone formation process at early healing period; if the inhibitor effect were not transient during early healing period, the overall bone formation process would be impaired at 4 weeks. Another parameter increased by NFAT inhibitor was Tb.Th; there was no change in the parameters Tb.Sp and Tb.N.

In spite of sustained release of BMPs from collagen sponges, the synthetic biodegradable polymer/interconnected-porous calcium hydroxyapatite ceramics composite is also commonly used as a

delivery system for rhBMP-2 in clinical application [153]. Unfortunately, ceramic bone substitutes rapidly release BMP-2, resulting in bone resorption at an early stage in vivo [136]. This initial burst release of rhBMP-2 exposes the tissue environment to a high concentration of rhBMP-2, which is the main cause of high-dose rhBMP-2-mediated resorption, even though it is a transient process. Therefore, NFAT as a target molecule is therapeutically recommendable to inhibit the RANKL-NFAT pathway of osteoclastogenesis if locally administered. An additional beneficial property of NFAT inhibitor is selective interference with the calcineurin-NFAT interaction without affecting calcineurin phosphatase activity; NFAT inhibitor is also regarded to be less toxic than current drugs [152]. However, identification of another target factor is still needed, because NFAT is a critical regulator both of bone formation and resorption [148]. The potential uses of a RANKL inhibitor have been extensively explored in the preclinical setting and in numerous models using various RANKL binders such as OPG [154], RANK-Fc, and anti-RANKL antibodies (including denosumab) [155]. Denosumab is very specific for the inhibition of RANKL activity and is approved by the FDA for use in postmenopausal women with risk of osteoporosis; it is designed to inhibit RANKL by mimicking the OPG role in osteoclastogenesis [34]. Thus, a combined local treatment with these RANKL inhibitors might be another alternative to suppress the early bone resorption when supra-physiological doses of rhBMP-2 are applied. Further studies are necessary to verify which ratio of rhBMP-2 and NFAT inhibitor dose is optimal and whether NFAT inhibitor effect is better or worse for long term effects of rhBMP-2 on bone regeneration. In addition, it is necessary to investigate NFAT inhibitor only group in vivo to verify

its deleterious effect on osteoblast cell populations, and to observe any other unexpected phenotypes.

Part Ⅲ

Estrogen Modulates Bone Morphogenetic Protein-Induced Sclerostin Expression Through the Wnt Signaling Pathway

Part of this work was published in Journal of Tissue Eng Part A. 2015 Jul;21(13-14):2076-88

A. Materials and Methods

1. Chemicals

17b-Estradiol (E2) was purchased from Sigma-Aldrich (St. Louis, MO). TCF/LEF reporter for Wnt and Smad signaling was obtained from Qiagen (Hilden, Germany). The Dual-Luciferase Reporter Assay system was purchased from Promega (Fitchburg, WI). ERa and Smad4 siRNAs were purchased from Santa Cruz Biotechnology (Santa Cruz, CA). Transfections for the reporter assay and siRNA were performed using Lipofectamine® 2000 reagent (Invitrogen, Carlsbad, CA). Antibodies for total/active b-catenin, ERa, and Smad4 were obtained from Cell Signaling Technology® (Danvers, MA), Abcam (Burlingame, CA), and Santa Cruz Biotechnology, respectively. Enzyme-linked immunosorbent assay (ELISA) reagents for sclerostin, Opg, and insulin-like growth factor-1 (IGF1) were obtained from R&D Systems (Minneapolis, MN). The Smad inhibitor, dorsomorphin, was obtained from Calbiochem® (Gibbstown, NJ), and the Wnt inhibitor, ICI 182,780, was purchased from R&D Systems. Recombinant human BMP2 (rhBMP2), prepared from Escherichia coli, was obtained from Novosis®-Dent, BioAlpha, Inc., (Gyeonggi-do, South Korea); we demonstrated its osteogenic activity in a previous study [116].

2. Isolation and culture of hMSCs and human osteoblasts

Bone marrow was obtained from the iliac crest of three

nonosteoporotic, healthy female donors (19 - 25 years old) who provided informed consent. Procedures were approved by the local ethics committee of Seoul National University Dental Hospital, according to the legal regulations for human tissue and organs in Korea (CRI05008). hMSCs from bone marrow were cultured as described previously [140, 156]. Nucleated cells that concentrated at the interface after Ficoll-Paque (Amersham Biosciences, Uppsala, Sweden) treatment were collected and washed with phosphate-buffered saline (PBS). Collected cells were plated at a density of $200x10^4$ cells/100mm and cultured in expansion medium comprising lowglucose Dulbecco's modified Eagle's medium (DMEM; Welgene, Inc., Daegu, South Korea), 100 U/mL penicillin, 100mg/mL streptomycin, and 10% heat-inactivated fetal bovine serum (HI-FBS) under a humidified atmosphere of 5% CO2 at 37℃, with medium changes every 3 or 4 days. Cells were passaged when they reached 70% confluence and reseeded in a new culture plate at a density of $30x\ 10^4$ cells/cm^2. Cells from the second to fifth passages were used for all experiments. The ability of hMSCs to differentiate into osteoblasts, chondrocytes, or adipocytes was confirmed according to previously published protocols [140].

Primary human osteoblasts were derived from mandible biopsy specimens of four healthy, female human donors (19 - 25 years old) who provided informed consent. To obtain bone-derived cells, bone samples were minced and washed twice with PBS. The samples were incubated for 40min with gentle shaking in a solution containing 0.1% type I collagenase (Sigma-Aldrich) and 0.2% dispase (Roche, Indianapolis, IN) in serum-free DMEM at 37℃. This process was performed twice, and the cells that were obtained were combined for each case and cultured separately. To investigate the effect of

estrogen on SOST expression in association with BMP signaling and osteoblast differentiation, hMSCs were treated with E2 or a combination of E2 and BMP2 in osteogenic differentiation medium with DMEM supplemented with ascorbic acid (50 μg/mL) and b-glycerophosphate (10mM) without dexamethasone (DEX), added at 1 or 2 days postplating when the cells were confluent.

3. Transient transfection and luciferase reporter assays

Transient transfections for luciferase reporter assays were performed using Lipofectamine 2000 reagent (Invitrogen). hMSCs were transfected with 1 ng/μL of TOPFlash luciferase reporter plasmids or Smad reporter plasmids in serum-free DMEM without antibiotics. Positive and negative reporters, corresponding to each reporter assay, were also included according to the manufacturer's instruction. After 5 h of transfection, the cells were stabilized by culturing overnight in DMEM with 10% HI-FBS, and then plated in 96-well plates (5000 cells/well). The next day, the cells were treated with E2 (100 nM), BMP2 (200 ng/mL), E2/BMP2, or no treatment for 24 h. The cells were washed once with PBS and lysed with 1x passive lysis buffer. Luciferase activity was measured using a Turner 20/20 luminometer with a Dual-Luciferase Reporter Assay kit (Promega) according to the manufacturer's instructions. Luciferase activity was calculated as the ratio of firefly luciferase activity to that of *Renilla* luciferase.

4. Gene silencing using siRNA targeting ERa or

SMAD

Endogenous *ERa* or *SMAD4* expression was knocked down by siRNA transfection using human ERa siRNA (sc-29305) or Smad4 siRNA (sc-29484), which refers to a pool of four target-specific 19 to 25 oligonucleotide siRNAs. siRNA-A, a nontargeting 20 to 25 oligonucleotide (sc-37007), was used as the control. hMSCs were transfected with human sequence-specific ERa/Smad4 siRNA or control siRNA-A at a final concentration of 30pM using Lipofectamine 2000 reagent in serum-free DMEM without antibiotics for 5 - 6 h, according to the manufacturer's instructions (Invitrogen). After transfection, the cells were stabilized by culturing overnight in DMEM with 10% HIFBS, and then the medium was replaced with DMEM with 1% HI-FBS. After incubation for 24 h, the cells were treated with E2 (100 nM), BMP2 (200 ng/mL), or E2/BMP2 or left untreated.

5. Quantitative real-time reverse transcription - polymerase chain reaction

Total RNAs were extracted by the addition of 0.5mL of TRIzol reagent (Life Technologies, Waltham, MA) to cells on a plate as described in the manufacturer's instructions. One microgram of RNA was subjected to cDNA synthesis with SuperScript Reverse Transcriptase II and oligo 12 - 18 primers (Invitrogen). We used SYBR® Green PCR Master Mix (Applied Biosystems, Foster City, CA) to detect the accumulation of PCR product during cycling with the ABI Prism 7700 Sequence Detection System (Applied Biosystems).

The thermocycling conditions were as follows: predenaturation at 95℃ for 10 min; 40 cycles of denaturation at 95℃ for 15 s, and annealing and extension at 60℃ for 1min, followed by a final dissociation cycle at 95℃ for 15 s, 60℃ for 1 min, and 95℃ for 15 s. Real-time reverse transcription-polymerase chain reaction (RT-PCR) was carried out in triplicate in at least three independent experiments ($n > 3$). Oligonucleotide primers were designed using real-time RT-PCR system sequence detection software v1.3 (Applied Biosystems) and their sequences are provided in Table 4. Fold differences in the expression level of each gene were calculated for each treatment group using CT values normalized to transcript levels of the housekeeping gene, *18S rRNA*, according to the manufacturer's instructions.

6. Alkaline phosphatase assay

We assayed alkaline phosphatase (ALP) activity by measuring the amount of ρ-nitrophenol produced using ρ-nitrophenol phosphate substrate. Cell lysates were mixed with alkaline buffer solution and gently shaken for 10 min. ALP substrate was added at room temperature for 30 min. After the reaction was stopped with 0.05N NaOH, the absorbance at 405 nm was read and compared with a standard curve prepared with ρ-nitrophenol standard solution. Enzyme activity was normalized to the protein concentration of the cell layer determined using a protein assay (Bio-Rad, Hercules, CA).

7. Enzyme-linked immunosorbent assay

Sclerostin or Opg levels in the culture supernatants were determined using an ELISA kit (R&D Systems). After centrifugation, cell culture supernatants (n = 4 - 5) were added to 96-well ELISA plates. Standards for cytokines (0 - 1000 pg/mL) were run in each series. After incubation, aspiration, and washing, a human conjugate of each protein (100 μL/well) was added according to the manufacturer's instructions. The OD of each well was determined within 30 min using a microplate reader set to a 450-nm wavelength with correction for optical imperfections in the plate.

8. Western blotting

Total cell lysates of cultured hMSCs were prepared by lysing cells in RIPA buffer containing 50mM Tris buffer (pH 7.5), 50mM NaCl, 1% Triton X-100, 1mM ethylene glycol tetraacetic acid, 10mM Na4P2O9, 5mM Na3VO4, 50mM NaF, and protease inhibitors (10 μg/mL leupeptin, 10 μg/mL aprotinin, 10 μg/mL pepstatin A, 0.1mM phenylmethylsulfonyl fluoride, and 1mM dithiothreitol). Nuclear and cytoplasmic fractionation of cultured hMSCs was performed using NE-PER nuclear and cytoplasmic extraction reagents (Thermo Scientific, Rokford, IL) according to the manufacturer's instructions. Total cell lysates (20 μg/lane) or nuclear/cytoplasmic fractions (15 μg/lane) were subjected to electrophoresis through a 10% sodium dodecyl sulfate - polyacrylamide gel and transferred to PolyScreen polyvinylidene difluoride membranes (PerkinElmer Life Sciences, Hopkinton, MA). Membranes were blocked with 5% nonfat dry milk in TBST buffer (0.1M Tris-buffered saline [pH 7.5]/0.1% Tween) and probed with antibodies. The following antibodies were used in this study: polyclonal rabbit anti-total b-catenin (Abnova, Taipei, Taiwan);

polyclonal rabbit anti-nonphospho (active) b-catenin antibody, diluted 1:2000; polyclonal rabbit anti-ERa antibody, diluted 1:200; monoclonal mouse anti-Smad4 antibody, diluted 1:200; and monoclonal mouse anti-a-tubulin antibody, diluted 1:200. Primary antibodies were detected with horseradish peroxidase (HRP)-conjugated anti-rabbit immunoglobulin G (IgG; Santa Cruz Biotechnology) for total/active b-catenin and ERa or with HRP-conjugated antimouse IgG (Dako, Glostrup, Denmark) for Smad4 and a-tubulin. Finally, blots were stained with an enhanced chemiluminescence detection system (Amersham Biosciences) according to the manufacturer's instructions.

9. Immunofluorescent staining

Sclerostin or b-catenin expression in hMSCs was detected at an average cell density of 3000 cells per coverslip. Cells were washed thrice with PBS, fixed in 4% paraformaldehyde for 30 min, and blocked in blocking solution for 30 min. Cells were incubated with antibody against sclerostin (anti-rabbit, 1:100; Abnova) or active b-catenin (anti-rabbit, 1:400; Cell Signaling Technology, Inc.) overnight at 4℃, washed twice with PBS, and then incubated with secondary antibody labeled with fluorescein isothiocyanate (anti-rabbit IgG, 1:500; Biomeda) for 1 h. Primary antibody controls were processed in parallel using only the secondary antibody. Slides were washed in PBS for 10 min and incubated with PBS-buffered 4',6-diamino-2-phenylindole solution (1 mg/mL; Santa Cruz Biotechnology) using a dilution ratio of 1:1000 for nuclear staining. Section images of the stained cells were captured using an Olympus Fluoview FV300 confocal laser scanning microscope and Fluoview software (Olympus Optical Co., Ltd.).

10. Statistical analyses

All data are presented as mean±standard error of the mean. Statistical analyses were performed using SPSS 20 (IBM Co., Armonk, NY). Differences between two groups were evaluated using two-tailed Student's t-test, and the comparison of data for more than two groups was performed using two-way analysis of variance post hoc through the Bonferroni method. Differences with $p < 0.05$ were considered significant.

B. Results

1. Induction of SOST by BMP2 in hMSCs

Treatment of hMSCs and human osteoblasts with the BMPs, BMP-2, -4, and -6, has been reported to induce SOST [77]. We confirmed that BMP2 treatment (200 ng/mL) induced SOST expression in primary hMSCs prepared from three female donors. In contrast to SOST induction in murine cells [20], SOST induction by BMP2 in human cells gradually increased with time, consistent with a previous report [77]. Although SOST upregulation differed among the donors, it showed a time-dependent increase in all cases (Figure 16). In two of the tested hMSC cultures (#1 and 2), SOST expression was significantly increased by BMP2 from day 3, and a noticeable increase in SOST expression was generally observed at day 7 after treatment in all tested cells (Figure 16). However, in untreated hMSCs, the basal level of SOST did not increase over time from day 1. BMP2 treatment also enhanced the expression of the bone-forming markers, ALP and IGF1, which are BMP2-responsive genes, in all three hMSC cultures.

2. Effects of estrogen on BMP2-mediated SOST induction

The effect of estrogen on BMP2 signaling was investigated at day 7 because all cultures of hMSCs showed SOST upregulation at this point. We used 100nM of E2, a concentration that was shown in a previous report to stimulate the greatest extent of osteoblast

differentiation in hMSCs [157]. SOST expression was examined at day 7 after treatment of cells with BMP2 (200 ng/mL), E2 (100 nM), or both BMP2 and E2, and the results were compared with those of nontreated cultures (Figure 17). E2 alone had no effect on the basal expression of SOST in hMSCs, whereas BMP2 increased its expression ($p < 0.01$) in all three hMSC lines (#1, 2, and 3). Interestingly, there was a marked decrease in the level of SOST expression ($p < 0.01$ compared with BMP treatment) when hMSCs were cotreated with E2 and BMP2 (Figure 17A).

SOST expression was further examined at the protein level using ELISA and immunofluorescent staining in hMSC#1 and #2 (data are presented for hMSCs#1), which showed a similar phenotype after treatment with E2, BMP2, or E2/BMP2. Extracellular release of sclerostin was not affected by E2 alone, but was increased by 65.7% by BMP2 compared with the nontreated control group (Figure 17B).Moreover, consistent with the transcriptional expression of SOST, treatment of cells with a combination of E2 and BMP2 decreased Sost protein expression by 28.3% relative to BMP2 treatment alone. Immunofluorescent detection of intracellular sclerostin expression at day 7 was intense in the cytosol, but not in the nuclei, with a similar pattern to the ELISA results (Figure 17C). We also examined the expression of other BMP2-responsive genes after E2 treatment (Figure 17D). Similar to SOST expression, E2 alone had no effect on the basal expression of ALP, IGF1, or BMP2 in hMSCs, whereas BMP2 treatment significantly upregulated the expression of these markers (data shown for hMSC line#1). Likewise, expression of the ALP, IGF1, and BMP2 genes decreased when the cells were treated with both E2 and BMP2, as observed for SOST expression. The expression of OPG, a presumed target of estrogen, was not

influenced by E2 treatment, but was downregulated by BMP2 ($p < 0.01$). However, the real-time RT-PCR analysis to detect RANKL expression was the same as that of the negative control without cDNA in all test groups, indicating that RANKL expression in hMSCs is too low to be detected. Cotreatment of hMSCs with E2 and BMP had no effect on OPG expression, which was maintained at a reduced level after BMP2 treatment. This pattern was consistent in all tested hMSCs. Consistent with realtime RT-PCR data, Opg expression by ELISA was decreased by 20.0% ($p < 0.01$) by BMP2 or by 23.9% ($p < 0.01$) by E2/BMP2 treatment compared with the nontreated control group, whereas there was no change in the E2 only group (Figure 17F). ALP activity showed the same trend as expression by real-time RT-PCR (Figure 17G).

3. Involvement of Wnt/b-catenin/ERa signaling in the E2-mediated suppression of SOST induction by BMP2

Both the Smad and Wnt signaling pathways have been implicated in modulating the suppressive effect of E2 on BMP2-mediated SOST induction [158]. First, we investigated the effect of the Wnt pathway on E2- and BMP2-mediated SOST induction in hMSCs#2. We tested whether E2 increases the transcriptional activity of b-catenin using a TCF/LEFresponsive vector (Figure 18A). There was a significant (17.8-fold, $p < 0.01$) increase in TOPFlash luciferase activity in E2-treated cells compared with nontreated controls, whereas cells treated with BMP2 alone did not show any change. Combined treatment with E2 and BMP2 resulted in a 3.7-fold increase over the

control ($p < 0.01$), which corresponded to a reduction compared with E2 alone ($p < 0.01$), but an increase compared with BMP2 alone ($p < 0.01$). Positive and negative controls functioned as expected in the TOPFlash luciferase assay.

The effect of the Wnt pathway on E2- and BMP2-mediated SOST induction was assessed by treatment with the Wnt inhibitor, ICI 182,780 (100 nM), as an antagonist of ERa [159]. Treatment with ICI 182,780 partially recovered the E2-mediated suppression of SOST to levels similar to those after BMP2 treatment alone, but did not affect BMP2-mediated SOST induction (Figure 18B). We confirmed sclerostin expression at the protein level using ELISA (Figure 18C). Consistent with the results of real-time RT-PCR, ICI 182,780 treatment recovered sclerostin expression of cells cotreated with BMP2 and estrogen similar to the level of sclerostin observed in BMP2-treated cells, but had little effect on sclerostin induction by BMP2. These results implicate involvement of the Wnt pathway or ERa in the action of E2 on sclerostin suppression through cross talk with BMP signaling.

4. Effect of ERa gene silencing on E2 signaling in association with BMP2 signaling

Because the Wnt inhibitor used in this study targets ERa, we investigated the involvement of ERa in the Wnt pathway during estrogen signaling. Blocking of ERa expression using ERa siRNA was confirmed by western blotting using anti-ERa antibody (Figure 18E). In cells transfected with control siRNA, there was a noticeable difference in the level of active b-catenin after E2 treatment, whereas total b-catenin level showed little difference from the nontreated

control. However, the enhanced expression of active b-catenin induced by E2 was slightly decreased by combined treatment with BMP2, consistent with results of the TOPFlash reporter assay.

Transfection with ERa siRNA resulted in lower expression of b-catenin after E2 treatment (alone and with BMP2) compared with the same groups transfected with control siRNA. Real-time RT-PCR showed that transcriptional SOST expression after transfection with ERa siRNA was consistent with the effects of the Wnt inhibitor, ICI 182,780 (Figure 18D). BMP2 still increased SOST expression 3.9-fold, but the suppressive effect of E2 on BMP-mediated SOST induction was not evident in cells transfected with ERa siRNA, indicating that ERa plays a role in SOST regulation through interaction between estrogen and BMP2.

Additionally, we observed nuclear localization of activated b-catenin after estrogen treatment. Immunofluorescent staining using an antibody specific for active b-catenin on subcellular fractions confirmed that estrogen increased the level of cytoplasmic b-catenin compared with that of control cells (Figure 18F). Active b-catenin expression in the cytosolic fraction was more apparent after estrogen treatment, compared with the control. Nuclear localization of active bcatenin was clearly detected at 1 hr after estrogen treatment, while it was diminished at 3 h.

Western blotting at the time points of 1 and 24 h under the same conditions as in Figure 3E showed a similar trend to immunofluorescent staining (Figure 18G). In cells transfected with control siRNA or ERa siRNA, estrogen alone enhanced cytosolic expression of active b-catenin at 1 and 24 h compared with the nontreated control. However, the nuclear fraction of active b-catenin was slightly increased at 1 h, and then decreased with time, showing

little expression at 24 h in all treatments (estrogen, BMP, estrogen + BMP). Transfection with ERa siRNA resulted in less expression of active b-catenin in the cytosolic and nuclear fractions after E2 treatment (alone and with BMP2), especially at 24 h, compared with the same groups transfected with control siRNA. Total catenin expression was mainly observed in the cytosolic fraction with little difference between treatments, which was also independent of blocking ERa.We confirmed the absence of cross-contamination between nuclear and cytoplasmic fractions (data not shown).

5. Noninvolvement of the Smad pathway in the modulation of SOST expression by E2 coupled with BMP signaling

BMP2 activates intracellular mediators such as Smad proteins to induce SOST however, it is unclear whether the interaction between E2 and BMP2 signaling involves the Smad pathway. The transcriptional activity of SMAD4 was not affected by E2 treatment in the Smad-luciferase reporter assay, whereas it was significantly increased by BMP2 treatment (BMP2 alone and E2/BMP2) compared with the nontreated control, with no difference between BMP2 alone and BMP2 plus E2 (Figure 19A). SOST expression was assessed after treatment with dorsomorphin (10 μM), a Smad inhibitor, using real-time RT-PCR and ELISA, which led to a complete blockage of SOST induction by BMP2 treatment, with or without E2 (Figure 19B, C) [160]. Further investigation using Smad4 siRNA showed a similar trend to treatment with dorsomorphin. Silencing of the SMAD4 gene using anti-Smad4 antibody was confirmed by western blotting, which

showed a definite reduction in BMP2-induced expression after transfection with Smad4 siRNA transfection compared with the same group with control siRNA (Figure 19D). There was little difference in the levels of active bcatenin between cells transfected with control siRNA or Smad4 siRNA. There was a complete blockage of SOST induction in cells transfected with Smad4 siRNA after BMP2 treatment, with or without E2, as seen after treatment with the Smad inhibitor, dorsomorphin (Figure 19E).

6. Effect of estrogen on BMP2-induced upregulation of SOST in human osteoblasts

To determine whether estrogen had the same effect on BMP2 signaling in undifferentiated hMSCs and differentiated osteoblasts, we examined the effects of estrogen on primary human osteoblasts derived from the mandibles of four females. We pursued the same strategy as for hMSCs, using real-time RT-PCR and ELISA to assess the effects of E2 on BMP2-induced SOST expression. In contrast to the common response of all three hMSC cultures to E2, the effect of E2 on SOST induction by BMP2 differed among the human osteoblast lines (Figure 20A). Of the four different cell lines, two cell lines (#1 and #2) showed the same pattern as seen in hMSCs, that is, E2 had an inhibitory effect on BMP2-mediated SOST upregulation, whereas in the other two cell lines (#3 and #4), E2 did not change the BMP2-induced level of SOST. Representative cell line #1, in which E2 had an inhibitory effect, expressed sclerostin protein by ELISA in a manner similar to the SOST levels determined by real-time RT-PCR (Figure 20A, B).

An interesting finding was that combined treatment of osteoblasts

with E2 and BMP2 did not suppress the upregulated expression of other BMP2-responsive genes, such as ALP or IGF1, in any of the tested osteoblasts, independent of whether estrogen was able to suppress the BMP2-mediated increase in SOST expression (Figure 20C). In addition, we found that ALP expression in human osteoblasts was not significantly increased in response to BMP2 treatment, in contrast to hMSCs. However, OPG expression was consistent with that in hMSCs and was not changed by E2 treatment compared with the control, but was downregulated by BMP2. Cotreatment with E2 and BMP had no effect on OPG expression, which was maintained at a reduced level similar to that after BMP2 treatment. The protein levels of ALP and Opg were consistent with their transcriptional levels following treatment with E2, BMP2, or E2/BMP2 (Figure 20D, E). Unlike hMSCs, ALP activity did not show significant increases with BMP2 treatment. Furthermore, there was no relationship between SOST and ALP activity in any of the cell lines. In vitro matrix mineralization determined by von Kossa staining showed little difference from the control group in the four osteoblast cell lines after treatment with Dex, E2, BMP2, or E2/BMP2 (Figure 20F).

7. Relationship between SOST expression and the ratio of RANKL to OPG expression in human osteoblasts

Using human osteoblast cell lines #1 and #2, which showed estrogen-mediated suppression of SOST induction by BMP2, we investigated the effect of BMP2 or E2 dose on SOST expression (data shown are for osteoblast line #1). SOST expression was

examined at increasing concentrations of BMP2 (100, 200, and 300 ng/mL) and was found to reach a maximum at 200 ng/mL and then decrease at 300 ng/mL (Figure 21A). The expression level of the osteoclast marker, RANKL, differed among individuals and either followed a similar pattern to SOST expression or did not change appreciably as the dose of BMP2 increased. However, OPG expression was decreased by BMP2 treatment independent of the BMP2 dose. Nevertheless, the relative ratio of RANKL to OPG showed an identical pattern to that of SOST expression with increasing doses of BMP2, indicating that the increase in the ratio of RANKL to OPG is probably caused by the induction of SOST by BMP2 (Figure 21B). The effect of the E2 dose was investigated by incubating cells with increasing concentrations of E2 (1, 10, and 100 nM) at a fixed concentration of BMP2 (200 ng/mL) (Figure 21C). E2 had a suppressive effect on SOST induction regardless of the dose. The relationship between the E2 dose and expression of RANKL and OPG was not definite. However, the resulting ratio of RANKL to OPG expression showed a similar pattern to SOST expression and was significantly decreased by E2 compared with that of cells treated with BMP2 only, independent of the E2 dose.

C. Discussion

There is a growing interest in sclerostin-based treatment as a novel potential anabolic therapy for postmenopausal osteoporosis. An antibody to sclerostin dramatically increased bone formation in ovariectomized rats and intact monkeys, without affecting bone resorption [70, 72]. Although these data implicate a suppressive effect of estrogen on sclerostin production, the precise molecular mechanism by which estrogen regulates the transcriptional expression of SOST remains unclear. Interestingly, previous studies showed that BMPs are potential inducers of SOST expression in mouse- and human-derived MSCs or osteoblasts [20, 77], whereas growth factors such as IGF1 or transforming growth factor b had no such effect in hMSCs [77]. Therefore, this study aimed to elucidate the mechanism of estrogen modulation of SOST expression in human bone cells in association with BMP2 signaling, which would provide a logical basis for recent therapies targeting sclerostin in osteoporotic patients.

BMP2 upregulates SOST expression through the Smad pathway [20, 161]. In contrast to other BMP antagonists such as noggin or chordin, which inhibit BMP2 signaling by directly binding the BMP receptor [21], the produced sclerostin has no direct effect on BMP signaling involving Smad phosphorylation and Smad-driven transcriptional reporter activation [162]. Instead, sclerostin inhibits the Wnt signaling that is required for BMP-stimulated osteoblastic differentiation, which explains the high bone mass in diseases associated with SOST mutations, such as sclerosteosis and van Buchem disease [163, 164]. The induction of SOST by BMPs is a controversial component of BMP action. It is reported that this catabolic activity of BMP is modulated by several steroids at the

transcriptional level [165]. DEX has been shown to be an antagonist of SOST in BMP4-treated cells; in contrast, retinoic acid or 1,25(OH)2D3 enhances the levels of SOST in vitro [77]. A recent study reported that estrogen inhibits BMP2 signaling, including the expression of ALP and osteocalcin, in the murine stem cell line, C2C12 [166]. This tendency was also observed in the current studies using human MSCs and osteoblasts. Estrogen showed an inhibitory action on the upregulation of the catabolic marker, SOST, as well as anabolic markers (ALP and IGF1) by BMP2. Although there was no direct effect of estrogen alone on SOST expression in vitro, these results imply a molecular link between estrogen signaling and SOST expression with indirect modulation through BMP2 signaling.

We found that the Wnt/ERa/b-catenin signaling pathway participates in estrogen signaling for SOST suppression. Consistent with previous reports in cell lines derived from rodents, our findings showed that estrogen activated the Wnt/ERa/b-catenin signaling pathway in hMSCs [79, 167]. E2 alone increased transcriptional activity of b-catenin and the level of active b-catenin, whereas BMP2 failed to do so. b-Catenin expression with combined treatment of E2 and BMP2 was higher than that induced by BMP2 treatment alone, but lower than that induced by E2 treatment alone. The role of ERa was critical in estrogen-mediated b-catenin activation and SOST suppression. The suppressive effect of E2 on SOST induction by BMP2 was abolished both in ERasilenced cells and by treatment with the Wnt inhibitor, ICI 182,780, which causes ERa degradation [168], whereas BMP2 signaling in SOST induction was not affected under the same conditions. These results suggest that even in the presence of BMP2 signals, which suppress the Wnt pathway, estrogen/ERa exerts positive control in the activation of b-catenin. The current

findings support the initial suggestion that estrogen and BMP signaling converge on SOST expression and Wnt pathways in bone cells [23, 65, 169, 170]. Sutherland et al. suggested participation of steroid hormone receptor complexes created with DEX, which may interfere with the binding of SMADs or create an inactive complex, resulting in a decrease in the BMP-induced transcription of SOST, thus tuning BMP2 activity toward favoring bone formation when BMPs upregulate antagonists such as SOST [77]. Current findings suggest that estrogen is such a modulating factor that downregulates SOST levels induced by BMP2 in human bone-forming cells by activating the Wnt/b-catenin pathway through ERa.

This study also investigated the role of the Smad pathway in estrogen signaling. It is reported that BMP2 upregulates SOST expression through the Smad pathway, ultimately blocking the Wnt pathway [20, 161]. The current finding that E2 inhibited BMP2-mediated SOST expression suggests that there is a connection between ERa/b-catenin and the Smad pathway. Our experiments targeting Smad4 expression indicated that the Smad pathway plays a critical role in BMP2-mediated SOST induction, as seen in a previous report [20]. However, estrogen did not exert any influence on Smad4 activity. Because of lack of evidence from the current study, modulation of the Smad pathway by activated bcatenin needs to be explored further. This question might be explained by previous studies [158, 166]. It was reported that in the presence of E2, ERa suppresses the prodifferentiation actions of BMP2 by inhibiting BMP2-induced activation of Smads and Smad-mediated transcription [158]. In addition, it is also speculated that the inhibitory effect of E2 on BMP2 signaling is mediated by phosphorylation of ERKs in the Smad1 linker region, which in turn increases the proteasomal

degradation of Smad1 and ultimately contributes to the suppressive effect of estrogens on osteoblastogenesis [166]. Taken together, these results imply that estrogen signaling is probably not linked directly to the Smad-related signaling pathway, but instead indirectly inhibits the Smad pathway in the presence of BMP2.

The current results indicate that the effect of E2 on BMP2 signaling changes according to the stage of osteoblast development. E2 had an inhibitory effect on the BMP2-responsive genes, ALP, IGF1, and SOST, in undifferentiated hMSCs independent of the donor. However, in human osteoblasts, the effect of E2 showed individual differences. Specifically, E2-mediated inhibition of SOST induction by BMP2 was observed in two of the tested osteoblast lines, whereas E2 did not inhibit ALP or IGF1 expression in any of the osteoblast lineages tested, in contrast to the observations for hMSCs. To confirm the cell specificity of these stimuli, we examined the effects of estrogen and BMP2 in other types of human cells, such as skin fibroblasts and liver cells. There was no estrogen-mediated suppression of SOST induction by BMP2 in either cell line, although the fibroblasts showed SOST induction by BMP2. These results indicate that estrogen-mediated suppression of BMP signaling is specific to bone cells and might be more apparent in the undifferentiated state.

A unique point is that estrogen does not inhibit BMP2-mediated bone-forming activity in cells that have differentiated into osteoblasts, but still suppresses the antibone-forming activity of BMP2 signaling in an individual-dependent manner. All of the osteoblast cell lines used in this study failed to show a significant increase in ALP activity after treatment with BMP2, as seen in hMSCs [140]. Moreover, the development of in vitro mineralization exhibited little difference after treatment with E2, BMP2, E2/BMP2, or DEX from

the nontreated control group, although all experimental groups, including the control group, were positively stained. These data imply that all of the osteoblast cell lines might be at a later stage of osteogenic differentiation at the time of isolation. Nevertheless, SOST expression was different and highly dependent on the individual donor. Taken together, our data imply that estrogen might be a modulator of BMP2 activity that antagonizes SOST activity at all stages of osteoblast development in adult hMSCs and human osteoblasts. However, this leaves the question of whether this action of estrogen coupled with BMP signaling differs according to the differentiation state of bone cells or has individual variations. The estrogen response implies that estrogen plays a dynamic role in enhancing bone formation at the level of osteoblast cells.

SOST activity is linked to BMP-BMPR1A signaling in osteoblasts and triggers RANKL-OPG pathway-induced osteoclastogenesis in vivo [166]. We aimed to identify a downstream marker of BMP2-mediated SOST induction in hMSCs or human osteoblasts. The current results showed that OPG was significantly downregulated when hMSCs were treated with BMP2, whereas there was no basal expression of RANKL. In contrast to the absence of basal RANKL expression in hMSCs, there was a distinct relationship between SOST expression and the ratio of RANKL to OPG in human osteoblasts. A previous animal study using Bmpr1a-deficient mice showed that the effect of BMP was mediated through Bmpr1A and that Bmp increased SOST expression, as well as the ratio of RANKL to OPG expression [166]. In contrast to this animal study, clinical studies showed that treatment of postmenopausal women with estrogen did not induce any changes in Opg levels, whereas estrogen significantly reduced the levels of serum sclerostin and other markers

of bone resorption [65]. Current data using human samples showed that OPG expression was downregulated by BMP2, but the addition of E2 did not influence the BMP2-mediated inhibition of OPG expression in either hMSCs or osteoblasts.

The effects of BMP2 and E2 on RANKL expression differed depending on the individual. Above all, the ratio of RANKL to OPG expression was consistent with that of SOST expression, which was increased by BMP2 and decreased by cotreatment with E2 and BMP2 in differentiated osteoblasts, but not in hMSCs. Notably, the inhibitory effect of estrogen on the ratio of RANKL to OPG expression was similarly independent of the E2 dose, meaning that E2 is active at low doses. This result is similar to data reported by a study of Bmpr1a-modified mice, in which the ratio of RANKL to OPG expression was a determining factor when Bmpr1a was deficient or constitutively expressed [166]. Consistent with these data, we also demonstrated in a recent publication that the ratio of RANKL/OPG s correlated with in vivo boneresorbing activity of rhBMP-2 during the early healing period [115]. Taken together, these findings suggest that the target of SOST inhibition by E2 in bone metabolism might be the ratio of RANKL to OPG rather than the concentration of OPG or RANKL alone at the osteoblast level. However, further study is required to elucidate which factor is linked to individual differences in the effect of estrogen on SOST expression.

Conclusions

This study approached HCS-mediated BMP-2 delivery as an alternative to overcome limitations of high dose BMP-2 application. We proved the advantage of HCS use in BMP-2 delivery on the basis that HCS induces a lower burst and subsequent sustained release of BMP-2. This led to less initial bone resorption at the surrounding tissue, alleviated heterotopic ossification, and enhanced compact regeneration at the target bone defect over a longer period. However, HCS-BMP does not accelerate early osseous healing of the target area at 4 weeks, presumably due to a simultaneous increase in bone formation and resorption, despite the fact that HCS-BMP had a greater increase in bone forming activity than ACS-BMP. HCS is a useful alternative to lessen early adverse effects and continue bone formation over a longer period in high-dose BMP therapy.

And current study investigated in vivo BMP-2 signaling on bone resorption and formation which occurs during early healing period when high-dose rhBMP-2 was implanted at local bone defect, and thereby a new strategy for anti-resorption was attempted using a target molecule. In vivo signaling of rhBMP-2 loaded on a collagen sponge showed a definite dose-dependent increase in the expression of both bone formation- and resorption-related markers during early healing period. High dose rhBMP-2 (20 μg) induced osteoclast activation at a greater level over low dose (5 μg) through increased ratio of RANKL to OPG, which signals activation of the NFATc1 pathway in vivo. Although high-dose rhBMP-2 concurrently promoted osteoblastogenesis during early healing period, it led to little difference in new bone formation with the low-dose rhBMP-2 group after 4 weeks healing period, probably due to dominant effect of

activated osteoclasts. Blocking NFAT in vivo was effective on the suppression of osteoclast activation increased by high-dose rhBMP-2 during the early healing period, while NFAT inhibitor also reduced the expression of bone formation markers. Ratio of RANKL/OPG might be an index which indicates bone resorbing activity of rhBMP-2 during early healing period. A new strategy by a cocktail treatment of rhBMP-2 and NFAT inhibitor into target site enhanced new bone formation at 4 weeks more than high-dose rhBMP-2 group (20 μg) alone. Blocking NFAT might be an alternative strategy to avoid early resorption and improve bone formation in high-dose rhBMP-2 applications.

we investigated the molecular mechanism by which estrogen regulates SOST expression in association with BMP2 signaling. We demonstrated that the mechanism of E2 action on SOST expression involved activation of the Wnt pathway involving ERa and b-catenin. In differentiated osteoblasts, the effect of E2 on SOST expression differed among individuals. It is intriguing that the relative ratio of RANKL to OPG expression after BMP2 or E2 treatment was a downstream marker of SOST expression in differentiated osteoblasts, but was indeterminate in hMSCs because of the extremely low-level expression of RANKL. The strength of this study is the demonstration of cross talk between estrogen and BMP2 signaling in SOST regulation, which is probably one of the mechanisms involved in bone homeostasis by estrogen at the level of human osteoblast cells. Therefore, this study provides a logical basis for recent therapies targeting sclerostin in osteoporotic patients. However, further studies are needed to more precisely define why estrogen signaling requires interaction with BMP signaling to regulate SOST expression and whether the effect of estrogen on BMP2 signaling

differs depending on the differentiated state or among individuals.

References

[1] MistryAS,MikosAG.Tissueengineeringstrategiesforboneregeneration. Advancesinbiochemicalengineering/biotechnology.2005;94:1-22.

[2] Doll B, Sfeir C, Winn S, Huard J, Hollinger J. Critical aspects of tissue-engineered therapy for bone regeneration. Critical reviews in eukaryotic gene expression. 2001;11:173-98.

[3] Petite H, Viateau V, Bensaid W, Meunier A, de Pollak C, Bourguignon M, et al. Tissue-engineered bone regeneration. Nature biotechnology. 2000;18:959-63.

[4] Wikesjo UM, Guglielmoni P, Promsudthi A, Cho KS, Trombelli L, Selvig KA, et al. Periodontal repair in dogs: effect of rhBMP-2 concentration on regeneration of alveolar bone and periodontal attachment. Journal of clinical periodontology. 1999;26:392-400.

[5] Valentin-Opran A, Wozney J, Csimma C, Lilly L, Riedel GE. Clinical evaluation of recombinant human bone morphogenetic protein-2. Clinical orthopaedics and related research. 2002:110-20.

[6] Govender S, Csimma C, Genant HK, Valentin-Opran A, Amit Y, Arbel R, et al. Recombinant human bone morphogenetic protein-2 for treatment of open tibial fractures: a prospective, controlled, randomized study of four hundred and fifty patients. The Journal of bone and joint surgery American volume. 2002;84-A:2123-34.

[7] Termaat MF, Den Boer FC, Bakker FC, Patka P, Haarman HJ. Bone morphogenetic proteins. Development and clinical efficacy in the treatment of fractures and bone defects. The Journal of bone and joint surgery American volume. 2005;87:1367-78.

[8] Wong DA, Kumar A, Jatana S, Ghiselli G, Wong K. Neurologic impairment from ectopic bone in the lumbar canal: a potential complication of off-label PLIF/TLIF use of bone morphogenetic

protein-2 (BMP-2). The spine journal : official journal of the North American Spine Society. 2008;8:1011-8.
[9] Kaneko H, Arakawa T, Mano H, Kaneda T, Ogasawara A, Nakagawa M, et al. Direct stimulation of osteoclastic bone resorption by bone morphogenetic protein (BMP)-2 and expression of BMP receptors in mature osteoclasts. Bone. 2000;27:479-86.
[10] Zara JN, Siu RK, Zhang X, Shen J, Ngo R, Lee M, et al. High doses of bone morphogenetic protein 2 induce structurally abnormal bone and inflammation in vivo. Tissue engineering Part A. 2011;17:1389-99.
[11] McClellan JW, Mulconrey DS, Forbes RJ, Fullmer N. Vertebral bone resorption after transforaminal lumbar interbody fusion with bone morphogenetic protein (rhBMP-2). Journal of spinal disorders & techniques. 2006;19:483-6.
[12] Martin T, Gooi JH, Sims NA. Molecular mechanisms in coupling of bone formation to resorption. Critical reviews in eukaryotic gene expression. 2009;19:73-88.
[13] Martin TJ, Sims NA. Osteoclast-derived activity in the coupling of bone formation to resorption. Trends in molecular medicine. 2005;11:76-81.
[14] Bougioukli S, Jain A, Sugiyama O, Tinsley BA, Tang AH, Tan MH, et al. Combination therapy with BMP-2 and a systemic RANKL inhibitor enhances bone healing in a mouse critical-sized femoral defect. Bone. 2015;84:93-103.
[15] Jensen ED, Pham L, Billington CJ, Jr., Espe K, Carlson AE, Westendorf JJ, et al. Bone morphogenic protein 2 directly enhances differentiation of murine osteoclast precursors. Journal of cellular biochemistry. 2010;109:672-82.
[16] Teitelbaum SL. Bone resorption by osteoclasts. Science.

2000;289:1504-8.
[17] Boyce BF, Xing L. Biology of RANK, RANKL, and osteoprotegerin. Arthritis research & therapy. 2007;9 Suppl 1:S1.
[18] Ulsamer A, Ortuno MJ, Ruiz S, Susperregui AR, Osses N, Rosa JL, et al. BMP-2 induces Osterix expression through up-regulation of Dlx5 and its phosphorylation by p38. J Biol Chem 2008;283:3816-26.
[19] Noth U, Tuli R, Seghatoleslami R, Howard M, Shah A, Hall DJ, et al. Activation of p38 and Smads mediates BMP-2 effects on human trabecular bone-derived osteoblasts. Exp Cell Res 2003;291:201-11.
[20] Kamiya N, Kobayashi T, Mochida Y, Yu PB, Yamauchi M, Kronenberg HM, et al. Wnt inhibitors Dkk1 and Sost are downstream targets of BMP signaling through the type IA receptor (BMPRIA) in osteoblasts. J Bone Miner Res 2010;25:200-10.
[21] Zimmerman, L.B., De Jesus-Escobar, J.M., and Harland, R.M. The Spemann organizer signal noggin binds and inactivates bone morphogenetic protein 4. Cell 86, 599, 1996.
[22] Li X, Zhang Y, Kang H, Liu W, Liu P, Zhang J, et al. Sclerostin binds to LRP5/6 and antagonizes canonical Wnt signaling. J Biol Chem 2005;280:19883-7.
[23] Kamiya N, Ye L, Kobayashi T, Mochida Y, Yamauchi M, Kronenberg HM, et al. BMP signaling negatively regulates bone mass through sclerostin by inhibiting the canonical Wnt pathway. Development. 2008;135:3801-11.
[24] Glass 2nd DA, Bialek P, Ahn JD, Starbuck M, Patel MS, Clevers H, et al. Canonical Wnt signaling in differentiated osteoblasts controls osteoclast differentiation. Dev Cell 2005;8:751-64.
[25] Boyce BF, Schwarz EM, Xing L. Osteoclast precursors: cytokine-stimulated immunomodulators of inflammatory bone disease.

Curr Opin Rheumatol 2006;18:427-32.
[26] Wada T, Nakashima T, Hiroshi N, Penninger JM. RANKL-RANK signaling in osteoclastogenesis and bone disease. Trends Mol Med 2006;12:17-25.
[27] Sharma SM, Hu R, Bronisz A, Meadows N, Lusby T, Fletcher B, et al. Genetics and genomics of osteoclast differentiation: integrating cell signaling pathways and gene networks. Crit Rev Eukar Gene 2006;16:253-77.
[28] Dougall WC, Glaccum M, Charrier K, Rohrbach K, Brasel K, De Smedt T, et al. RANK is essential for osteoclast and lymph node development. Genes & development. 1999;13:2412-24.
[29] Itoh K, Udagawa N, Katagiri T, Iemura S, Ueno N, Yasuda H, et al. Bone morphogenetic protein 2 stimulates osteoclast differentiation and survival supported by receptor activator of nuclear factor-kappaB ligand. Endocrinology. 2001;142:3656-62.
[30] Takayanagi H, Ogasawara K, Hida S, Chiba T, Murata S, Sato K, et al. T-cell-mediated regulation of osteoclastogenesis by signalling cross-talk between RANKL and IFN-gamma. Nature. 2000;408:600-5.
[31] Kostenuik PJ. Osteoprotegerin and RANKL regulate bone resorption, density, geometry and strength. Current opinion in pharmacology. 2005;5:618-25.
[32] Jin Q, Cirelli JA, Park CH, Sugai JV, Taba M, Jr., Kostenuik PJ, et al. RANKL inhibition through osteoprotegerin blocks bone loss in experimental periodontitis. Journal of periodontology. 2007;78:1300-8.
[33] Boyce BF, Xing L. Functions of RANKL/RANK/OPG in bone modeling and remodeling. Archives of biochemistry and biophysics. 2008;473:139-46.
[34] Kostenuik PJ, Nguyen HQ, McCabe J, Warmington KS, Kurahara

C, Sun N, et al. Denosumab, a fully human monoclonal antibody to RANKL, inhibits bone resorption and increases BMD in knock-in mice that express chimeric (murine/human) RANKL. Journal of bone and mineral research : the official journal of the American Society for Bone and Mineral Research. 2009;24:182-95.
[35] Ominsky MS, Stouch B, Schroeder J, Pyrah I, Stolina M, Smith SY, et al. Denosumab, a fully human RANKL antibody, reduced bone turnover markers and increased trabecular and cortical bone mass, density, and strength in ovariectomized cynomolgus monkeys. Bone. 2011;49:162-73.
[36] Dempster DW, Lambing CL, Kostenuik PJ, Grauer A. Role of RANK ligand and denosumab, a targeted RANK ligand inhibitor, in bone health and osteoporosis: a review of preclinical and clinical data. Clinical therapeutics. 2012;34:521-36.
[37] Wiley SR, Schooley K, Smolak PJ, Din WS, Huang CP, Nicholl JK, et al. Identification and characterization of a new member of the TNF family that induces apoptosis. Immunity. 1995;3:673-82.
[38] Schwarz EM, Ritchlin CT. Clinical development of anti-RANKL therapy. Arthritis research & therapy. 2007;9 Suppl 1:S7.
[39] Tsai HY, Lin HY, Fong YC, Wu JB, Chen YF, Tsuzuki M, et al. Paeonol inhibits RANKL-induced osteoclastogenesis by inhibiting ERK, p38 and NF-kappaB pathway. European journal of pharmacology. 2008;588:124-33.
[40] He X, Andersson G, Lindgren U, Li Y. Resveratrol prevents RANKL-induced osteoclast differentiation of murine osteoclast progenitor RAW 264.7 cells through inhibition of ROS production. Biochemical and biophysical research communications. 2010;401:356-62.
[41] Lewiecki EM. New targets for intervention in the treatment of postmenopausal osteoporosis. Nat Rev Rheumatol 2011;7:631 - 8

[42] Costa AG, Bilezikian JP, Lewiecki EM. Update on romosozumab: a humanizedmonoclonal antibody to sclerostin. Expert Opin Biol Ther 2014;14:697 - 707.
[43] Ke HZ, Richards WG, Li X, Ominsky MS. Sclerostin and Dickkopf-1 as therapeutictargets in bone diseases. Endocr Rev 2012;33:747 - 83.
[44] Takayanagi H. The role of NFAT in osteoclast formation. Annals of the New York Academy of Sciences. 2007;1116:227-37.
[45] Huang H, Chang EJ, Ryu J, Lee ZH, Lee Y, Kim HH. Induction of c-Fos and NFATc1 during RANKL-stimulated osteoclast differentiation is mediated by the p38 signaling pathway. Biochemical and biophysical research communications. 2006;351:99-105.
[46] Huang H, Ryu J, Ha J, Chang EJ, Kim HJ, Kim HM, et al. Osteoclast differentiation requires TAK1 and MKK6 for NFATc1 induction and NF-kappaB transactivation by RANKL. Cell death and differentiation. 2006;13:1879-91.
[47] Zhao Q, Wang X, Liu Y, He A, Jia R. NFATc1: functions in osteoclasts. The international journal of biochemistry & cell biology. 2010;42:576-9.
[48] Song I, Kim JH, Kim K, Jin HM, Youn BU, Kim N. Regulatory mechanism of NFATc1 in RANKL-induced osteoclast activation. FEBS letters. 2009;583:2435-40.
[49] Kim K, Kim JH, Lee J, Jin HM, Lee SH, Fisher DE, et al. Nuclear factor of activated T cells c1 induces osteoclast-associated receptor gene expression during tumor necrosis factor-related activation-induced cytokine-mediated osteoclastogenesis. The Journal of biological chemistry. 2005;280:35209-16.
[50] Zhou S, Glowacki J, Yates KE. Comparison of TGF-beta/BMP pathways signaled by demineralized bone powder and BMP-2 in

human dermal fibroblasts. Journal of bone and mineral research : the official journal of the American Society for Bone and Mineral Research. 2004;19:1732-41.
[51] Strobel C, Bormann N, Kadow-Romacker A, Schmidmaier G, Wildemann B. Sequential release kinetics of two (gentamicin and BMP-2) or three (gentamicin, IGF-I and BMP-2) substances from a one-component polymeric coating on implants. Journal of controlled release : official journal of the Controlled Release Society. 2011;156:37-45.
[52] Kempen DH, Lu L, Heijink A, Hefferan TE, Creemers LB, Maran A, et al. Effect of local sequential VEGF and BMP-2 delivery on ectopic and orthotopic bone regeneration. Biomaterials. 2009;30:2816-25.
[53] Eghbali-Fatourechi G, Khosla S, Sanyal A, Boyle WJ, Lacey DL, Riggs BL. Role of RANK ligand in mediating increased bone resorption in early postmenopausal women. The Journal of clinical investigation. 2003;111:1221-30.
[54] Falahati-Nini A, Riggs BL, Atkinson EJ, O'Fallon WM, Eastell R, Khosla S. Relative contributions of testosterone and estrogen in regulating bone resorption and formation in normal elderly men. The Journal of clinical investigation. 2000;106:1553-60.
[55] Khosla S, Melton LJ, 3rd, Atkinson EJ, O'Fallon WM, Klee GG, Riggs BL. Relationship of serum sex steroid levels and bone turnover markers with bone mineral density in men and women: a key role for bioavailable estrogen. The Journal of clinical endocrinology and metabolism. 1998;83:2266-74.
[56] Chow J, Tobias JH, Colston KW, Chambers TJ. Estrogen maintains trabecular bone volume in rats not only by suppression of bone resorption but also by stimulation of bone formation. The

Journal of clinical investigation. 1992;89:74-8.
[57] Bain SD, Bailey MC, Celino DL, Lantry MM, Edwards MW. High-dose estrogen inhibits bone resorption and stimulates bone formation in the ovariectomized mouse. Journal of bone and mineral research : the official journal of the American Society for Bone and Mineral Research. 1993;8:435-42.
[58] Nakamura T, Imai Y, Matsumoto T, Sato S, Takeuchi K, Igarashi K, et al. Estrogen prevents bone loss via estrogen receptor alpha and induction of Fas ligand in osteoclasts. Cell. 2007;130:811-23.
[59] Heino TJ, Hentunen TA, Vaananen HK. Osteocytes inhibit osteoclastic bone resorption through transforming growth factor-beta: enhancement by estrogen. Journal of cellular biochemistry. 2002;85:185-97.
[60] Hughes DE, Dai A, Tiffee JC, Li HH, Mundy GR, Boyce BF. Estrogen promotes apoptosis of murine osteoclasts mediated by TGF-beta. Nature medicine. 1996;2:1132-6.
[61] Weitzmann MN, Roggia C, Toraldo G, Weitzmann L, Pacifici R. Increased production of IL-7 uncouples bone formation from bone resorption during estrogen deficiency. The Journal of clinical investigation. 2002;110:1643-50.
[62] Hofbauer LC, Khosla S, Dunstan CR, Lacey DL, Spelsberg TC, Riggs BL. Estrogen stimulates gene expression and protein production of osteoprotegerin in human osteoblastic cells. Endocrinology. 1999;140:4367-70.
[63] Mirza FS, Padhi ID, Raisz LG, Lorenzo JA. Serum sclerostin levels negatively correlate with parathyroid hormone levels and free estrogen index in postmenopausal women. The Journal of clinical endocrinology and metabolism. 2010;95:1991-7.
[64] Cidem M, Usta TA, Karacan I, Kucuk SH, Uludag M, Gun K.

Effects of sex steroids on serum sclerostin levels during the menstrual cycle. Gynecologic and obstetric investigation. 2013;75:179-84.
[65] Modder UI, Clowes JA, Hoey K, Peterson JM, McCready L, Oursler MJ, et al. Regulation of circulating sclerostin levels by sex steroids in women and in men. Journal of bone and mineral research : the official journal of the American Society for Bone and Mineral Research. 2011;26:27-34.
[66] Hannon R, Blumsohn A, Naylor K, Eastell R. Response of biochemical markers of bone turnover to hormone replacement therapy: impact of biological variability. Journal of bone and mineral research : the official journal of the American Society for Bone and Mineral Research. 1998;13:1124-33.
[67] Modder UI, Roforth MM, Hoey K, McCready LK, Peterson JM, Monroe DG, et al. Effects of estrogen on osteoprogenitor cells and cytokines/bone-regulatory factors in postmenopausal women. Bone. 2011;49:202-7.
[68] Wijenayaka AR, Kogawa M, Lim HP, Bonewald LF, Findlay DM, Atkins GJ. Sclerostin stimulates osteocyte support of osteoclast activity by a RANKL-dependent pathway. PloS one. 2011;6:e25900.
[69] Bellido T, Roodman GDD. Direct Cell-To-Cell Interactions Between Osteocytes and Multiple Myeloma (MM) Cells Upregulate Sost and Downregulate OPG Expression In Osteocytes: Evidence For Osteocytic Contributions To MM-Induced Bone Disease. Blood. 2013;122:3140-.
[70] Ominsky MS, Vlasseros F, Jolette J, Smith SY, Stouch B, Doellgast G, et al. Two doses of sclerostin antibody in cynomolgus monkeys increases bone formation, bone mineral density, and bone strength. Journal of bone and mineral research : the official journal of

the American Society for Bone and Mineral Research. 2010;25:948-59.
[71] Ominsky MS, Niu QT, Li C, Li X, Ke HZ. Tissue-level mechanisms responsible for the increase in bone formation and bone volume by sclerostin antibody. Journal of bone and mineral research : the official journal of the American Society for Bone and Mineral Research. 2014;29:1424-30.
[72] Li X, Ominsky MS, Warmington KS, Morony S, Gong J, Cao J, et al. Sclerostin antibody treatment increases bone formation, bone mass, and bone strength in a rat model of postmenopausal osteoporosis. Journal of bone and mineral research : the official journal of the American Society for Bone and Mineral Research. 2009;24:578-88.
[73] Li X, Warmington KS, Niu QT, Asuncion FJ, Barrero M, Grisanti M, et al. Inhibition of sclerostin by monoclonal antibody increases bone formation, bone mass, and bone strength in aged male rats. Journal of bone and mineral research : the official journal of the American Society for Bone and Mineral Research. 2010;25:2647-56.
[74] Ominsky MS, Li C, Li X, Tan HL, Lee E, Barrero M, et al. Inhibition of sclerostin by monoclonal antibody enhances bone healing and improves bone density and strength of nonfractured bones. Journal of bone and mineral research : the official journal of the American Society for Bone and Mineral Research. 2011;26:1012-21.
[75] Keller H, Kneissel M. SOST is a target gene for PTH in bone. Bone. 2005;37:148-58.
[76] Kamiya N. The role of BMPs in bone anabolism and their potential targets SOST and DKK1. Current molecular pharmacology. 2012;5:153-63.
[77] Sutherland MK, Geoghegan JC, Yu C, Winkler DG, Latham JA. Unique regulation of SOST, the sclerosteosis gene, by BMPs and

steroid hormones in human osteoblasts. Bone. 2004;35:448-54.
[78] Sutherland MK, Geoghegan JC, Yu C, Turcott E, Skonier JE, Winkler DG, et al. Sclerostin promotes the apoptosis of human osteoblastic cells: a novel regulation of bone formation. Bone. 2004;35:828-35.
[79] Kouzmenko AP, Takeyama K, Ito S, Furutani T, Sawatsubashi S, Maki A, et al. Wnt/beta-catenin and estrogen signaling converge in vivo. The Journal of biological chemistry. 2004;279:40255-8.
[80] Yamamoto T, Saatcioglu F, Matsuda T. Cross-talk between bone morphogenic proteins and estrogen receptor signaling. Endocrinology. 2002;143:2635-42.
[81] Zhang R, Oyajobi BO, Harris SE, Chen D, Tsao C, Deng HW, et al. Wnt/beta-catenin signaling activates bone morphogenetic protein 2 expression in osteoblasts. Bone. 2013;52:145-56.
[82] Hollinger JO, Uludag H, Winn SR. Sustained release emphasizing recombinant human bone morphogenetic protein-2. Advanced drug delivery reviews. 1998;31:303-18.
[83] Talwar R, Di Silvio L, Hughes FJ, King GN. Effects of carrier release kinetics on bone morphogenetic protein-2-induced periodontal regeneration in vivo. Journal of clinical periodontology. 2001;28:340-7.
[84] Hunziker EB, Enggist L, Kuffer A, Buser D, Liu Y. Osseointegration: the slow delivery of BMP-2 enhances osteoinductivity. Bone. 2012;51:98-106.
[85] Hernandez A, Sanchez E, Soriano I, Reyes R, Delgado A, Evora C. Material-related effects of BMP-2 delivery systems on bone regeneration. Acta biomaterialia. 2012;8:781-91.
[86] Uludag H, D'Augusta D, Palmer R, Timony G, Wozney J. Characterization of rhBMP-2 pharmacokinetics implanted with biomaterial carriers in the rat ectopic model. Journal of biomedical

materials research. 1999;46:193-202.
[87] Winn SR, Uludag H, Hollinger JO. Carrier systems for bone morphogenetic proteins. Clinical orthopaedics and related research. 1999:S95-106.
[88] Kempen DH, Lu L, Hefferan TE, Creemers LB, Maran A, Classic KL, et al. Retention of in vitro and in vivo BMP-2 bioactivities in sustained delivery vehicles for bone tissue engineering. Biomaterials. 2008;29:3245-52.
[89] Kirker-Head CA. Potential applications and delivery strategies for bone morphogenetic proteins. Advanced drug delivery reviews. 2000;43:65-92.
[90] Kim HD, Valentini RF. Retention and activity of BMP-2 in hyaluronic acid-based scaffolds in vitro. Journal of biomedical materials research. 2002;59:573-84.
[91] Woo BH, Fink BF, Page R, Schrier JA, Jo YW, Jiang G, et al. Enhancement of bone growth by sustained delivery of recombinant human bone morphogenetic protein-2 in a polymeric matrix. Pharmaceutical research. 2001;18:1747-53.
[92] Liu T, Wu G, Wismeijer D, Gu Z, Liu Y. Deproteinized bovine bone functionalized with the slow delivery of BMP-2 for the repair of critical-sized bone defects in sheep. Bone. 2013;56:110-8.
[93] Ruhe PQ, Boerman OC, Russel FG, Spauwen PH, Mikos AG, Jansen JA. Controlled release of rhBMP-2 loaded poly(dl-lactic-co-glycolic acid)/calcium phosphate cement composites in vivo. Journal of controlled release : official journal of the Controlled Release Society. 2005;106:162-71.
[94] Fu YC, Nie H, Ho ML, Wang CK, Wang CH. Optimized bone regeneration based on sustained release from three-dimensional fibrous PLGA/HAp composite scaffolds loaded with BMP-2.

Biotechnology and bioengineering. 2008;99:996-1006.
[95] Rahman CV, Ben-David D, Dhillon A, Kuhn G, Gould TW, Muller R, et al. Controlled release of BMP-2 from a sintered polymer scaffold enhances bone repair in a mouse calvarial defect model. Journal of tissue engineering and regenerative medicine. 2014;8:59-66.
[96] Jeon O, Song SJ, Kang SW, Putnam AJ, Kim BS. Enhancement of ectopic bone formation by bone morphogenetic protein-2 released from a heparin-conjugated poly(L-lactic-co-glycolic acid) scaffold. Biomaterials. 2007;28:2763-71.
[97] Ruppert R, Hoffmann E, Sebald W. Human bone morphogenetic protein 2 contains a heparin-binding site which modifies its biological activity. European journal of biochemistry / FEBS. 1996;237:295-302.
[98] Yang HS, La WG, Bhang SH, Jeon JY, Lee JH, Kim BS. Heparin-conjugated fibrin as an injectable system for sustained delivery of bone morphogenetic protein-2. Tissue engineering Part A. 2010;16:1225-33.
[99] Chung YI, Ahn KM, Jeon SH, Lee SY, Lee JH, Tae G. Enhanced bone regeneration with BMP-2 loaded functional nanoparticle-hydrogel complex. Journal of controlled release : official journal of the Controlled Release Society. 2007;121:91-9.
[100] Bhakta G, Rai B, Lim ZX, Hui JH, Stein GS, van Wijnen AJ, et al. Hyaluronic acid-based hydrogels functionalized with heparin that support controlled release of bioactive BMP-2. Biomaterials. 2012;33:6113-22.
[101] Geiger M, Li RH, Friess W. Collagen sponges for bone regeneration with rhBMP-2. Advanced drug delivery reviews. 2003;55:1613-29.
[102] Alonso N, Tanikawa DY, Freitas Rda S, Canan L, Jr., Ozawa TO, Rocha DL. Evaluation of maxillary alveolar reconstruction using

a resorbable collagen sponge with recombinant human bone morphogenetic protein-2 in cleft lip and palate patients. Tissue engineering Part C, Methods. 2010;16:1183-9.
[103] Bhakta G, Lim ZX, Rai B, Lin T, Hui JH, Prestwich GD, et al. The influence of collagen and hyaluronan matrices on the delivery and bioactivity of bone morphogenetic protein-2 and ectopic bone formation. Acta biomaterialia. 2013;9:9098-106.

[104] Shields LB, Raque GH, Glassman SD, Campbell M, Vitaz T, Harpring J, et al. Adverse effects associated with high-dose recombinant human bone morphogenetic protein-2 use in anterior cervical spine fusion. Spine (Phila Pa 1976). 2006;31:542-7.

[105] Neovius E, Lemberger M, Docherty Skogh AC, Hilborn J, Engstrand T. Alveolar bone healing accompanied by severe swelling in cleft children treated with bone morphogenetic protein-2 delivered by hydrogel. J Plast Reconstr Aesthet Surg. 2013;66:37-42.
[106] Brown KV, Li B, Guda T, Perrien DS, Guelcher SA, Wenke JC. Improving bone formation in a rat femur segmental defect by controlling bone morphogenetic protein-2 release. Tissue Eng Part A. 2011;17:1735-46.
[107] Koo KH, Lee JM, Ahn JM, Kim BS, La WG, Kim CS, et al. Controlled delivery of low-dose bone morphogenetic protein-2 using heparin-conjugated fibrin in the posterolateral lumbar fusion of rabbits. Artif Organs. 2013;37:487-94.
[108] Smucker JD, Rhee JM, Singh K, Yoon ST, Heller JG. Increased swelling complications associated with off-label usage of rhBMP-2 in the anterior cervical spine. Spine (Phila Pa 1976). 2006;31:2813-9.
[109] Irie A, Takami M, Kubo H, Sekino-Suzuki N, Kasahara K, Sanai Y. Heparin enhances osteoclastic bone resorption by inhibiting

osteoprotegerin activity. Bone. 2007;41:165-74.
[110] Kim SE, Song SH, Yun YP, Choi BJ, Kwon IK, Bae MS, et al. The effect of immobilization of heparin and bone morphogenic protein-2 (BMP-2) to titanium surfaces on inflammation and osteoblast function. Biomaterials. 2011;32:366-73.
[111] Lee DW, Yun YP, Park K, Kim SE. Gentamicin and bone morphogenic protein-2 (BMP-2)-delivering heparinized-titanium implant with enhanced antibacterial activity and osteointegration. Bone. 2012;50:974-82.
[112] Shen H, Hu X, Yang F, Bei J, Wang S. Cell affinity for bFGF immobilized heparin-containing poly(lactide-co-glycolide) scaffolds. Biomaterials. 2011;32:3404-12.
[113] Yang HS, La WG, Cho YM, Shin W, Yeo GD, Kim BS. Comparison between heparin-conjugated fibrin and collagen sponge as bone morphogenetic protein-2 carriers for bone regeneration. Exp Mol Med. 2012;44:350-5.
[114] Johnson MR, Boerckel JD, Dupont KM, Guldberg RE. Functional restoration of critically sized segmental defects with bone morphogenetic protein-2 and heparin treatment. Clin Orthop Relat Res. 2011;469:3111-7.
[115] Kim RY, Oh JH, Lee BS, Seo YK, Hwang SJ, Kim IS. The effect of dose on rhBMP-2 signaling, delivered via collagen sponge, on osteoclast activation and in vivo bone resorption. Biomaterials. 2014;35:1869-81.
[116] Kim IS, Lee EN, Cho TH, Song YM, Hwang SJ, Oh JH, et al. Promising efficacy of Escherichia coli recombinant human bone morphogenetic protein-2 in collagen sponge for ectopic and orthotopic bone formation and comparison with mammalian cell recombinant human bone morphogenetic protein-2. Tissue Eng Part A.

2011;17:337-48.
[117] Shah DK, Doyle LW, Anderson PJ, Bear M, Daley AJ, Hunt RW, et al. Adverse neurodevelopment in preterm infants with postnatal sepsis or necrotizing enterocolitis is mediated by white matter abnormalities on magnetic resonance imaging at term. J Pediatr. 2008;153:170-5, 5 e1.
[118] Seeherman HJ, Li XJ, Bouxsein ML, Wozney JM. rhBMP-2 induces transient bone resorption followed by bone formation in a nonhuman primate core-defect model. J Bone Joint Surg Am. 2010;92:411-26.
[119] Seeherman H, Li R, Bouxsein M, Kim H, Li XJ, Smith-Adaline EA, et al. rhBMP-2/calcium phosphate matrix accelerates osteotomy-site healing in a nonhuman primate model at multiple treatment times and concentrations. J Bone Joint Surg Am. 2006;88:144-60.
[120] Hakeda Y, Kobayashi Y, Yamaguchi K, Yasuda H, Tsuda E, Higashio K, et al. Osteoclastogenesis inhibitory factor (OCIF) directly inhibits bone-resorbing activity of isolated mature osteoclasts. Biochem Biophys Res Commun. 1998;251:796-801.
[121] Kwan Tat S, Padrines M, Theoleyre S, Heymann D, Fortun Y. IL-6, RANKL, TNF-alpha/IL-1: interrelations in bone resorption pathophysiology. Cytokine Growth Factor Rev. 2004;15:49-60.
[122] Hofbauer LC, Dunstan CR, Spelsberg TC, Riggs BL, Khosla S. Osteoprotegerin production by human osteoblast lineage cells is stimulated by vitamin D, bone morphogenetic protein-2, and cytokines. Biochem Biophys Res Commun. 1998;250:776-81.
[123] Sato MM, Nakashima A, Nashimoto M, Yawaka Y, Tamura M. Bone morphogenetic protein-2 enhances Wnt/beta-catenin signaling-induced osteoprotegerin expression. Genes Cells.

2009;14:141-53.
[124] Kim RY, Yang HJ, Song YM, Kim IS, Hwang SJ. Estrogen Modulates Bone Morphogenetic Protein-Induced Sclerostin Expression Through the Wnt Signaling Pathway. Tissue Eng Part A. 2015;21:2076-88.
[125] Linde A, Hedner E. Recombinant bone morphogenetic protein-2 enhances bone healing, guided by osteopromotive e-PTFE membranes: an experimental study in rats. Calcif Tissue Int. 1995;56:549-53.
[126] Zellin G, Linde A. Importance of delivery systems for growth-stimulatory factors in combination with osteopromotive membranes. An experimental study using rhBMP-2 in rat mandibular defects. J Biomed Mater Res. 1997;35:181-90.
[127] Luginbuehl V, Meinel L, Merkle HP, Gander B. Localized delivery of growth factors for bone repair. Eur J Pharm Biopharm. 2004;58:197-208.
[128] Li RH, Wozney JM. Delivering on the promise of bone morphogenetic proteins. Trends Biotechnol. 2001;19:255-65.
[129] Seo YK, Song KY, Kim YJ, Park JK. Wound healing effect of acellular artificial dermis containing extracellular matrix secreted by human skin fibroblasts. Artif Organs 2007;31:509-20.
[130] Abe E, Yamamoto M, Taguchi Y, Lecka-Czernik B, O'Brien CA, Economides AN, et al. Essential requirement of BMPs-2/4 for both osteoblast and osteoclast formation in murine bone marrow cultures from adult mice: antagonism by noggin. J Bone Miner Res 2000;15:663-73.
[131] Kanatani M, Sugimoto T, Kaji H, Kobayashi T, Nishiyama K, Fukase M, et al. Stimulatory effect of bone morphogenetic protein-2 on osteoclast-like cell formation and bone-resorbing activity. J Bone

Miner Res 1995;10:1681-90.
[132] Okamoto M, Murai J, Yoshikawa H, Tsumaki N. Bone morphogenetic proteins in bone stimulate osteoclasts and osteoblasts during bone development. J Bone Miner Res 2006;21:1022-33.
[133] Miyazono K, Maeda S, Imamura T. BMP receptor signaling: transcriptional targets, regulation of signals, and signaling cross-talk. Cytokine Growth Factor Rev 2005;16:251-63.
[134] Leboy PS. Regulating bone growth and development with bone morphogenetic proteins. Ann N Y Acad Sci 2006;1068:14-8.
[135] Gautschi OP, Frey SP, Zellweger R. Bone morphogenetic proteins in clinical applications. Aust Nz J Surg 2007;77:626-31.
[136] King WJ, Krebsbach PH. Growth factor delivery: how surface interactions modulate release in vitro and in vivo. Adv Drug Deliv Rev 2012;64:1239-56.
[137] Toth JM, Boden SD, Burkus JK, Badura JM, Peckham SM, McKay WF. Shortterm osteoclastic activity induced by locally high concentrations of recombinant human bone morphogenetic protein-2 in a cancellous bone environment. Spine 2009;34:539-50.
[138] Sciadini MF, Johnson KD. Evaluation of recombinant human bone morphogenetic protein-2 as a bone-graft substitute in a canine segmental defect model. J Orthop Res 2000;18:289-302.
[139] Katagiri T, Yamaguchi A, Komaki M, Abe E, Takahashi N, Ikeda T, et al. Bone morphogenetic protein-2 converts the differentiation pathway of C2C12 myoblasts into the osteoblast lineage. J Cell Biol 1994;127:1755-66.
[140] Kim IS, Song YM, Cho TH, Park YD, Lee KB, Noh I, et al. In vitro response of primary human bone marrow stromal cells to recombinant humanbbone morphogenic protein-2 in the early and late stages of osteoblast differentiation. Dev Growth Differ 2008;50:553-64.

[141] Wan M, Cao X. BMP signaling in skeletal development. Biochem Biophys Res Commun 2005;328:651-7.
[142] Zhang F, Qiu T, Wu X, Wan C, Shi W, Wang Y, et al. Sustained BMP signaling in osteoblasts stimulates bone formation by promoting angiogenesis and osteoblast differentiation. J Bone Miner Res 2009;24:1224-33.
[143] Ito Y, Miyazono K. RUNX transcription factors as key targets of TGF-beta superfamily signaling. Curr Opin Genet Dev 2003;13:43-7.
[144] Tang W, Yang F, Li Y, de Crombrugghe B, Jiao H, Xiao G, et al. Transcriptional regulation of Vascular Endothelial Growth Factor (VEGF) by osteoblastspecific transcription factor Osterix (Osx) in osteoblasts. J Biol Chem 2012;287:1671-8.
[145] Saftig P, Hunziker E, Wehmeyer O, Jones S, Boyde A, Rommerskirch W, et al. Impaired osteoclastic bone resorption leads to osteopetrosis in cathepsin-Kdeficient mice. Proc Natl Acad Sci U S A 1998;95:13453-8.
[146] Miyaji H, Sugaya T, Kato K, Kawamura N, Tsuji H, Kawanami M. Dentin resorption and cementum-like tissue formation by bone morphogenetic protein application. J Periodontal Res 2006;41:311-5.
[147] Takayanagi H, Kim S, Koga T, Nishina H, Isshiki M, Yoshida H, et al. Induction and activation of the transcription factor NFATc1 (NFAT2) integrate RANKL signaling in terminal differentiation of osteoclasts. Developmental cell. 2002;3:889-901.
[148] Winslow MM, Pan M, Starbuck M, Gallo EM, Deng L, Karsenty G, et al. Calcineurin/NFAT signaling in osteoblasts regulates bone mass. Dev Cell 2006;10:771-82.
[149] Zhao Q, Wang X, Liu Y, He A, Jia R. NFATc1: functions in

osteoclasts. Int J Biochem Cell Biol 2010;42:576-9.
[150] Asagiri M, Sato K, Usami T, Ochi S, Nishina H, Yoshida H, et al. Autoamplification of NFATc1 expression determines its essential role in bone homeostasis. J Exp Med 2005;202:1261-9.
[151] Koga T, Matsui Y, Asagiri M, KodamT, de Crombrugghe B, Nakashima K, et al. NFAT and Osterix cooperatively regulate bone formation. Nat Med 2005;11:880-5.
[152] Aramburu J, Yaffe MB, Lopez-Rodriguez C, Cantley LC, Hogan PG, Rao A. Affinity-driven peptide selection of an NFAT inhibitor more selective than cyclosporin A. Science 1999;285:2129-33.
[153] Hsu EL, Ghodasra JH, Ashtekar A, Nickoli MS, Lee SS, Stupp SI, et al. A comparative evaluation of factors influencing osteoinductivity among scaffolds designed for bone regeneration. Tissue Eng Part A 2013;19:1764-72.
[154] Kearns AE, Khosla S, Kostenuik PJ. Receptor activator of nuclear factor kappaB igand and osteoprotegerin regulation of bone remodeling in health and disease. Endocr Rev 2008;29:155-92.
[155] Lacey DL, Boyle WJ, Simonet WS, Kostenuik PJ, Dougall WC, Sullivan JK, et al. Bench to bedside: elucidation of the OPG-RANK-RANKL pathway and the development of denosumab. Nat Rev Drug Discov 2012;11:401-19.
[156] Caterson, E.J., Nesti, L.J., Danielson, K.G., and Tuan, R.S. Human marrow-derived mesenchymal progenitor cells: isolation, culture expansion, and analysis of differentiation. Mol Biotechnol 20, 245, 2002.
[157] Zhao, J.W., Gao, Z.L., Mei, H., Li, Y.L., and Wang, Y. Differentiation of human mesenchymal stem cells: the potential mechanism for estrogen-induced preferential osteoblast versus adipocyte differentiation. Am J Med Sci 341, 460, 2011.

[158] Kousteni, S., Almeida, M., Han, L., Bellido, T., Jilka, R.L., and Manolagas, S.C. Induction of osteoblast differentiation by selective activation of kinase-mediated actions of the estrogen receptor. Mol Cell Biol 27, 1516, 2007.
[159] Wakeling, A.E. Similarities and distinctions in the mode of action of different classes of antioestrogens. Endocr Relat Cancer 7, 17, 2000.
[160] Yu, P.B., Hong, C.C., Sachidanandan, C., Babitt, J.L., Deng, D.Y., Hoyng, S.A., Lin, H.Y., Bloch,K.D., and Peterson, R.T. Dorsomorphin inhibits BMP signals required for embryogenesis and iron metabolism. Nat Chem Biol 4, 33, 2008.
[161] Li, X., Zhang, Y., Kang, H., Liu, W., Liu, P., Zhang, J., Harris, S.E., and Wu, D. Sclerostin binds to LRP5/6 and antagonizes canonical Wnt signaling. J Biol Chem 280, 19883, 2005.
[162] van Bezooijen, R.L., Svensson, J.P., Eefting, D., Visser, A., van der Horst, G., Karperien, M., Quax, P.H., Vrieling, H., Papapoulos, S.E., ten Dijke, P., and Lowik, C.W. Wnt but not BMP signaling is involved in the inhibitory action of sclerostin on BMP-stimulated bone formation. J Bone Miner Res 22, 19, 2007.
[163] Balemans,W., Ebeling, M., Patel, N., Van Hul, E., Olson, P., Dioszegi, M., Lacza, C., Wuyts, W., Van Den Ende, J., Willems, P., Paes-Alves, A.F., Hill, S., Bueno, M., Ramos, F.J.,Tacconi, P., Dikkers, F.G., Stratakis,C., Lindpaintner,K., Vickery, B., Foernzler, D., and Van Hul, W. Increased bone density in sclerosteosis is due to the deficiency of a novel secreted protein (SOST). Hum Mol Genet 10, 537, 2001.
[164] Balemans, W., Patel, N., Ebeling, M., Van Hul, E., Wuyts, W., Lacza, C., Dioszegi, M., Dikkers, F.G., Hildering, P., Willems, P.J., Verheij, J.B., Lindpaintner, K., Vickery, B., Foernzler, D., and Van

Hul, W. Identification of a 52 kb deletion downstream of the SOST gene in patients with van Buchem disease. J Med Genet 39, 91, 2002.
[165] Yanagi, Y., Suzawa, M., Kawabata, M., Miyazono, K., Yanagisawa, J., and Kato, S. Positive and negative modulation of vitamin D receptor function by transforming growth factor-beta signaling through smad proteins. J Biol Chem 274, 12971, 1999.
[166] Almeida, M., Martin-Millan, M., Ambrogini, E., Bradsher, R., 3rd, Han, L., Chen, X.D., Roberson, P.K., Weinstein, R.S., O'Brien, C.A., Jilka, R.L., and Manolagas, S.C. Estrogens attenuate oxidative stress and the differentiation and apoptosis of osteoblasts by DNA-binding-independent actions of the ERalpha. J Bone Miner Res 25, 769, 2010.
[167] Bhukhai, K., Suksen, K., Bhummaphan, N., Janjorn, K., Thongon, N., Tantikanlayaporn, D., Piyachaturawat, P., Suksamrarn, A., and Chairoungdua, A. A phytoestrogen diarylheptanoid mediates estrogen receptor/Akt/glycogen synthase kinase 3beta protein-dependent activation of the Wnt/beta-catenin signaling pathway. J Biol Chem 287, 36168, 2012.
[168] Mbalaviele, G., Sheikh, S., Stains, J.P., Salazar, V.S., Cheng, S. L., Chen, D., and Civitelli, R. Beta-catenin and BMP-2 synergize to promote osteoblast differentiation and new bone formation. J Cell Biochem 94, 403, 2005.
[169] McCarthy, T.L., Kallen, C.B., and Centrella, M. Betacatenin independent cross-control between the estradiol and Wnt pathways in osteoblasts. Gene 479, 16, 2011.
[170] Nakashima, A., Katagiri, T., and Tamura, M. Cross-talk between Wnt and bone morphogenetic protein 2 (BMP-2) signaling in differentiation pathway of C2C12 myoblasts. J Biol Chem 280, 37660, 2005.

Table 1. Rat oligonucleotide primers used for real time RT-PCR

Target gene	GenBank Accession Nr.	Sequences		Expected size (bp)
		Forward (5'-3')	Reverse (5'-3')	
b-acin	BC063166	CCT GAG GAG CAC CCT GTG CTG CT	CAA CAC AGC CTG GAT GGC TAC GT	129
ALP	NM013059	ATG TCT GGA ACC GCA CTG AAC	TTC TTT GTC AGG ATC CGG AGG	166
VEGF	BC168708	TTT CTC CGC TCT GAA CAA GGC	TGC AGA TCA TGC GGA TCA AAC	142
Osterix	AY177399	AGC TCT TCT GAC TGC CTG CCT AGT	TTG GGC TTA TAG ACA TCT TGG GGT	347
Cbfa 1	AB1145746	ACC ATG GTG GAG ATC ATC GC	GCC ATG ACG GTA ACC ACG G	173
Trap	NM019144	ACT TCC CCA GCC CTT ACT ACC G	TCA GCA CAT AGC CCA CAC CG	381
cathepsin K	NM031560.2	CTT GTG GAC TGT GTG ACT	AAC ACT GCA TGG TTC ACA	338
NFAT c1	NM001244933.1	GGC ATC TCA GCT GTT CCT TC	ACG TCT TCC ACC TCC ACA TC	206
c-Fos	NM022197.2	TCA CCC TGC CTC TTC TCA AT	GAA GGA ACC AGA CAG GTC CA	179
RANKL	NM057149.1	ACT CTG GAG AGC GAA GAC ACA GAA	ATC AGG TTA TGC GAA CTT GGG ATT	461
OPG	NM012870.2	GGA GAG TGA GGC AGG CTA TTT GA	CTA CAA ATG GGA TAA GGC TCG TG	375
OCN	M23637.1	AAA GCC CAG CGACTC TC	CTA AAC GGT GGT GCC ATA GAT	99
OPN	AB001382	CGA CGG CCG AGG TGA TAG CTT	CAT GGC TGG TCT TCC CGT TGC C	317

Primers are designed according to rat sequence of each gene. Abbreviations: *ALP, alkaline phosphatase*; *VEGF, vascular endothelial growth factor* ; *Cbfa 1, core binding factor a1; Trap, Tartrate-resistant acid phosphatase; NFATc1, Nuclear factor of activated T-cells; RANKL, Nuclear factor kappa-B ligand; OPG, osteoprotegerin; OCN, osteocalcin; OPN, osteopontin*

Table 2. Quantitative analysis of new bone using 3D mCT

A. Central defect region

	Weeks	ACS-CON	ACS-BMP	HCS-CON	HCS-BMP
BV/real defect (%)	4	9.51±1.24	13.66±2.50	70.93±12.79**	88.33±10.09**
	8	11.61±1.40	19.34±1.29	86.63±9.96**	113.23±11.57**
	12	22.77±3.23	21.70±4.78	126.89±5.26**	155.58±7.90**
BMD (g/cm^3)	4	1.14±0.00	1.15±0.01	1.21±0.02**	1.23±0.01**
	8	1.15±0.00	1.15±0.00	1.25±0.01**	1.28±0.01**
	12	1.17±0.01	1.16±0.01	1.33±0.01**	1.36±0.01**
Tb.Sp (mm)	4	1.68±0.10	1.30±0.13	1.21±0.17**	1.09±0.14
	8	1.19±0.05	1.61±0.12	0.91±0.12	0.78±0.10**
	12	1.40±0.11	0.97±0.06	0.60±0.03**	0.53±0.03**
Tb.N (mm^{-1})	4	0.07±0.01	0.11±0.02	0.73±0.15**	0.85±0.09**
	8	0.08±0.01	0.13±0.01	0.62±0.07**	1.00±0.14**
	12	0.12±0.01	0.16±0.03	0.79±0.03**	1.06±0.04**
Tb.Th (mm)	4	0.44±0.02	0.39±0.01	0.31±0.01**	0.32±0.01**
	8	0.42±0.03	0.44±0.02	0.43±0.01	0.35±0.02**
	12	0.60±0.04	0.41±0.03	0.49±0.01	0.45±0.03*

B. Full region

	Weeks	ACS-CON	HCS-CON	ACS-BMP	HCS-BMP
BV/TV (%)	4	3.62±0.46	3.74±0.47	22.54±0.86**	18.51±1.69**
	8	2.97±0.40	5.12±0.40	32.11±2.50**	27.34±2.28**
	12	6.00±0.57	16.44±1.86	33.92±2.08**	39.80±3.35**
TV (mm^3)	4	97.66±8.07	144.24±7.41	241.56±23.13**	197.42±6.21**
	8	170.31±12.83	138.68±3.54	169.26±13.25	189.77±15.02**
	12	141.20±8.06	74.92±4.82	140.07±3.28	148.76±6.16**
BMD (g/cm^3)	4	1.14±0.00	1.15±0.01	1.21±0.00**	1.22±0.01**
	8	1.14±0.00	1.16±0.00	1.28±0.01**	1.27±0.01**
	12	1.16±0.00	1.22±0.01	1.30±0.01**	1.32±0.02**
Tb.Sp (mm)	4	1.26±0.06	1.30±0.12	1.16±0.11	1.29±0.09
	8	1.50±0.09	1.57±0.20	0.75±0.06**	1.14±0.15*
	12	1.54±0.04	0.56±0.03	0.70±0.05**	0.69±0.08
Tb.N (mm^{-1})	4	0.08±0.01	0.10±0.01	0.77±0.05**	0.74±0.06**
	8	0.06±0.01	0.12±0.01	0.79±0.08**	0.87±0.10**
	12	0.10±0.01	0.36±0.04	0.69±0.03**	0.88±0.05**
Tb.Th (mm)	4	0.47±0.03	0.39±0.01	0.30±0.01**	0.25±0.01**
	8	0.46±0.05	0.43±0.03	0.41±0.02	0.32±0.02*
	12	0.60±0.04	0.46±0.03	0.49±0.01*	0.46±0.03

Table 3. Rat oligonucleotide primers used for real time RT-PCR

Target gene	GenBank Accession Nr.	Sequences		Expected size (bp)
		Forward (5'-3')	Reverse (5'-3')	
b-acin	BC063166	CCT GAG GAG CAC CCT GTG CTG CT	CAA CAC AGC CTG GAT GGC TAC GT	129
ALP	NM013059	ATG TCT GGA ACC GCA CTG AAC	TTC TTT GTC AGG ATC CGG AGG	166
VEGF	BC168708	TTT CTC CGC TCT GAA CAA GGC	TGC AGA TCA TGC GGA TCA AAC	142
Osterix	AY177399	AGC TCT TCT GAC TGC CTG CCT AGT	TTG GGC TTA TAG ACA TCT TGG GGT	347
Cbfa 1	AB1145746	ACC ATG GTG GAG ATC ATC GC	GCC ATG ACG GTA ACC ACG G	173
Trap	NM019144	ACT TCC CCA GCC CTT ACT ACC G	TCA GCA CAT AGC CCA CAC CG	381
cathepsin K	NM031560.2	CTT GTG GAC TGT GTG ACT	AAC ACT GCA TGG TTC ACA	338
NFAT c1	NM001244933.1	GGC ATC TCA GCT GTT CCT TC	ACG TCT TCC ACC TCC ACA TC	206
c-Fos	NM022197.2	TCA CCC TGC CTC TTC TCA AT	GAA GGA ACC AGA CAG GTC CA	179
RANKL	NM057149.1	ACT CTG GAG AGC GAA GAC ACA GAA	ATC AGG TTA TGC GAA CTT GGG ATT	461
OPG	NM012870.2	GGA GAG TGA GGC AGG CTA TTT GA	CTA CAA ATG GGA TAA GGC TCG TG	375

Primers are designed according to rat sequence of each gene. Abbreviations: *ALP, alkaline phosphatase*; *VEGF, vascular endothelial growth factor* ; *Cbfa 1, core binding factor a1; Trap, Tartrate-resistant acid phosphatase* ; *NFATc1, Nuclear factor of activated T-cells; RANKL, Nuclear factor kappa-B ligand ;OPG, osteoprotegerin* ;

Table 4. Human oligonucleotide primers used for real time RT-PCR.

Target gene	GenBank Accession Nr.	Sequences		Expected size (bp)
		Forward (5'-3')	Reverse (5'-3')	
IGF1	M27544	TGG TGG ATG CTC TTC AGT TCG	TTA GAT CAC AGC TCC GGA AGC	135
BMP2	M22489	AAG CCA AAC ACA AAC AGC GG	TTC TCC GTG GCA GTA AAA GGC	137
OPG	U94332	ACG TCA AGC AGG AGT GCA ATC	CAG CTT GCA CCA CTC CAA ATC	126
RANKL	AF019047	CAG GGC GAC GCT GCA GAC AA	GCC GCG CCA GCA GAG ACT AC	194
SOST	NM025237	CCG GTT CAT GGT CTT GTT GT	GAG CCT GTG CTA CTG GAA GG	220
ALP	AH005272	ACC ATG AAG GAA AAG CCA AGC	CCA CCA AAT GTG AAG ACG TGG	142
18S rRNA	X01117.1	CGC GGT TCT ATT TTG TTG GT	AGT CGG CAT CGT TTA TGG TC	219

Abbreviations: *ALP*, alkaline phosphatase; *BMP2*, bone morphogenic protein-2; *IGF1,* insulin-like growth factor-1; *OPG,* osteoprotegerin; *RANKL*, receptor activator of nuclear factor kappa-B ligand; *SOST*, sclerostin; *18S rRNA,* 18S ribosomal RNA.

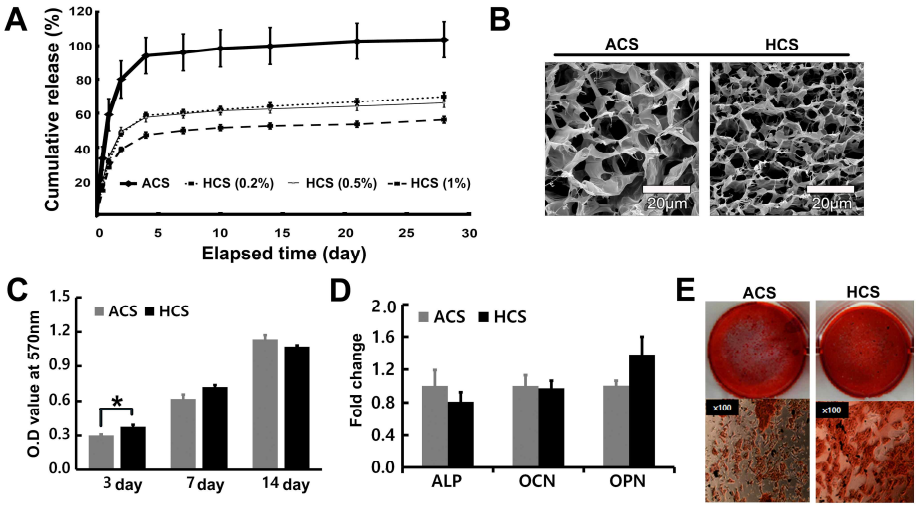

Figure 1. Characterization of HCS *(A) In vitro* release of BMP-2 from ACS and HCS at different heparin concentrations (0.2, 0.5, 1 %) over a 28 day period. Significant difference between ACS and each HCS, $p^{*}<0.05$, $p^{**}<0.01$. (B) SEM images of surface sections in ACS and HCS (0.5 %). (C) Proliferation of rat BM-MSC cultured on ACS and HCS (0.5 %) for 3, 7, and 14 days. Significant difference between ACS and each HCS, $p^{*}<0.05$, $p^{**}<0.01$. (D) Gene expression of *ALP*, *OCN,* and *OPN* in BM-MSCs cultured on ACS and HCS (0.5 %) for 14 days with osteogenic differentiation media. (E) *In vitro* mineralization determined by Alizarin red s staining of BM-MSCs cultured on ACS- and HCS- (0.5 %) coated plates with osteogenic differentiation media for 14 days.

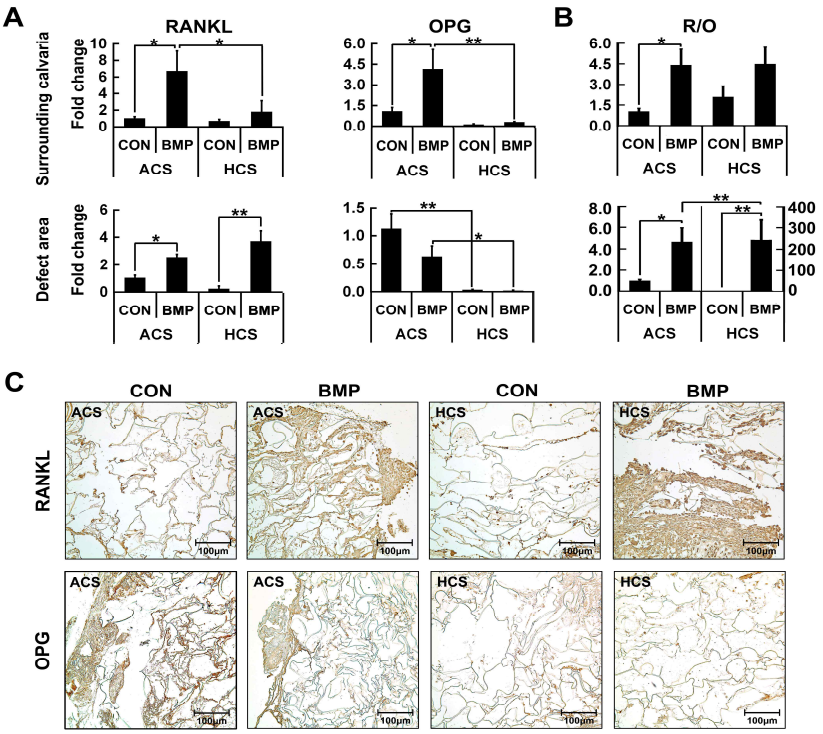

Figure 2. *RANKL* and *OPG* expression at the initial phase of high-dose rhBMP-2 delivery using ACS and HCS. Calvaria containing an 11-mm radius around the defect from vehicle alone (CON) and rhBMP treatment (BMP) of ACS or HCS were removed 7 days after surgery and separated into collagen sponges and the surrounding calvaria adjacent to the defect. Then, total RNA was extracted from the collagen sponge or bone of each group. (A) The expression of *RANKL* and *OPG* in the collagen sponge of the defect area and surrounding calvaria. Significant difference between two groups, $p^{*}<0.05$, $p^{**}<0.01$. (B) The relative ratio of *RANKL* to *OPG* (R/O). Significant difference between two groups, $p^{*}<0.05$, $p^{**}<0.01$. (C) Representative IHC staining for Rankl and Opg expression are presented to show intracellular RANKL and OPG expression. Scale bar indicates 100 μm.

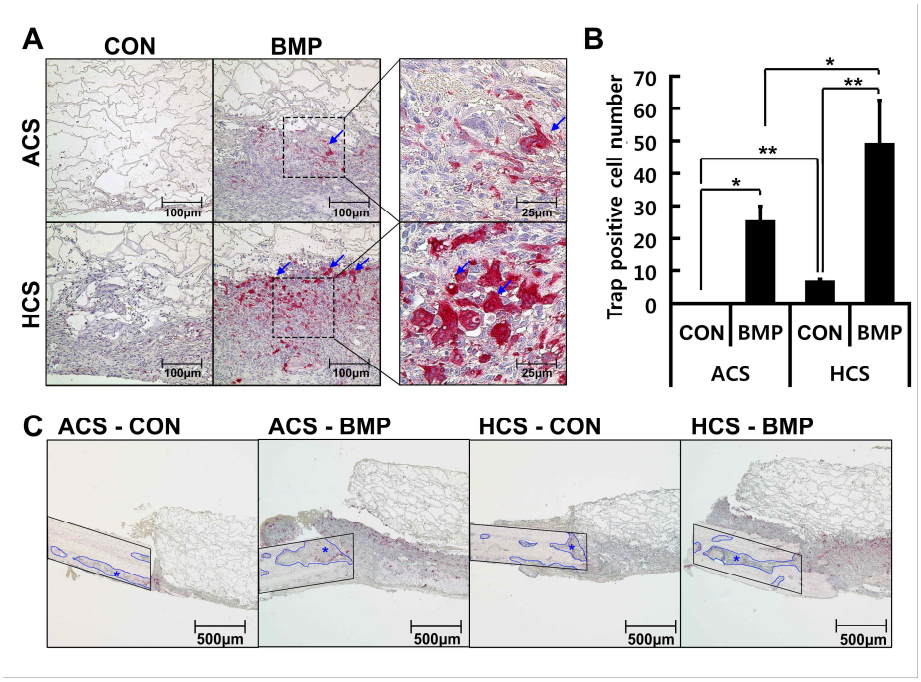

Figure 3. Early bone resorption in ACS-BMP and HCS-BMP groups. A calvaria containing an 11-mm radius around the defect after vehicle alone (CON) and rhBMP treatment (BMP) of ACS or HCS was removed at 7 days after surgery and stained with TRAP and H&E. (A) Representative images of TRAP staining on implanted sponges. Blue arrows indicate TRAP-positive MNCs. Scale bar indicates 50 μm. (B) Osteoclast activation was determined by counting TRAP-positive cells with more than three nuclei under an inverted-phase contrast microscope. Significant differences between groups are indicated by $p*<0.05$, $p**<0.01$. (C) Bone erosion in the marginal region (black-lined area) which is merged into the scaffold, which is designated with asterisks (*) in the blue-lined area after TRAP and H&E staining. Scale bar indicates 500 μm.

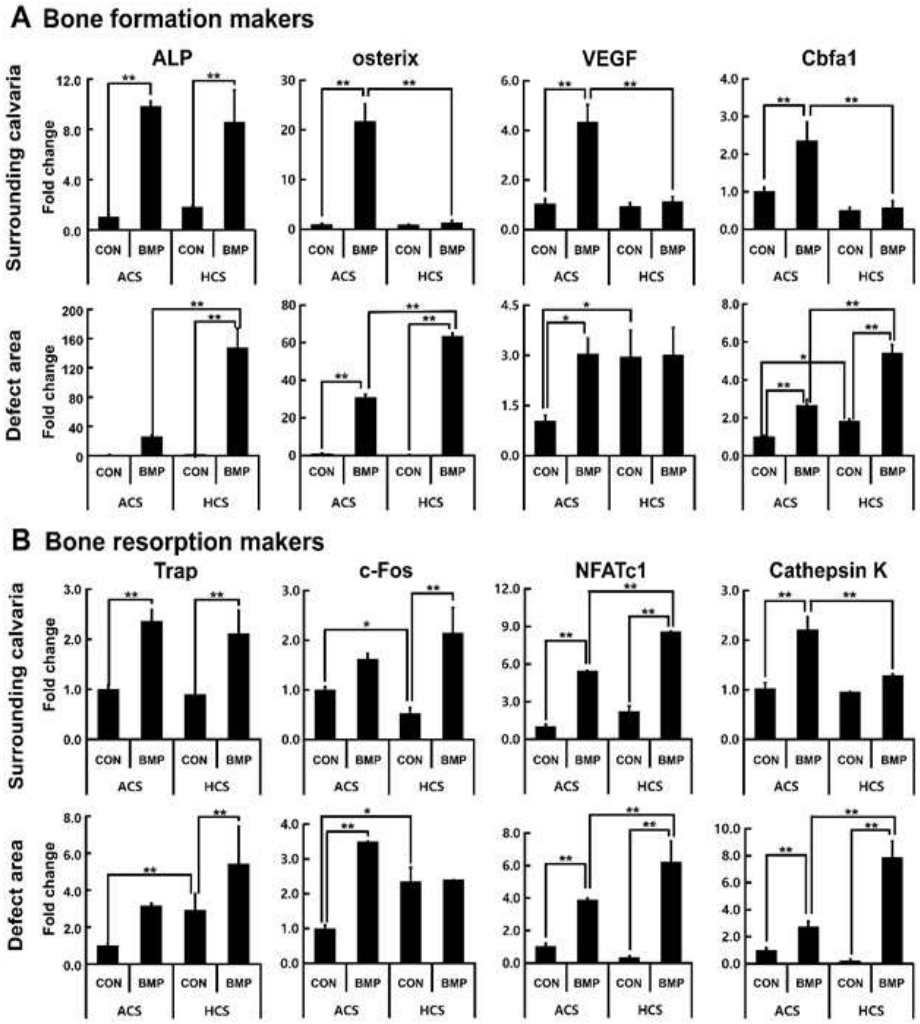

Figure 4. The effect of rhBMP-2 on the expression of bone formation- and resorption- related markers *in vivo*. Total RNA was prepared as described in Figure 2. Real time-PCR analysis was performed for (A) the expression of bone formation-related markers, including *ALP, osterix, VEGF,* and *Cbfa1,* and (B) the expression of bone resorption-related markers including *Trap, c-fos, NFATc1,* and *Cathepsin K*. Significant differences between groups are indicated by $p*<0.05$, $p**<0.01$.

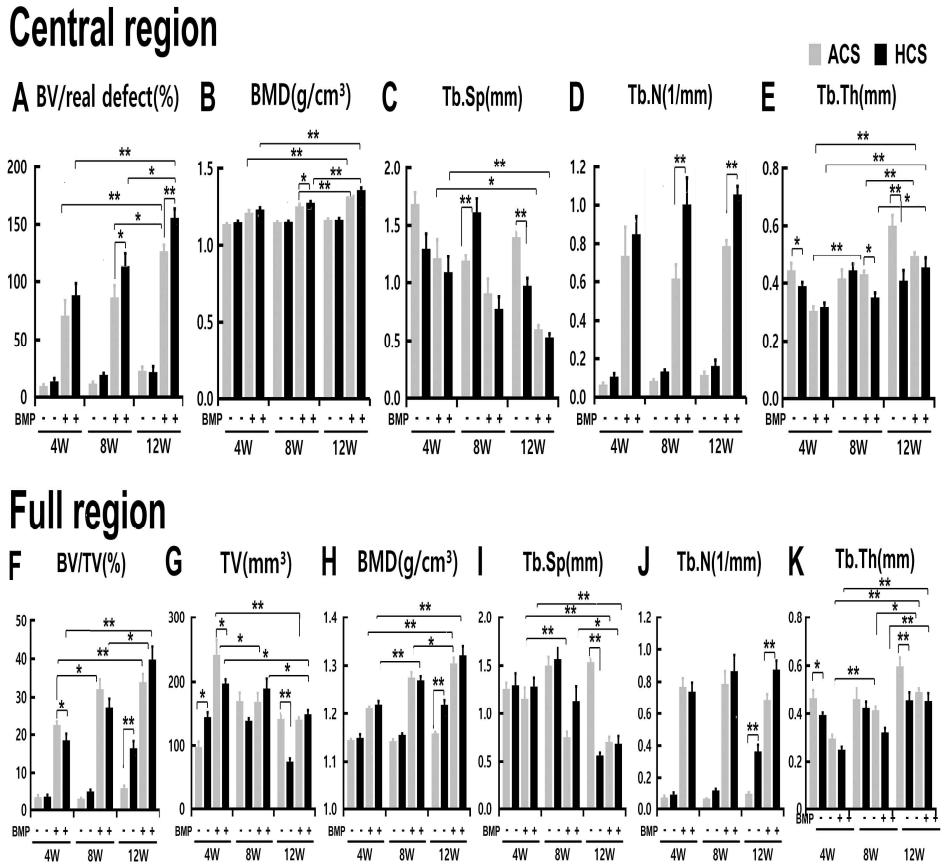

Figure 5. Quantitative micro-CT analysis of the effects of BMP-2 delivery from ACS and HCS on bone formation in rat calvaria defects. The experimental groups were implanted with ACS or HCS disks of buffer-loaded control (ACS-CON and HCS-CON) or rhBMP-2-treated disks (40 μg/defect; ACS-BMP, HCS-BMP). Micro-CT-based evaluation for new bone formation was performed for two regions after a 4, 8, or 12-week healing period; one region is the real defect (A-E), and the other is the full region, which includes the real defect and the defect exterior (F-K). (A) BV/real defect TV (%), (B) BMD (g/cm^3), (C) Tb.Sp (mm), (D) Tb.N (1/mm), and (E) Tb.Th (mm) of newly ossified tissue in the central defect area are

expressed as mean±SD in each group. Significant differences between groups: $*p<0.05$, $**p<0.01$. New bone formation in full region was analyzed for (F) BV/TV (%), (G) TV (mm^3), (H) BMD (g/cm^3), (I) Tb.Sp (mm), (J) Tb.N (1/mm), and (K) Tb.Th (mm). All parameters are expressed as mean±SD in each group. Significant differences between groups: $*p<0.05$, $**p<0.01$.

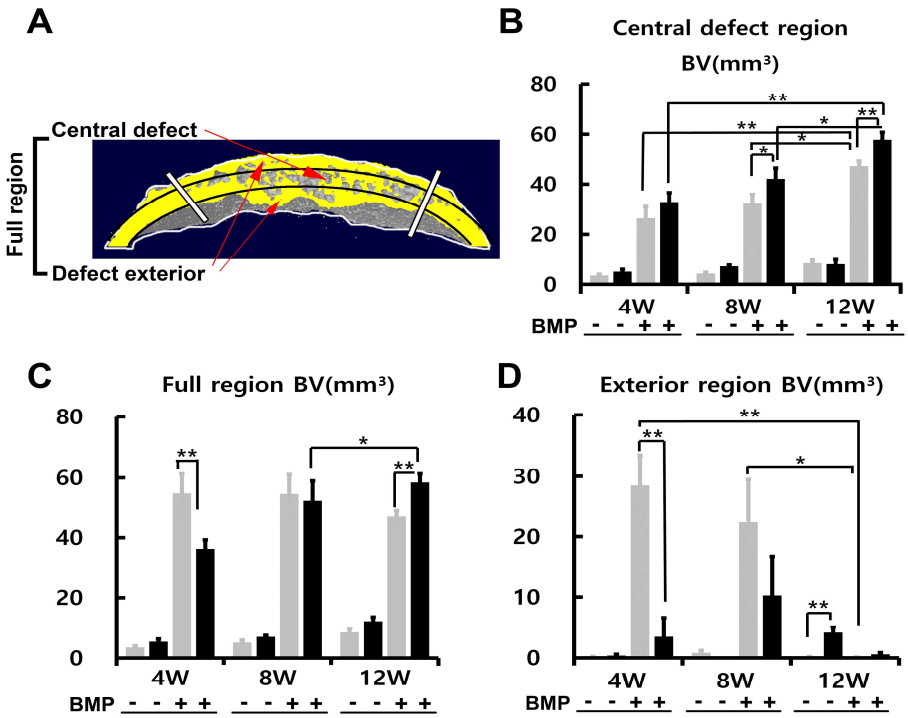

Figure 6. Comparison of the effect of HCS-BMP and ACS-BMP on heterotopic ossification or bone regeneration. (A) Schematic images for two areas on micro-CT scanning in a calvarial defect regeneration. The exterior region was outside the real defect region. The central defect region indicates the size of the real defect. The full region includes the regions of central defect and the up/down exterior of the defect. Micro-CT analysis was compared for (B) BV (mm^3)of the central defect region, (C) BV (mm^3) of the full region, and (D) BV (mm^3) of the exterior region after a 4, 8, and 12-week healing period. The BV of the central defect and the exterior region is related to compact bone formation and heterotopic ossification, respectively. HCS-BMP was effective in compact bone formation, but less so in heterotopic ossification and longer term bone regeneration.

All data are expressed as mean±SD. There was a significance (p**<0.01) between ACS-CON and ACS-BMP or HCS-CON and HCS-BMP at all time points in central defect and full region, respectively; significance was not marked. Significant differences between ACS-CON and ACS-BMP or HCS-CON and HCS-BMP at each time point in defect exterior region, $^{\dagger\dagger}p$<0.01. Significant differences between groups, *p<0.05, **p<0.01.

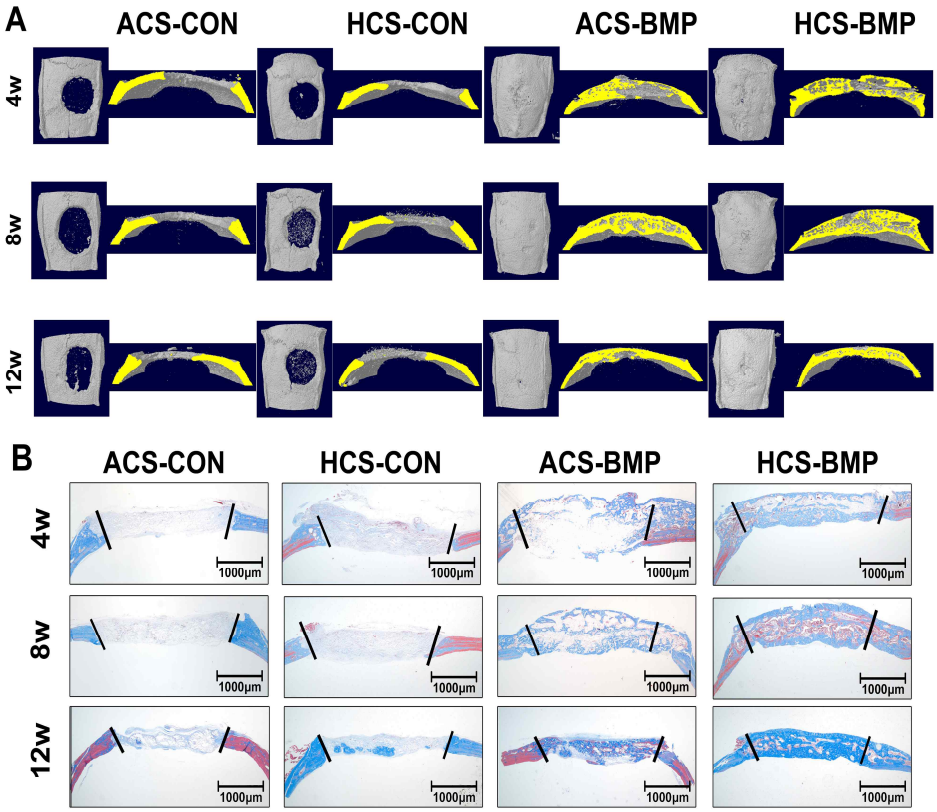

Figure 7. 3D reconstructed images and histological staining of regenerated defects. (A) 3D images from micro-CT are presented both in cross- and horizontal sections in ACS-CON, ACS-BMP, HCS-CON, and HCS-BMP. The yellow color (lower side) corresponds to a slice perpendicular to the calvarial surface axis, which was obtained at the middle position of the calvarial defect. The dotted circle indicates the position and dimensions of the 8 mm defect. (B) Histological appearance of calvarial defect after 4, 8, and 12 weeks of healing. All groups were stained with Masson trichrome (MT) at a 4, 8, and 12 weeks after implantation. The bars represent 1000 μm in 12.5×. *indicates new bone, and arrows indicate existing bone. Defect area was lined.

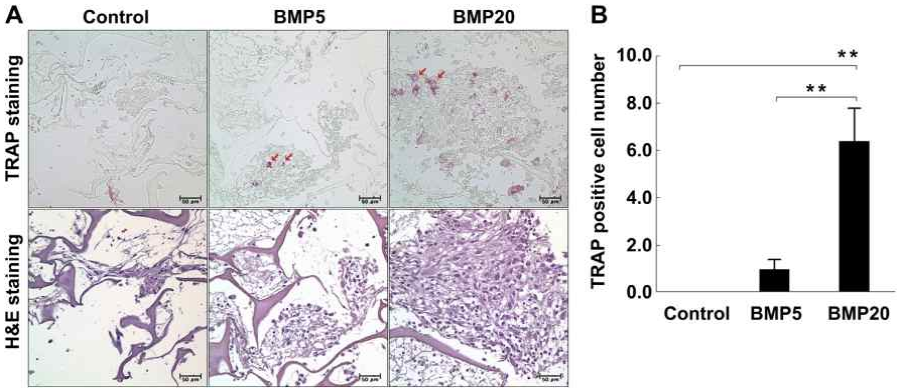

Figure 8. Dose-dependent effect of rhBMP-2 on osteoclast activation in vivo. Collagen disks implanted into 8 mm calvarial defects of buffer-loaded control, rhBMP-2 (5 μg/defect; BMP5) and rhBMP-2 (20 μg/defect; BMP20) groups were removed after the early healing period of 7 days after surgery. (A) Representative images of TRAP and H&E staining of implanted collagen sponges. Red arrows indicate the multinucleated TRAP-positive cells. Scale bar indicates 50 μm. (B) Osteoclast activation was determined by counting TRAP-positive cells having more than three nuclei under an inverted-phase contrast microscope. Significant differences between two groups, at $p^{**} < 0.01$.

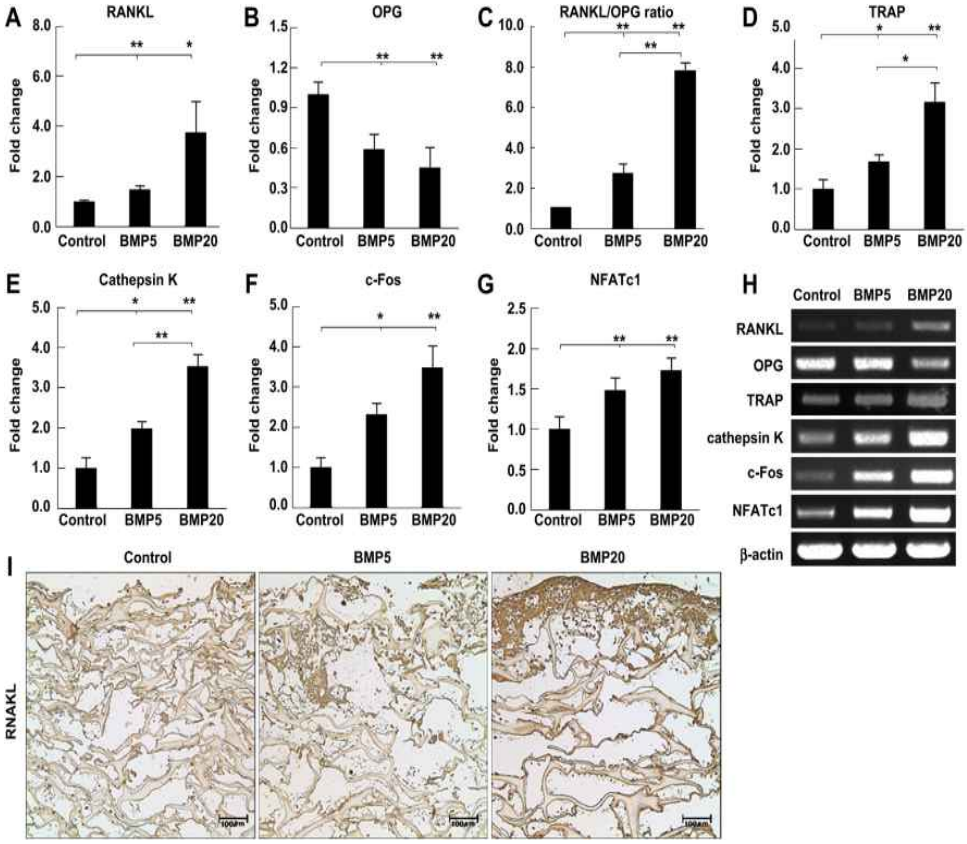

Figure 9. High-dose effect of rhBMP-2 on the expression of bone resorption markers in vivo in comparison with low dose. Total RNA was extracted from the collagen disks implanted into calvarial defects of vehicle control, 5 μg rhBMP-2 (BMP5), and 20 μg rhBMP-2 (BMP20) groups after the early healing period of 7 days after surgery. Real-time RT-PCR analysis was performed to measure the expression of bone resorption-related markers including (A) RANKL and (B) OPG. (C) The relative ratio of RANKL to OPG was calculated based on the expression levels in Figure 9A and B. (D) TRAP, (E) Cathepsin K, (F) c-Fos, and (G) NFATc1 expression were assessed using real-time RT-PCR as well. Significant

differences between two groups are indicated by p* < 0.05, p** < 0.01. (H) Representative RT-PCR images are presented for RANKL, OPG, TRAP, Cathepsin K, c-Fos, NFATc1, and b-actin. (I) Representative images of IHC staining for RANKL expression are presented to show the intracellular RANKL expression. 20x magnification. Scale bar indicates 100 μm.

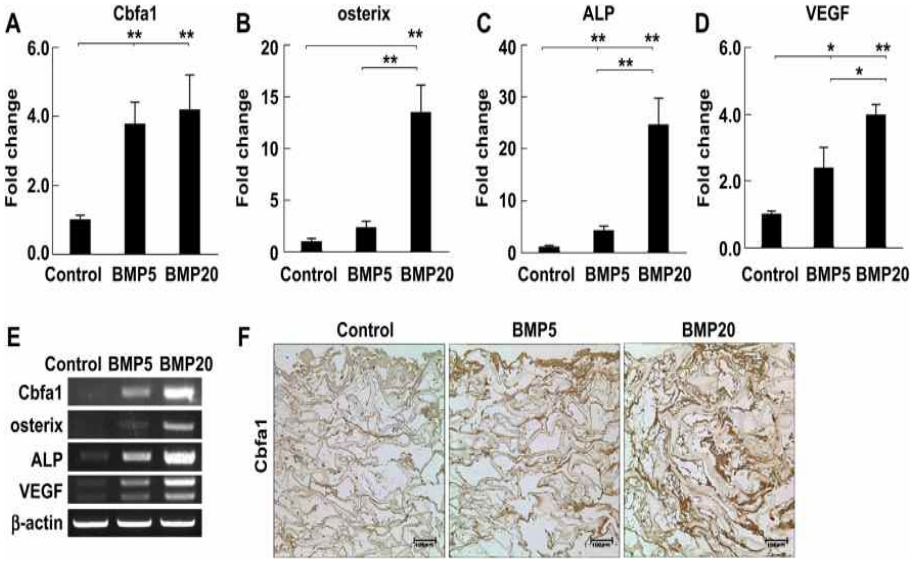

Figure 10. Dose-dependent effect of rhBMP-2 on the expression of bone formation markers in vivo. Total RNA was isolated from the implanted collagen sponge as described in Figure 9. Real time-PCR analysis was performed for the expression of bone resorption-related markers including (A) Cbfa1, (B) osterix, (C) ALP, and (D) VEGF. Significant differences between two groups are indicated by p* < 0.05, p** < 0.01. (E) Representative RT-PCR images are presented for Cbfa1, osterix, ALP, VEGF, and b-actin. (F) Representative images of IHC staining for Cbfa1 expression are presented. 20x magnification. Scale bar indicates 100 μm.

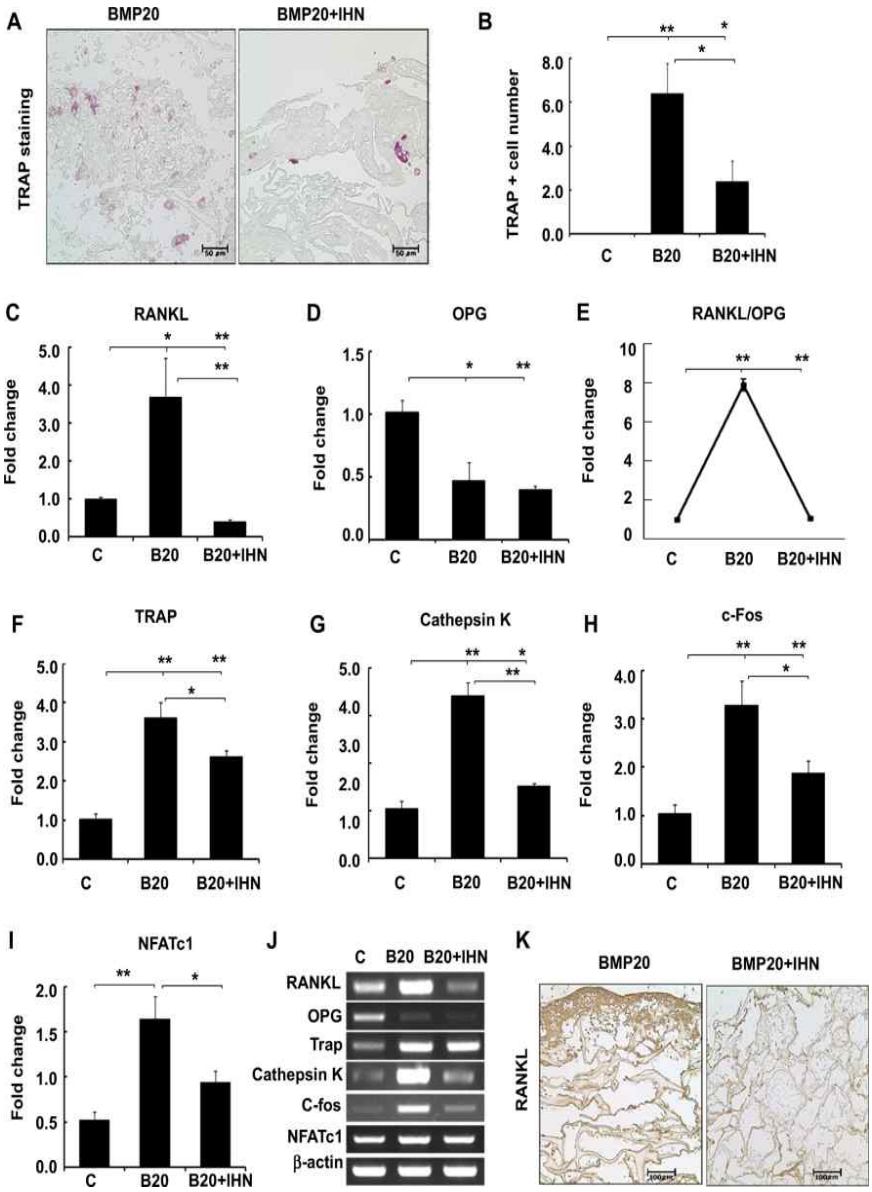
A
BMP20
BMP20+IHN
TRAP staining
B
TRAP + cell number
C
B20
B20+IHN
C
RANKL
Fold change
D
OPG
E
RANKL/OPG
F
TRAP
G
Cathepsin K
H
c-Fos
I
NFATc1
J
RANKL
OPG
Trap
Cathepsin K
C-fos
NFATc1
β-actin
K
BMP20
BMP20+IHN
RANKL

Figure 11. Involvement of NFAT signaling in high-dose rhBMP-2-mediated osteoclastogenesis in vivo. Combined treatment of NFAT inhibitor (IHN; 150 μM; 7.5 μg/defect) with high-dose rhBMP-2 (20 μg/defect) was implanted in the same animal model as described in Figures 8-10. (A) Collagen disks implanted into calvarial defects were removed after the early healing period of 7 days after surgery with the same scheme as Figure 8. Osteoclast activation was determined by counting TRAP-positive cells having more than three nuclei under an inverted-phase contrast microscope. C, B20 and B20/IHN indicate vehicle control, 20 μg of rhBMP-2, and 20 μg of rhBMP-2+NFAT inhibitor, respectively. Significant differences between two groups at $p^{**} < 0.01$. (B) Representative images of TRAP and H&E staining of implanted collagen sponges. Red arrows indicate the multinucleated TRAP-positive cells. Real-time RT-PCR analysis was performed to measure the expression of bone resorption-related markers including (C) RANKL and (D) OPG from collagen disks as described in Figure 9. (E) The relative ratio of RANKL to OPG was calculated based on the expression levels in Figure 9A and B. (F) TRAP, (G) Cathepsin K, (H) c-Fos, and (I) NFATc1 expression were assessed using real-time RT-PCR as well. Significant differences between two groups are indicated by $p^{*} < 0.05$, $p^{**}<0.01$. (J) Representative RT-PCR images are presented for RANKL, OPG, TRAP, Cathepsin K, c-Fos, NFATc1, and b-actin. (K) Representative images of IHC staining for RANKL expression are presented to show the intracellular RANKL expression. 20x magnification. Scale bar indicates 100 μm.

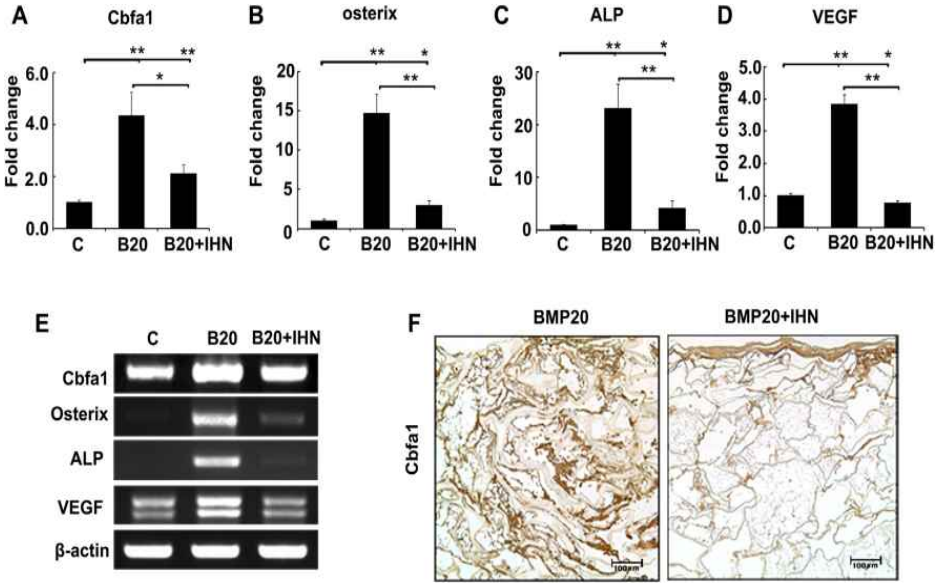

Figure 12. Effect of NFAT inhibitor on osteoblastogenesis mediated by high-dose rhBMP-2 in vivo. Real-time RT-PCR analysis was performed to measure the expression of bone formation-related markers including (A) Cbfa1, (B) osterix, (C) ALP, and (D) VEGF from the same disks as described in Figure 11 with combined treatment of NFAT inhibitor (IHN; 150 μM) with high-dose rhBMP-2 (20 μg/defect). C, B20 and B20/IHN indicate vehicle control, 20 μg of rhBMP-2, and 20 μg of rhBMP-2+NFAT inhibitor, respectively. Significant differences between two groups are indicated by p* < 0.05, p** < 0.01. (E) Representative RT-PCR images are presented for Cbfa1, osterix, ALP, VEGF, and b-actin. (F) Representative images of IHC staining for Cbfa1 expression are presented. 20x magnification. Scale bar indicates 100 μm.

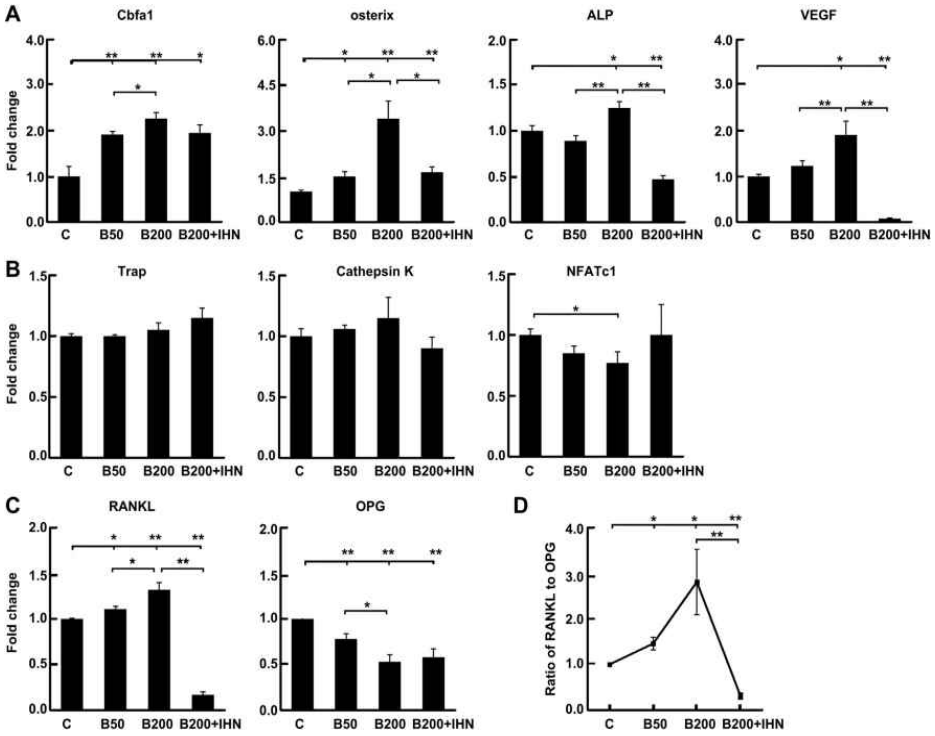

Figure 13. NFAT effect on the BMP-2 mediated signaling in rMSCs in vitro. rMSCs were treated with 50 ng/mL of rhBMP-2, 200 ng/mL of rhBMP-2, or 200 ng/mL of rhBMP-2+NFAT inhibitor (IHN; 200 nM). Real-time RT-PCR was performed after 7 days of culture for the expression of (A) bone-formation markers including (A) Cbfa1, osterix, ALP, and VEGF, (B) bone-resorption markers including TRAP, Cathepsin K, and NFATc1. (C) RANKL and OPG expression were examined using real-time RT-PCR. Significant differences between two groups are indicated by p* < 0.05, p** < 0.01. (D) The relative ratio of RANKL to OPG was calculated based on the expression levels in Figure 13C. (E) Representative RT-PCR images are presented for all genes of Fig. 13A-C. C, B50, B200 and B200+IHN indicate vehicle control, 50 ng/ML of rhBMP-2, 200 ng/mL of rhBMP-2, and 200 mL of rhBMP-2+NFAT inhibitor, respectively.

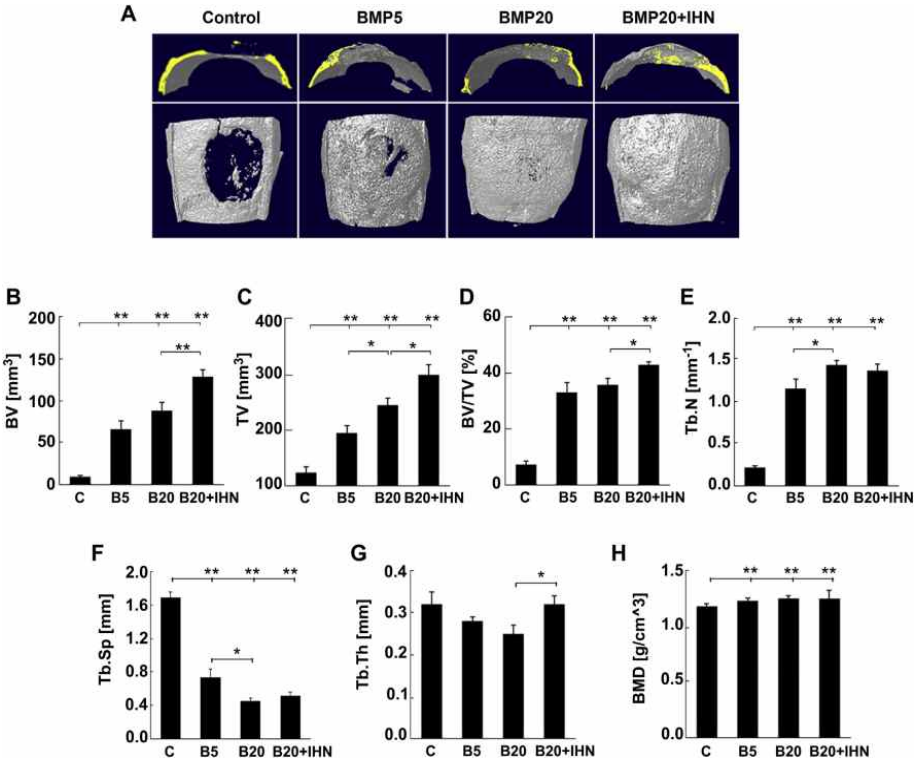

Figure 14. Effect of NFAT inhibitor on high-dose rhBMP-2 implantation on bone regeneration. The experimental groups were implanted with buffer-loaded collagen sponge control, rhBMP-2 (5 μg/defect), rhBMP-2 (20 μg/defect), and rhBMP-2 (20 μg/defect) + NFAT inhibitor (IHN; 150 μM). Micro-CT-based evaluation was performed after a 4-week healing period. (A) 3D images from micro-CT were presented both in cross and horizontal section. The yellow color (upper side) corresponds to a slice perpendicular to the calvarial surface axis, which was obtained at the middle position of the calvarial defect. The dotted circle indicates the position and dimensions of the 8 mm defect. (B) BV (mm3), (C) TV (mm3), (D) BV/TV (%), (E) Tb.N (1/mm), (F) Tb.Sp, (G) Tb.Th, and (H) BMD (g/cm3) of newly ossified tissue are expressed as mean SD in

rhBMP-2-treated groups and untreated controls. Significant differences between groups: *p < 0.05, **p < 0.01. C, BMP5, BMP20, and BMP20+IHN indicate control, 5 μg of rhBMP-2, 20 μg of rhBMP-2, and 20 μg of rhBMP-2+NFAT inhibitor, respectively.

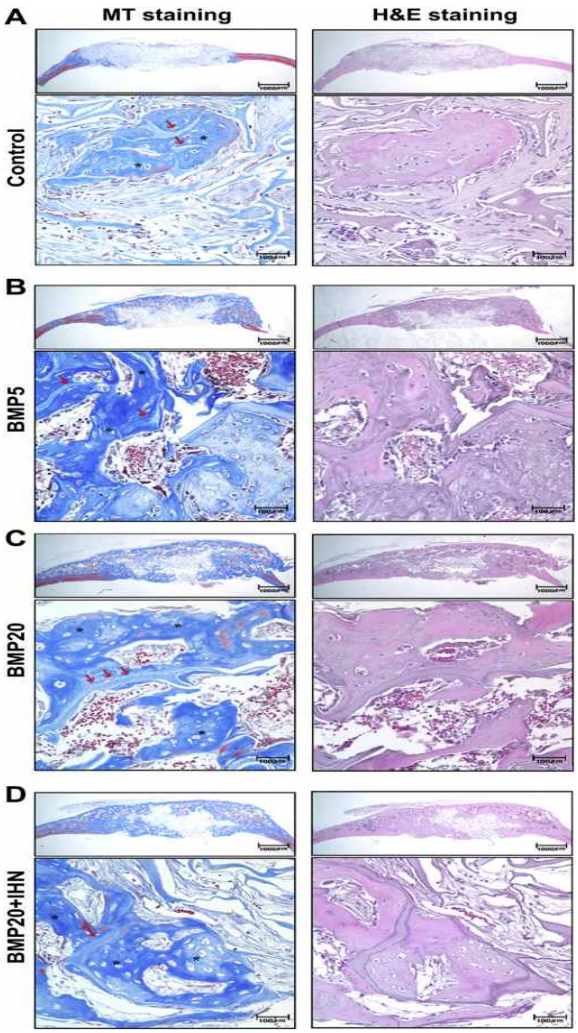

Figure 15. Histological appearance of calvarial defect a four weeks healing period. Histological sections of (A) control; buffer-loaded collagen sponge alone, (B) BMP5; 5 μg rhBMP-2, (C) BMP20; 20 μg rhBMP-2, and (D) BMP20+IHN; 20 μg rhBMP-2+NFAT inhibitor using the same specimens described in Figure 14. All groups were stained with Masson trichrome (MT) and with H&E at 4 weeks after implantation. The bars represent 1000 μm in 12.5x and 100 μm in 200x. *indicates new bone, and arrows indicate existing collagen fiber.

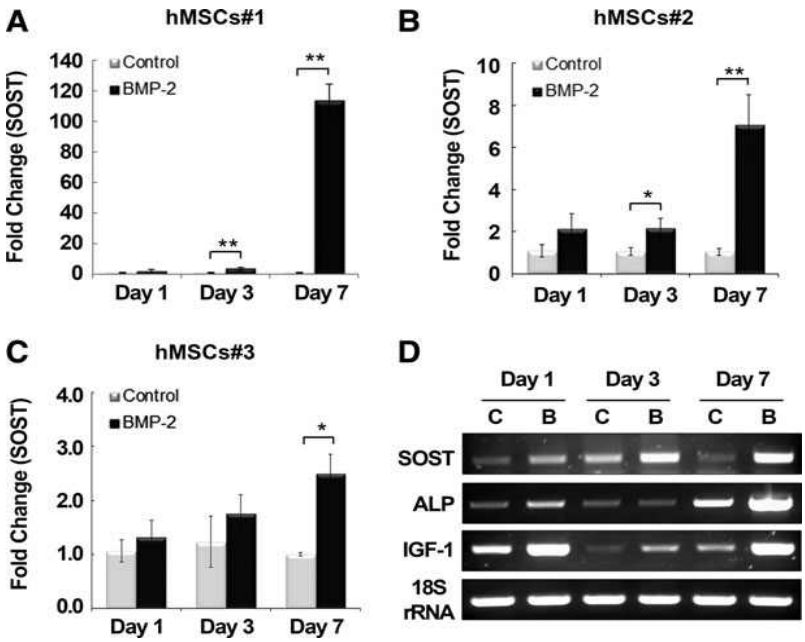

Figure 16. Time course of sclerostin (SOST) expression in human mesenchymal stromal cells (hMSCs) treated with bone morphogenetic protein (BMP)2. Three different cell lines of primary hMSCs (hMSCs#1, 2, 3) were prepared from the bone marrow of healthy female donors. SOST expression was examined using real-time reverse transcription-polymerase chain reaction (RT-PCR) at days 1, 3, and 7 after treatment with BMP2 (200 ng/mL). Values are expressed relative to those of nontreated hMSCs at day 1 with normalization to *18S rRNA* for hMSCs#1 (A), #2 (B), and #3 (C). Significant differences from the nontreated control for each day are indicated by $*p < 0.05$, $**p < 0.01$. (D) Representative RT-PCR images for hMSCs#1 are presented for alkaline phosphatase (ALP), insulin-like growth factor-1 (IGF1), BMP2, SOST, and 18S rRNA in the control (C) and BMP2-treated (B) group.

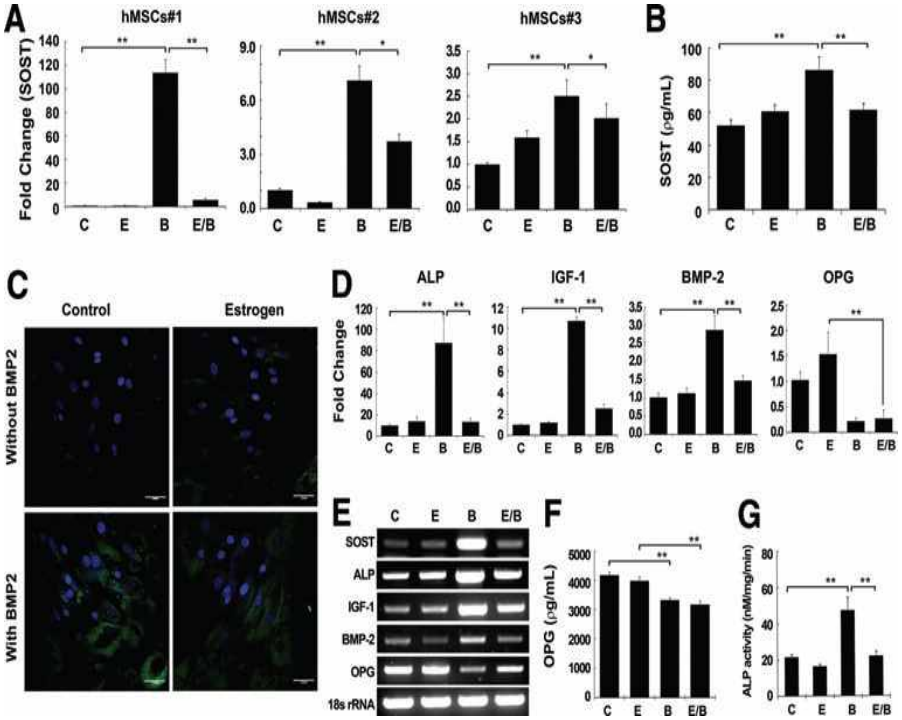

Figure 17. Suppressive effect of estrogen on BMP2 signaling in hMSCs. The three different lines of primary hMSCs (hMSCs#1, 2, 3) used in Figure 16 were treated with E2 (E; 100 nM), BMP2 (B; 200 ng/mL), or E2 and BMP2 (E/B) for 7 days. (A) SOST expression was examined using real-time RT-PCR at day 7 in all three hMSC lines and compared with the nontreated control. Significant differences between two groups are indicated by *p < 0.05, **p < 0.01. (B) The extracellular release of SOST in hMSCs#1 was quantified in cell culture supernatants (n=4) at day 7 using an enzyme-linked immunosorbent assay (ELISA) kit. Significant differences between two groups are indicated by **p < 0.01. (C) Immunofluorescence and 4',6-diamino-2-phenylindole (DAPI) staining were carried out to detect SOST at the same time points and under the same culture conditions using hMSCs#1 as described for (A). Scale bars indicate

50 μm. (D) Real-time RT-PCR results for ALP, IGF1, BMP2, and osteoprotegerin (OPG) expression in hMSCs#1. Significant differences between two groups are indicated by **p < 0.01. (E) Representative RT-PCR images for hMSCs#1 are presented for ALP, IGF1, BMP2, SOST, and 18S rRNA. (F) The extracellular release of OPG in hMSCs#1 was quantified in cell culture supernatants (n=4) at day 7 using an ELISA kit. Significant differences between two groups are indicated by **p < 0.01. (G) ALP acitvity was assessed at the same condition as described in Figure 17D. Significantly different, **p < 0.01.

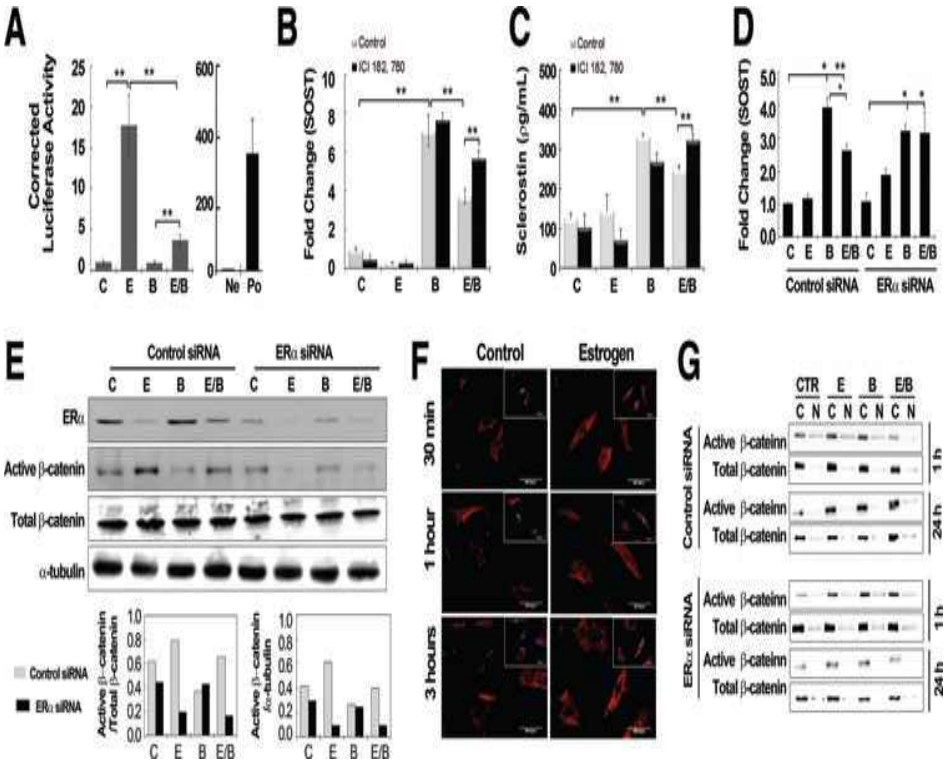

Figure 18. E2 activation of the Wnt/b-catenin/estrogen receptor (ER)a signaling pathway. (A) TOPFlash luciferase reporter assays were performed in hMSCs 24 h after no treatment (control; C) or treatment with E2 (E; 100 nM), BMP2 (B; 200 ng/mL), or E2 and BMP2 (E/B). Positive (Po) and negative (Ne) reporter assays provided by the manufacturer were also performed. Significant differences between two groups are indicated by **p < 0.01. (B) Treatment with ICI 182,780 (100 nM; Wnt inhibitor). hMSCs were cultured as described in Figure 17 for 3 days with no treatment (control; C) or treatment with E2 (E; 100 nM), BMP2 (B; 200 ng/mL), or E2 and BMP2 (E/B), and then treated with or without ICI 182,780 (100 nM; Wnt inhibitor)

for the last 3 days. The transcriptional expression of SOST was determined at day 7. Significant differences between two groups are indicated by **p < 0.01. (C) Extracellular release of sclerostin was determined at day 7 by ELISA analysis at the same condition as in (B). **p < 0.01. (D) Transfected cells with ERa siRNA or control siRNA were treated with none (control; C), E2 (E; 100 nM), BMP2 (B; 200 ng/mL), or E2 and BMP2 (E/B). Transcriptional expression of SOST was assessed using real-time RT-PCR 3 days after transfection. Significant differences between two groups are indicated by *p < 0.05, **p < 0.01. (E) Western blotting was performed to detect ERa, total b-catenin, active b-catenin, and a-tubulin using cell lysates prepared 24 h after culturing at the same condition as described in (D). a-Tubulin was used as an internal loading control. (F) Immunofluorescence and DAPI staining were carried out to detect activated bcatenin in hMSCs at 30 min, 1, and 3 h after pretreatment as described in (D). Cells were fixed and the subcellular localization of active b-catenin was determined by immunocytochemistry and confocal microscopy. Dual-stained cells with DAPI are presented at the upper right corner of each image. The scale bars indicate 50 μm. (G) Western blotting of cytoplasmic (C) and nuclear (N) fractions from hMSCs 1 and 24 h after the cells were treated as described in (D). CTR (control), E2 (E; 100 nM), BMP2 (B; 200 ng/mL), E2 and BMP2 (E/B). Data shown are representative findings from two separate experiments.

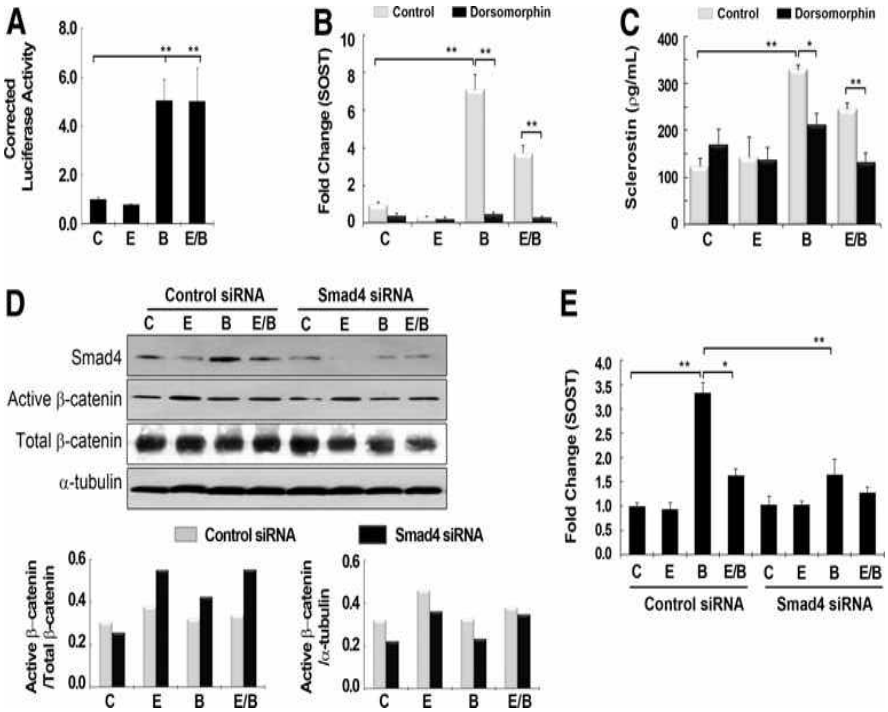

Figure 19. E2 signaling is independent of the Smad pathway. (A) Smad reporter assays were performed in hMSCs 24 h after no treatment (control; C) or treatment with E2 (E; 100 nM), BMP2 (B; 200 ng/mL), or E2 and BMP2 (E/B). Significant differences between two groups are indicated by **p < 0.01. (B) Treatment with dorsomorphin (Smad inhibitor). hMSCs were cultured as described in Figure 17 for 3 days without (control; C) or with treatment with E2 (E; 100 nM), BMP2 (B; 200 ng/mL), or E2 and BMP2 (E/B), and then treated with or without dorsomorphin (10 mM) for the last 3 days. The transcriptional expression of SOST was determined at day 7 by real-time RT-PCR. Significant differences between two groups are indicated by **p < 0.01. (C) Extracellular release of sclerostin was determined at day 7 by ELISA at the same condition as

described in (B). *p < 0.05, **p < 0.01. (D) Cells were transfected with Smad4 siRNA or control siRNA, and then untreated (control; C) or treated with E2 (E; 100 nM), BMP2 (B; 200 ng/mL), or E2 and BMP2 (E/B). Western blotting was performed to detect Smad4, total b-catenin, active b-catenin, and a-tubulin at 24 h after transfection. a-Tubulin was used as an internal loading control. (E) Transcriptional expression of SOST was assessed using real-time RT-PCR 3 days after culturing under the conditions described in (D). Significant differences between two groups are indicated by *p < 0.05, **p < 0.01.

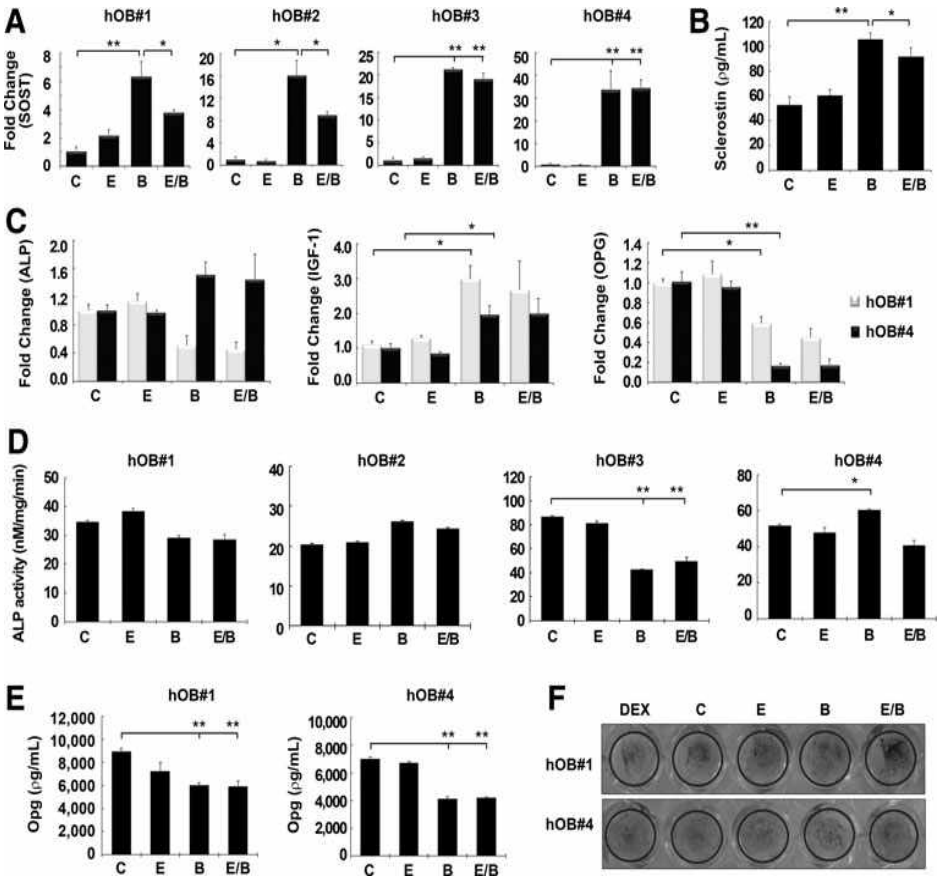

Figure 20. The response of human osteoblasts to estrogen in association with BMP2 signaling. Primary human osteoblasts derived from four different donors (hOB#1, 2, 3, and 4) were treated with none (control; C), E2 (E; 100 nM), BMP2 (B; 200 ng/mL), or E2 and BMP2 (E/B) for 7 days. (A) SOST expression was assessed at day 7 by real-time RT-PCR. (B) Extracellular release of sclerostin was quantified in cell culture supernatants of human osteoblasts #1 at day 7 using an ELISA kit. (C) ALP, IGF1, and OPG expression from two representative cell lines (hOB#1 and 4) was examined at day 7 by real-time RT-PCR. (D) ALP activity of hOB#1, 2, 3, and 4 was

assessed under the culture conditions described in (C). (E) Extracellular release of Opg from two representative cell lines (#1 and 4) was quantified in cell culture supernatants under the culture conditions described in (C) using an ELISA kit. Significant differences between two groups at (A - E) are indicated by *p < 0.05, **p < 0.01. (F) In vitro mineralization was observed by von Kossa staining at day 28 without treatment (control) or after treatment with none (control; C), dexamethasone (DEX, 10 nM), E2 (E; 100 nM), BMP2 (B; 200 ng/mL), or E2 and BMP2 (E/B) in two representative cell lines (hOB#1 and 4).

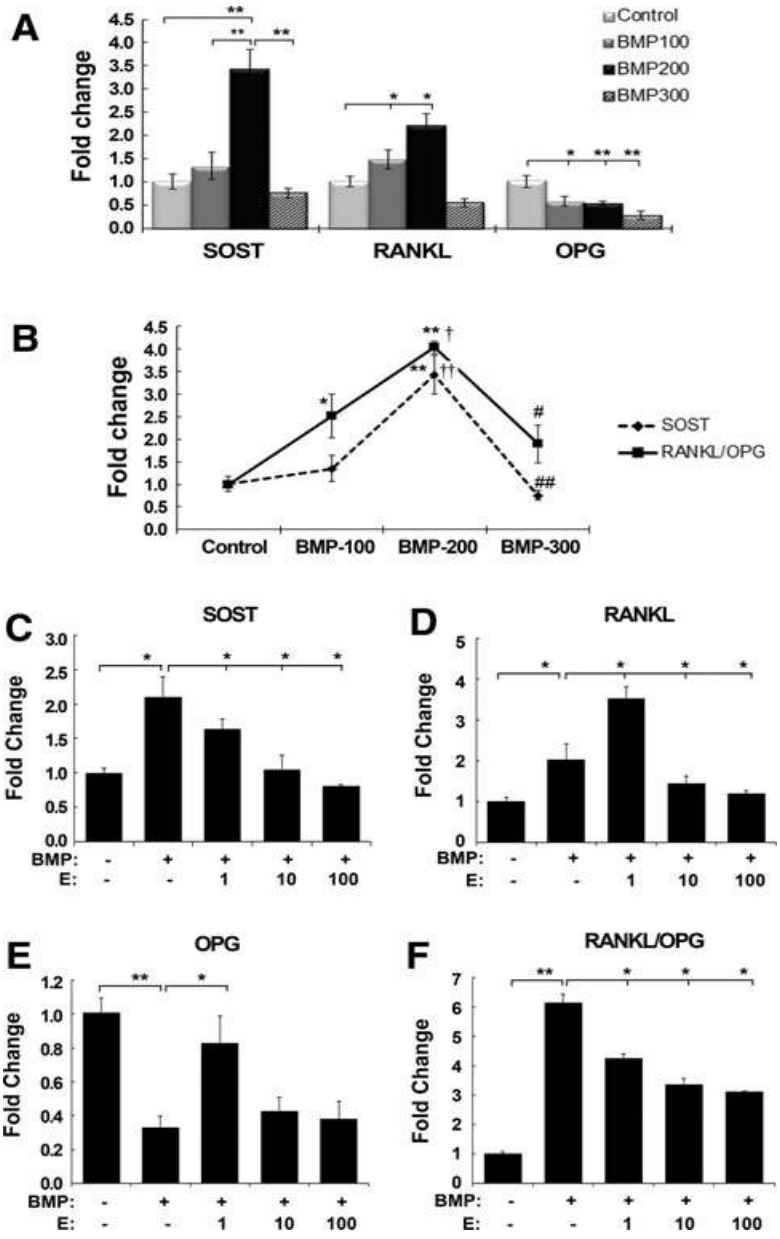
A
Fold change
Control
BMP100
BMP200
BMP300
SOST
RANKL
OPG
B
Fold change
SOST
RANKL/OPG
Control
BMP-100
BMP-200
BMP-300
C
SOST
Fold Change
BMP:
E:
D
RANKL
Fold Change
BMP:
E:
E
OPG
Fold Change
BMP:
E:
F
RANKL/OPG
Fold Change
BMP:
E:

Figure 21. Relationship between SOST expression and the ratio of receptor activator of nuclear factor kappa-B ligand (RANKL) to OPG expression in human osteoblasts. (A) Human osteoblast line #1 was treated with increasing doses of BMP2 (BMP; 100, 200, and 300 ng/mL). SOST, RANKL, and OPG expression was assessed at day 7 using real-time RT-PCR. Significant differences between two groups are indicated by *p < 0.05, **p < 0.01. (B) The relative ratio of RANKL to OPG was calculated based on the expression levels in (A). Significant differences between control and BMP2-treated groups are indicated by *p < 0.05, **p < 0.01; BMP2 100 ng/mL and BMP2 200 ng/mL groups are indicated by † p < 0.05, † † p < 0.01; BMP2 200 ng/mL and BMP2 300 ng/mL groups are indicated by #p < 0.05, ##p < 0.01. (C - E) Human osteoblast line #1 was treated with E2 (E; 1, 10, and 100 nM), BMP2 (200 ng/mL), and E2 and BMP2. Expression of SOST (C), RANKL (D), and OPG (E) was assessed at day 7 using real-time RT-PCR. (F) The relative ratio of RANKL to OPG was calculated based on the expression levels in (D, E). Significant differences between two groups are indicated by *p < 0.05, **p < 0.01.

-국문초록 -

고농도 골형성 단백질 2형 적용시 나타나는 초기 골 흡수 억제 전략

김 리 연
서울대학교 대학원 치의과학과 두 개악안면세포및발생생물학 전공
(지도교수 황 순 정)

1. 연구목적

인간유전자 재조합 2형 골형성단백질(recombinant human morphogenic protein-2 (rhBMP-2))는 중간엽줄기세포(mesenchymal stem cells(MSCs))를 연골세포와 조골세포로 분화시키며, 생체 내에서 골 형성을 이끄는 인자로 알려져 있으며, 골 형성을 통한 치료적 목적에 활용되고 있다. 그러나 이를 위한 고용량의 rhBMP-2 처리는 초기 골 흡수 유발을 포함한 다수의 부작용을 유발할 수 있다는 전 실험결과와 임상적 보고가 있다. 이 논문에서의 연구는 골 형성을 이끌기 위해 투여하는 고용량 rhBMP-2에 의해 유발되는 초기 골 흡수와 연관된 다양한 요인들을 파악하고, 이러한 결과를 바탕으로 초기 골 흡수를 억제할 수 있는 요인들을 선별하여, 이를 억제할 수 있는 생물학적인 시스템의 기반을 마련하고자 진행되었다. 우선, 생체 내 실험에서 rhBMP-2의 농도에 따른 초기 골 흡수 양상을 조사하고, 이 과정에서 분자생물학적인 실험을 기반으로 고용량의 rhBMP-2에 의한 초기 골 형성 및 골 흡수 관련 BMP-2 하위인자의 발현 양상 변화를 평가하고자 한다. 골 흡수 관련 인자 가운데, 파골 세포 분화에 관여하며 c-Fos 신호 기작을 통해서 골 흡수를 이끄는 것으로 알려져 있는 Nuclear factor of activated T-cells(NFAT)-c1에 대한 억제제 투여를 통해 고용량 rhBMP-2에 의해

유발되는 초기 골 흡수의 억제 양상과 장기간 신생 골 재생 양상을 분석하고자 한다. 더불어, Receptor activator of nuclear factor kappa-B ligand(RANKL)/Osteoprotegerin(OPG) 비율에 의해 조절되는 것으로 알려진 골 흡수 관련 인자 Sclerosteosis(SOST)의 rhBMP-2에 따른 발현 양상 변화와 SOST의 발현 조절과 연관되어 있는 에스트로겐과 BMP 신호기작의 연관성을 분자생물학적 기전 연구를 통해 살펴보고, 이를 통해 BMP-2에 의한 골 형성/흡수 기작 조절에 대한 초석을 마련하고자 한다. 또한 지지체에 의한 방출 속도의 차이가 rhBMP-2의 골 재생 효과에 영향을 미친다는 동역학적 연구 결과가 보고를 바탕으로, FDA의 허가를 받은 지지체인 흡수성 콜라겐 해면체(ACS)에 의한 rhBMP-2의 초기 과다 방출을 해결하기 위해, 다양한 생체 분자의 지연 방출을 야기하는 것으로 알려진 헤파린을 결합한 헤파린 콜라겐 해면체(HCS)를 이용하여 지연 방출 유도 시스템을 확립하고자 하며, 이에 따른 고용량의 rhBMP-2에 의한 초기 골 흡수 양상의 억제 효과 및 장기간 골 재생 효과와 더불어 주변골 침식과 이소성 골화의 억제 효과를 살펴보고자 한다. 이러한 일련의 실험을 통해 고용량의 rhBMP-2에 의한 파골 세포 활성화에 중요한 역할을 하는 목표 분자를 확인하고, 이러한 목표 분자의 조절과 더불어 지연 방출을 통해 골 흡수를 줄임으로써 rhBMP-2에 의한 장•단기적 골 형성 치료 효과를 높이는 것이 본 연구의 최종 목적이다.

2. 연구방법

백서의 8mm 두개골결손 모델을 이용하여 각 실험의 생체 내 골 흡수/골 형성 효과를 평가하였다. 특히, HCS에 대한 효과 실험에서는 실제 결함-지지체 부위와 주변 부위 뼈의 양상 차이를 확인하고자 각각의 부위로 나누고, 지지체 경계면의 주변 부위 뼈 1mm(BA)의 골 흡수 양상은 부식된 부위로 확인하였다. 이소성 골화를 확인하기 위해 신생 골 형성 부위를 실제 손상 내 형성 부위와 손상 바깥쪽 형성 부위로 나누어

각각 평가하였다. 이때, NFAT-c1 억제제의 효과를 평가하기 위해, 각각 실험군에 5, 20ug의 rhBMP-2와 150uM NFAT-c1 억제제를 ACS에 적용하였고 대조군으로는 완충제만을 처리한 ACS를 사용하였다. 헤파린의 rhBMP-2 지연 방출 효율을 확인하기 위해, 0, 0.2, 0.5, 1%의 HCS를 사용하여 5ug의 rhBMP-2의 상대적 방출량을 BMP-2 효소결합면역흡착법(ELISA assay)를 이용해 확인하였다. 주사전자현미경(Scanning Electron Microscope(SEM)), 세포 생존율 측정기법(MTT Assay), Alizarin red s 염색법을 통해서 헤파린 콜라겐 지지체의 특성을 분석하였다. 더불어 이러한 지연 방출의 생체 내 효과를 확인하기 위해 0.5% HCS에 40ug의 rhBMP-2을 적용하였고, 대조군으로는 완충제만을 처리한 ACS 또는 HCS를 사용하였다. 1차 인간 중간엽줄기세포와 1차 인간 조골세포를 실험에 따라 1ng/uL의 TOPFlash luciferase 또는 Smad reporter plasmids 그리고 30pM의 Estrogen receptor alpha(ER alpha) 또는 SMAD family member 4(Smad4) si-RNA를 포함하는 배양액에 배양하였으며, rhBMP-2 (50, 200ng), 100nM의 Estradiol(E2) 또는 200nM의 NFAT-c1 억제제를 처리하여 7일 간 배양하였다. 이후 각각의 샘플은 역전사 중합효소 연쇄반응(Reverse transcription polymerase chain reaction(RT-PCR))과 정량적 역전사 중합효소 연쇄 반응(quantitative reverse transcription polymerase chain reaction(qRT-PCR))을 이용하여 Insunlin-like Growth Factor-1(*IGF-1), BMP-2, SOST*와 골 흡수 관련 인자인 *RANKL, OPG, Tartrate-resistant acid phosphatase(TRAP), Cathepsin K, c-Fos, NFAT-c1* 그리고 골형성 관련 인자인 core binding factor α 1(*Cbfa1), osterix, Alkaline phosphatase(ALP), Vascular endothelial growth factor(VEGF)*의 messenger RNA(mRNA) 발현 양상을 확인하였다. 각각은 *18s RNA* 또는 Glyceraldehyde 3-phosphate dehydrogenase(*GAPDH)*로 상대적 정량이 이루어졌다. 더불어 RANKL/OPG 비율을 제시하였다. 뿐만 아니라, ELISA assay, Western blotting, ALP staining, TRAP staining, 그리고 면역형광염색법

(immunofluorescence(IF)) 또는 면역화학염색법 (immunohistochemistry(IHC))을 통해 Sost, Beta-catenin, ER alpha, Smad4, ALP, TRAP, Rankl, OPG, Cbfa1의 활성화 또는 단백질 발현 양상을 확인하였다. 미세단층촬영기(Micro-CT) 분석을 통해 bone volume (BV), tissue volume (TV), bone volume ratio (BV/TV), trabecular number (Tb.N), trabecular thickness (Tb.Th), trabecular separation (Tb.Sp), 골밀도(BMD) 양상을 확인하였으며, 이와 함께 조직학적 분석을 위하여 Masson Trichrome staining(MT staining)을 실시하였다. 모든 결과는 IBM SPSS statistic 22.0을 이용하여 양측 t 검정과 일원배치분산분석과 본페로니 검증을 포함한 이원배치분산분석을 이용하여 통계적인 검증을 실시하였으며, $p < 0.05$를 유의미한 차이로 고려하였다.

3. 연구결과

백서 두개골결손 모델에서 고용량(20ug, 40ug)의 rhBMP-2 처리는 저용량(5ug)을 처리하였을 때보다 골 형성 관련 인자들의 발현을 증가시켰으나, 파골 세포 활성화와, RANKL/OPG 비율, 그리고 NFAT-c1를 비롯한 골 흡수 관련 인자들의 발현의 증가도 유발하였다. 이때, NFAT-c1 억제제를 함께 처리하였을 때, 고용량의 rhBMP-2에 의한 파골 세포 형성과 RANKL/OPG 비율을 비롯한 골 흡수 관련 인자들의 발현이 모두 유의미하게 감소하였다. 그러나 NFAT-c1 억제제는 rhBMP-2에 의한 골 형성 관련 인자들의 증가 또한 억제하였다. Micro-CT를 통해 확인한 장기간 골 재생 양상에서, NFAT-c1 억제제를 고용량의 rhBMP-2와 함께 처리한 실험군은 rhBMP-2 단독 처리한 군과 비교하였을 때보다 BV과 BV/TV의 증가를 비롯한 더 나은 신생 골 형성 양상을 보였으며, BMD를 비롯한 인자들에서는 유사한 수준의 신생 골 형성 양상을 나타내었다. 이어진 실험에서, hMSCs에서는 200ng/mL의 rhBMP-2를 처리하였을 때 7일차에서 SOST 발현이 증가

하였다. 그러나, 이때 100nM의 E2를 함께 처리했을 경우 rhBMP-2에 의한 SOST의 증가가 유의미하게 감소하였으며, Wnt 신호 기작의 중요한 신호인자인 Beta-catenin의 활성이 크게 증가하였다. 반면에 Wnt 신호 기작의 억제제이자 ER alpha에 대한 길항제인 ICI 182,780과 ER alpha에 대한 siRNA는 Smad 의존 관계없이 E2 처리에 의한 SOST 증가 억제 효과를 경감시킬 뿐만 아니라, 활성화된 Beta-catenin의 증가를 감소시켰다. 앞선 양상을 분화된 조골 세포주에서 확인한 결과, 세포의 유래에 따라 hMSCs와 유사하거나 다른 결과를 나타내었다. 이때, hMSCs와 유사한 결과를 나타낸 두 조골 세포주에서 RANKL/OPG 비율은 SOST의 발현과 유사한 양상을 나타내었다. 끝으로 동역학적 관점에서, 헤파린은 HCS에서 0.2%부터 1%까지의 모든 농도에서 rhBMP-2의 지연 방출을 유도했으며, 이러한 양상은 4주차까지 유지되었다. 이때, 0.5% HCS는 결함-지지체 부위와 부위 주변 뼈에서 rhBMP-2에 의해 서로 다른 양상을 나타내었다. 초기, HCS는 결함-지지체 부위에서 OPG의 발현이 매우 낮았으며, rhBMP-2 처리 시 RANKL의 발현과 RANKL/OPG 비율이 14.9배와 145배로 크게 높아졌으며, 골 흡수 관련 인자들의 발현이 증가하였다. 특히 ACS 대비 HCS는 rhBMP-2에 의한 RANKL/OPG 비율 증가가 약 51.9배 높았으며, 파골 세포 활성화가 크게 증가하였다. 이러한 양상은 골 형성 관련 인자들에서도 유사하게 나타났다. Micro-CT 결과, rhBMP-2 처리 시, 결함-지지체 부위에서 HCS가 12주 차 BV, Tb.N 등에 있어서 다소 나은 결과를 나타내었다. 이러한 결과는 조직학적 결과에서도 나타났다. 반면에, 골부식 결과는 rhBMP2 처리 시 BA의 초기 주변골 침식이 ACS에서 HCS 대비 약간 증가한 것을 확인하였다. 그러나 rhBMP2 처리 시 4주차에 ACS에서만 결함-지지체 부위를 벗어난 이소성 골화가 발생하였다. 단, 12주차 이후 이러한 ACS의 이소성 골화 양상은 완전히 사라졌다.

4. 결 론

고용량의 rhBMP-2 처리는 생체 내에서 BMP-2 신호 기작과 연관된 골 형성 및 골 흡수 관련 인자의 발현을 조절하여 골 형성 유도뿐만 아니라 이른 시기의 골 흡수를 야기하였다. NFAT-c1의 억제제는 이러한 고용량 rhBMP-2에 의한 초기 골 흡수 관련 인자의 발현 증가를 효과적으로 낮추었을 뿐 만 아니라, 장기간 골 재생에 더욱 나은 골 형성 효과를 보였다. 그러나 이러한 양상은 백서의 중간엽줄기세포(rMSCs)에서는 나타나지 않았는데, 이는 rhBMP-2의 NFAT를 통한 신호전달 기작이 RANKL/OPG 기작에 의한 파골 세포 한정적인 변화일 수 있음을 제안한다. 이러한 결과들은 NFAT-c1에 의한 rhBMP-2 신호전달 기작의 초기 시기 한정적이며 파골 세포 선택적인 억제가 초기 골 흡수 억제와 장기간 골 재생 유도에 있어서 효과적인 전략이 될 수 있음을 나타낸다. 다만, NFAT-c1 억제제는 초기 골 흡수 인자 뿐만 아니라 초기 골 형성 인자의 발현 또한 낮춘다는 점과 장기간 골 재생에서의 효율 증가가 다소 미미하다는 점에서 이를 극복하기 위한 추가 실험이 필요해 보인다. 앞서 확인한 고용량 rhBMP-2에 의한 RANKL/OPG 비율 증가는 골 흡수 관련 인자인 SOST의 BMP-2에 의한 조절 가능성을 나타내었다. 이와 관련하여, SOST 발현을 조절할 수 있는 분자생물학적 신호 기작을 밝히고자 진행한 hMSCs를 통한 실험에서 에스트로겐은 BMP-2에 의한 SOST의 발현을 조절하며, 이러한 E2에 의한 SOST의 발현 조절은 Smad4 비의존적으로 ER alpha와 Beta-catenin을 포함하는 Wnt pathway의 활성이 관여함을 확인할 수 있었다. 이는 SOST 조절에 있어서 에스트로겐과 BMP-2 신호 기작 간의 상호작용을 의미할 수 있으며, 이러한 결과는 조골세포에서 이루어지는 에스트로겐에 의한 골 항상성 조절을 설명할 수 있을 것이다. 그러나 이러한 결과는 분화된 조골세포유래에 따라 다른 결과를 나타내었다. 추후 연구를 통하여 초기 골 흡수에 미치는 영향과 유래에 따른 차이에 대한 분자생물학적인 기전 연구가 비롯되어야 하겠지만, 에스트로겐에 의한 SOST 조절은 rhBMP-2에 의한 보다 나은 골 재생 양상을 이끄는데 적용될 수 있을 것으로 보인다. 끝으로 7일차부터 12주차까지 장기간 진행된 실험 결과는 HCS를

이용한 고용량 rhBMP-2 처리 시 ACS보다 적은 초기 방출과 향상된 지연 방출을 통해서 초기 주변부 골 침식과 이소성 골화를 낮추며, 장기적으로 ACS 대비 신생 골 생성에 있어서 다소 나은 결과를 나타내고 있다. 이러한 결과는 HCS에서의 rhBMP-2의 지연 방출이 야기한 rhBMP-2의 지지체 부위 집중과 헤파린 자체의 효과로 인한 것으로 보인다. 비록 통계적 유의성은 나타나지 않았지만, rhBMP-2에 의한 OPG의 부위 특이적 발현 조절이 이루어지는 것 또한 확인할 수 있었다. 다만, 이러한 고용량 rhBMP-2의 지연 방출에 의한 지지체 부위 집중은 초기 골 형성뿐만 아니라 결함-지지체 부위의 초기 골 흡수 역시 증가시키는 양상을 발견할 수 있었으며, 이러한 점은 지연 방출 시 이에 의한 초기 골 흡수 가능성 역시 고려되어야 함을 함의한다. 본 연구는 골 재생을 위한 고용량의 rhBMP-2의 사용으로 인한 부작용을 감소시키고 골 재생을 증가시킴으로서 보다 나은 임상적인 적용 효과를 얻고자 진행이 되었다. 본 연구 결과는 고용량의 rhBMP-2에 의한 초기 골 흡수 양상이 BMP2의 분자생물학적인 신호 기전의 특정 타겟을 억제하거나 이와 관련한 인자의 조절로 억제 가능할 수 있다는 것을 NFAT-c1의 억제에 의한 생체 내 초기 골 흡수 억제 효과를 통해 제시하였다. 이러한 관점에서 에스트로겐에 의한 BMP-2 유도 SOST의 발현 조절 양상은 향후 골 흡수 양상을 조절할 수 있는 분자생물학적 기전을 확립하는데 고려 될 수 있다. 이와 함께 rhBMP-2의 방출 지연을 이끄는 헤파린을 이용한 rhBMP-2의 방출량 조절은 초기 주변 골 침식과 이소성 골화를 낮출 수 있으며 장기적으로 더 나은 골 재생을 나타냄을 확인할 수 있었다. 끝으로 본 연구를 통해 확인한 분자생물학적인 기전들과 rhBMP-2 방출 조절에 의한 효과를 상호보완적으로 고려하여 적용시킬 수 있으리라는 추론을 함의하고 있다는 것 역시 본 연구의 큰 의의일 것으로 보인다.

주요어 : rhBMP-2, 신생골 생성, 초기 골 흡수, 헤파린, NFAT-c1 억제제, 에스트로겐, SOST